



LUND UNIVERSITY

Atomic Layer Deposition and Immobilised Molecular Catalysts Studied by In and Ex Situ Electron Spectroscopy

Shayesteh, Payam

2019

[Link to publication](#)

Citation for published version (APA):

Shayesteh, P. (2019). *Atomic Layer Deposition and Immobilised Molecular Catalysts Studied by In and Ex Situ Electron Spectroscopy*. [Doctoral Thesis (compilation), Department of Physics]. Lund University, Faculty of Science, Department of Physics.

Total number of authors:

1

General rights

Unless other specific re-use rights are stated the following general rights apply:

Copyright and moral rights for the publications made accessible in the public portal are retained by the authors and/or other copyright owners and it is a condition of accessing publications that users recognise and abide by the legal requirements associated with these rights.

- Users may download and print one copy of any publication from the public portal for the purpose of private study or research.
- You may not further distribute the material or use it for any profit-making activity or commercial gain
- You may freely distribute the URL identifying the publication in the public portal


Read more about Creative commons licenses: <https://creativecommons.org/licenses/>

Take down policy

If you believe that this document breaches copyright please contact us providing details, and we will remove access to the work immediately and investigate your claim.

LUND UNIVERSITY

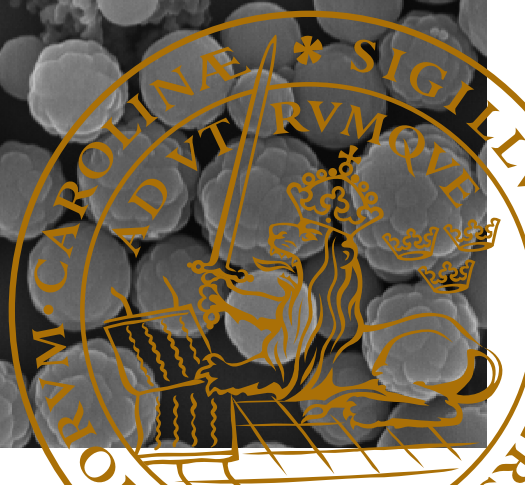
PO Box 117
221 00 Lund
+46 46-222 00 00

The background of the entire page is a scanning electron microscope (SEM) image showing a dense collection of spherical particles. Some particles are smooth and uniform in size, while others are more complex, appearing as clusters of smaller spheres or having a porous, textured surface. The particles are distributed across the entire frame, with a white text box overlaid in the center.

Atomic Layer Deposition and Immobilised Molecular Catalysts Studied by *In* and *Ex Situ* Electron Spectroscopy

PAYAM SHAYESTEH

DEPARTMENT OF PHYSICS | FACULTY OF SCIENCE | LUND UNIVERSITY



Atomic Layer Deposition and Immobilised Molecular Catalysts
Studied by *In* and *Ex Situ* Electron Spectroscopy

Atomic Layer Deposition and Immobilised Molecular Catalysts Studied by *In* and *Ex Situ* Electron Spectroscopy

Payam Shayesteh



LUND
UNIVERSITY

DOCTORAL DISSERTATION

by due permission of the Faculty of Science, Lund University, Sweden.
To be defended at the Rydberg Lecture Hall, Department of Physics on
15 March 2019 at 9.15 a.m.

Faculty opponent
Professor Georg Held

Organisation Department of Physics Box 118 SE-221 00 LUND Sweden	Document name DOCTORAL DISSERTATION	
Author(s) Payam Shayesteh	Date of disputation 2019-03-15	
Sponsoring organisation		
Title: Atomic layer deposition and immobilised molecular catalysts studied by <i>in</i> and <i>ex situ</i> electron spectroscopy		
Abstract The research work that I describe in my thesis deals with three different heterogenisation approaches for synthesising a heterogeneous transition metal catalyst used for direct C-H activation reactions. The three heterogenisation approaches considered in my research are: (1) heterogenisation of a molecular catalyst on a polymer support using covalent bonds, (2) heterogenisation of a catalyst on a reduced graphene oxide (rGO) support using non-covalent interactions and (3) immobilisation of a catalyst on an inorganic surface using covalent bonds and encapsulation in an inorganic matrix. Catalytic Pd complexes with one or two anchoring branches were successfully embedded in a polymer matrix by polymerisation, i.e. using the first approach. The catalyst samples were analysed using ultrahigh vacuum X-ray photoelectron spectroscopy (UHV XPS), transmission electron microscopy (TEM) and scanning electron microscopy (SEM). No sign of Pd in the metallic state (Pd ⁰) or nanoparticles was observed after synthesis and polymerisation and after using the catalyst for several cycles of oxygenation and halogenation reactions. In the second approach molecular Pd catalysts with one or two anthracene branches were immobilised on an rGO surface using π -stacking. These samples were used in oxygenation and halogenation reactions. XPS shows that the catalysts synthesis and immobilisation was successful, without any reduction in the oxidation state of the Pd. The results also show that the catalysts are stable and recyclable. The third approach aims at achieving a highly efficient and selective heterogeneous catalyst synthesis. The basic idea is to encapsulate a heterogenised molecular catalyst in an inorganic matrix, which is complementary to the target reaction product in size and shape. Since such a matrix conveniently can be produced by atomic layer deposition (ALD), I directed my focus on understanding the mechanism of oxide ALD. To this end, the ALD of HfO ₂ from tetrakis(dimethylamido)hafnium (TDMAHf) and water was on <i>In situ</i> -oxidised SiO ₂ /Si(111) was studied using <i>operando</i> ambient pressure x-ray photoelectron spectroscopy (APXPS). APXPS provides the possibility to bridge the pressure gap between standard UHV XPS investigation and the pressure conditions of the ALD process carried out in the mbar regime. It also offers the option of high temporal resolution on the second timescale, which made it possible to follow the precursor-surface and precursor-precursor interaction during the first two ALD half cycles. The <i>operando</i> study of ALD enable the study of the ALD reaction mechanisms by following the evolution of the different surface chemical species. Furthermore, combining the experimental data with density functional theory (DFT) calculations contributed to improving the understanding of the surface chemistry and reaction mechanism of HfO ₂ growth. In addition, a vapour phase study of two widely used precursors, tetrakis(dimethylamido)titanium (TDMAT) and TDMAHf, is also reported in my thesis. Experimental results AP XPS are combined with DFT calculations for a detailed analysis of the electronic structure of these two precursors. DFT calculations explain the difference in XPS results for the two precursor as being due to π -donation interactions between metals and ligands.		
Key words Ambient pressure XPS, catalysis, heterogenisation, atomic layer deposition, HfO ₂ , gas phase, TDMAHf, TDMAT		
Classification system and/or index terms (if any)		
Supplementary bibliographical information		
ISSN and key title	Price	ISBN
Recipient's notes	Language	978-91-7753-968-1 (print)
Number of pages 99	English	978-91-7753-969-8 (pdf)

I, the undersigned, being the copyright owner of the abstract of the above-mentioned dissertation, hereby grant to all reference sources permission to publish and disseminate the abstract of the above-mentioned dissertation.

Signature

Payam Shayesteh

Date 2019-02-04

Atomic Layer Deposition and Immobilised Molecular Catalysts Studied by *In* and *Ex Situ* Electron Spectroscopy

Payam Shayesteh



LUND
UNIVERSITY

Coverphoto: Copyright Payam Shayesteh

Description: SEM images of polymerised catalytic transition metal complex.

Copyright: pp 1-99 Payam Shayesteh

Paper 1 © John Wiley and Sons

Paper 2 © By the authors (manuscript unpublished)

Paper 3 © John Wiley and Sons

Paper 4 © By the authors (manuscript unpublished)

Paper 5 © By the authors (manuscript unpublished)

Paper 6 © By the authors (manuscript unpublished)

Faculty of Science

Department of Physics

Division of Synchrotron Radiation Research

ISBN: 978-91-7753-968-1 (print)

ISBN: 978-91-7753-969-8 (pdf)

Printed in Sweden by Media-Tryck, Lund University Lund 2019



Media-Tryck is an environmentally certified and ISO 14001:2015 certified provider of printed material. Read more about our environmental work at www.mediatryck.lu.se

MADE IN SWEDEN 

*Dedicated to
Those who always supported me...
My parents and
My lovely wife Mahsa.*

Table of Contents

List of Papers.....	10
Popular Science.....	12
Acknowledgement.....	14
1. Introduction	17
1.1. Heterogenisation Approaches in this Thesis.....	22
1.2. Surface Science	26
1.3. This Thesis: Organisation of the Work.....	27
2. Analysis Techniques.....	29
2.1. X-ray Photoelectron Spectroscopy	29
2.1.1. Principle and Theory	29
2.1.2. Core Level Shifts.....	35
2.1.3. XPS Instrumentation	38
2.2. Ambient Pressure X-ray Photoelectron Spectroscopy.....	40
2.3. Microscopy Techniques.....	43
2.3.1. Scanning Electron Microscopy.....	44
2.3.2. Transmission Electron Microscopy	46
2.4. Density Functional Theory	47
2.4.1. How Accurate is DFT?	48
2.4.2. DFT and Relation to Experiment.....	49
3. Atomic Layer Deposition.....	51
3.1. Ideal ALD Process.....	51
3.1.1. Adsorption Mechanisms in ALD.....	53
3.1.2. Temperature Dependency in ALD	54
3.2. ALD Precursors	55
3.3. HfO ₂ Growth on Si Surface Employing ALD	56
3.4. Gas Phase Study of TDMAHf and TDMAT	58
3.5. <i>Operando</i> Study of ALD Employing Ambient Pressure XPS.....	59

4.	Green Chemistry and Catalysis	73
4.1.	Homogenous and Heterogeneous Catalysts.....	75
4.2.	C-H Activation in Catalytic Oxygenation and Halogenation Chemistry	77
4.3.	XPS Studies of Catalyst Systems	78
5.	Conclusion and Remarks.....	87
6.	Outlook.....	89
7.	References	93

List of Papers

This doctoral thesis summarises my research work, which comprises an independent project on the surface chemistry of atomic layer deposition investigated by ambient pressure X-ray photoelectron spectroscopy and a collaboration project with the Department of Chemistry at Lund University. This thesis is structured based on the research papers listed below:

I. **Polymer-Supported Palladium(II) Carbene Complexes: Catalytic Activity, Recyclability and Selectivity in C-H Acetoxylation of Arenes**

Maitham H. Majeed, Payam Shayesteh, L. Reine Wallenberg, Axel R. Persson, Niclas Johansson, Lei Ye, Joachim Schnadt, Ola F. Wendt.
Chem. Eur. J. 23, (2017) 8457-8465.

I was responsible for preparing the samples and measuring the X-ray photoelectron spectroscopy and scanning electron microscopy data. I was main responsible for the analysis of the photoelectron spectroscopy data and the writing of the corresponding parts of the results and discussion sections in the paper. I also participated in the sample preparation for the transmission electron microscopy experiments.

II. **Direct C-H Halogenation Reactions Catalysed by Pd(II) Supported on Polymers Under Batch and Continuous Flow Conditions**

Maitham H. Majeed, Payam Shayesteh, Per Tunå, Axel R. Persson, Roman Gritcenko, L. Reine Wallenberg, Lei Ye, Christian Hultheberg, Joachim Schnadt, Ola F. Wendt.

In manuscript.

I was main responsible for preparing samples and the planning of the X-ray photoelectron spectroscopy and scanning electron microscopy measurements. I was main responsible for analysing the photoelectron spectroscopy data and the writing of the corresponding parts of the results and discussion sections in the paper.

III. **A Pd^{II} Carbene Complex with Anthracene Side-Arms for π -Stacking on Reduced Graphene Oxide (rGO): Activity Towards Undirected C-H Oxygenation of Arenes**

Maitham H. Majeedⁱ, Payam Shayestehⁱ, Axel R. Persson, L. Reine Wallenberg, Joachim Schnadt, Ola F. Wendt.
Eur. J. Org. Chem. 43 (2018) 4742-4746.

I was main responsible for sample preparation and for performing the X-ray photoelectron spectroscopy and scanning electron microscopy measurements. Prior to the final photoelectron spectroscopy experiments

ⁱ These authors contributed equally to this work.

at MAX IV, I carried out a pre-study at the Department of Biology at Lund University in order to confirm the synthesis and to be able choose the proper substrate for the final measurements. I was main responsible for the analysis of the photoelectron spectroscopy data and the writing of the corresponding parts of the results and discussion sections in the paper.

IV. Reduced Graphene Oxide supported Pd(II) Carbene Complex: Activity and Selectivity in Directed C-H Halogenation of Arenes

Maitham H. Majeed, Dino Redzic, Payam Shayesteh, Axel R. Persson, L. Reine Wallenberg, Joachim Schnadt, Ola F. Wendt.

In manuscript.

I was main responsible for the X-ray photoelectron spectroscopy and scanning electron microscopy measurements. I was main responsible for the analysis of the photoelectron spectroscopy data and the writing of the corresponding parts of the results and discussion sections in the paper.

V. Experimental and Theoretical Gas Phase Electronic Structure Study of Amido Transition Metal Complexes for Materials Deposition

Payam Shayesteh, Roman Tsyshevsky, Samuli Urpelainen, François Rochet, Fabrice Bournel, Jean-Jaques Gallet, Maija M. Kuklja, Joachim Schnadt, and Ashley R. Head.

Submitted for publication.

I was responsible for sample preparation and for the gas phase ambient pressure X-ray photoelectron spectroscopy experiments on the TDMAHf molecule. I was responsible for the analysis of the photoelectron spectroscopy data of both investigated compounds. I collaborated on writing the paper.

VI. Following the Evolution of the Surface Chemical Species During Atomic Layer Deposition of HfO₂ on SiO₂

Payam Shayesteh, Roman Tsyshevsky, Ashley R. Head, Jean-Jaques Gallet, Fabrice Bournel, François Rochet, Maija Kukla, Rainer Timm, and Joachim Schnadt.

In manuscript.

I was main responsible for planning and performing the X-ray photoelectron spectroscopy experiments, analysis of the data and writing the manuscript. I collaborated on the interpretation of the theoretical calculations.

Popular Science

The growing need for green processes in industry makes scientists design and develop processes that are more energy efficient than current processes. Naturally, some reactions require a high energy and long time to occur. This will cause high energy consumption and, typically, even more waste production. Therefore, many efforts have been done to design materials that can help to change the path of a chemical reaction and thus result in a decrease of the required energy for a particular chemical process. Such materials are called catalysts. Catalysts change the reaction chemistry in a way that the reaction can happen with consumption of less energy and in shorter time by changing the reaction path.

Catalysis has great impact on our lives, so much indeed that today we would not be able to do without catalysts. As an example, new medicines with less severe side effects on the human health are highly desired for the treatment of many illnesses. The development of such medicine cannot be done without a change of chemistry of the medicine, to avoid harmful substances and to limit side reactions that can occur in human body. Such a change of chemistry requires changes in the synthesis and production process of the medicine. Removing a harmful molecule/group or inserting a useful molecule/group is sometimes a complicated chemical process. In addition, an inserted molecule/group in a chemical structure should often have an orientation with respect to the rest of the molecular structure of the medicine. In my thesis, I have analysed newly synthesised catalysts that are designed for activating carbon-hydrogen bonds in order to substitute hydrogen with other groups or atoms – something which is extremely important for the production of fine chemicals such as medicines.

Catalysts can be divided into two groups: homogeneous and heterogeneous catalysts. A homogeneous catalyst, on the one hand, is a catalyst that acts in the same phase as the starting material and products of the desired chemical reaction. For instance, if all starting materials of the reaction are in the liquid phase, the catalysts that will catalyse the reaction between these substances is also in the liquid phase. On the other hand, a heterogeneous catalyst is in a different phase than the starting material and products. Often, the starting materials and products are in the gas phase and the catalyst is in the solid phase; the reaction is catalysed by a heterogeneous catalyst. My thesis focuses on the analysis of new Pd based heterogeneous catalysts and the study of the fundamental surface chemistry behind the synthesis of these catalysts.

Chemical reactions often happen on a surface. This implies a gas/liquid, gas/solid or liquid/solid interaction. Therefore, it is important to use techniques that can probe surfaces in order to have more insight in such chemical reactions. This can help improving the chemical reaction or design better catalysts for the use in catalysed

chemical processes. In this thesis I used X-rays photoelectron spectroscopy (XPS), which is a surface-sensitive technique, to investigate the structure of newly synthesised catalyst materials and, furthermore, study the chemistry of reactions at surfaces.

One interesting technique that can be used in the production of catalyst materials and is also widely used in electronics is atomic layer deposition (ALD). ALD is a thin film growth technique with high thickness precision, conformity and uniformity over the surface. In ALD of oxide materials one uses two different precursors in two separate half-cycles to grow thin films. Each half-cycle is followed by an evacuation or purge step. I have used XPS in ambient pressure conditions (i.e. I used *ambient pressure XPS* (APXPS)) to investigate the surface chemistry of ALD. Since this was done *during* the thin film growth, I use the term *operando* to describe the conditions of the investigation. The high time resolution that could be achieved helps in monitoring the surface reactions during the early stages of the precursor-solid interaction. I applied APXPS to the study of HfO_2 growth on SiO_2 and gained insight in surface chemical species and their interaction with the SiO_2 surface. Extremely useful input is gained in the reaction mechanism.

Acknowledgement

I would like to use the chance to thank all those who helped me during my PhD to follow my goal and complete my career. First and foremost, I thank my supervisor Prof. Joachim Schnadt not only for supervising me as a PhD student but also advising me with wise and helpful words at the right moments. There are ups and downs in life, and among these fluctuations, wise words can encourage a person to keep doing his/her best. Achim, you inspired me for doing my best in contributing to science and life.

I would like to express my gratitude to my co-supervisors, Prof. Ola Wendt, Prof. Lei Yi and Dr. Franz Hennies, for scientific discussions and inspirations. Ola, I will never forget the kick-off meeting with your group and the other occasion that I tasted Surströmming at your department for the first time. I agree with you and think that it tastes good!

I have great memories of all those who supported me or encouraged me to follow my dreams while I was pursuing my PhD. I learned to put more effort each time I faced a difficulty. I would like to give a deep thanks from my heart to those who always did their bests for me, *my parents*.

People in Centre of Analysis and Synthesis in chemistry department at Lund University are greatly acknowledged. Specially, I am indebted to Dr. Maitham H. Majeed not just as collaborator but also as a great friend. Maitham, this work was not possible to complete without your encouragements and great ideas. I gathered great knowledge by discussing the chemistry with you and learned many things during those fun and scientific night shifts at MAX IV. Maitham, do you know the difference between a real friend and blood? Blood goes in the heart and goes out but a true friend goes in the heart and stays there. Maitham, you mean more than just a friend and colleague for me, you are my brother.

I thank my dear friend and a man who stood with me during the hard time of finding a flat, Dr. Abdelrazek Mousa. Abdelrazek, I had such great time with you during my stay at your place. You are a friend that not everyone has the chance to have.

The Division of Synchrotron Radiation Research has had and has amazing people, and I would like to sincerely thank former and present members in this division. First of all, I would like to express my appreciation to Dr. Ashley Head for her great work in collaborating with me. Ashley, I learned many things from you in science and in life. You always have the best tips and suggestions for any problem in science or daily life. Ashley, I feel that our friendship is deep enough to say that you and your family are part of my family. As always I am missing your lovely daughter Emma and please pass my greetings to Jeff Head, the man with big heart and amazing smiles (Right on!)

I would like to thank Patrik Wirgin, the man of solutions and answers at the Division of Synchrotron Radiation Research. Patrik, you filled the work place with fun and sure it is “strålande”. I learned from you how to survive during Mondays and have fun during hard times no matter what and when. Patrik, I agree that it was funny that you had to sign so many papers for me every now and then.

I would like to give my thanks also to my former colleague Dr. Shabnam Oghbaie for helping me to prepare for my PhD position interview and also sharing her valuable experiences before and after I traveled to Sweden.

Special thanks to Dr. Shilpi Chaudhary for giving a hand and teaching me data analysis. My friend and former office mate Dr. Mohammad Alif Arman is also acknowledged for his patience and kind help during our scientific and non-scientific discussions.

My colleagues Dr. Niclas Johansson and Dr. Lisa Rullik are acknowledged for making the workplace a place of friendliness and free-time a place of fun and relaxation. Niclas, I appreciate all your help in IGOR programming and your patience, and Lisa I will never forget the tasty foods you cooked. Lisa, I still say that potatoes with the special sauce that you made taste even better than the chicken.

My Italian colleagues Stefano Albertin and Andrea Troian thank you for improving the working atmosphere so much that it feels more like home. My special thanks then should go for my friend Giulio D’Acunto from Roma who personally made the work and after work fun and fruitful (pastaful). Giulio, I appreciate that you are always helpful and kind. You are a good scientist and an amazing friend as you always say everything is done “nice and clean, clean and nice” and always Daje Roma!

Lund and physics are two important things that can make a complete picture of a good place to be for me when I think of MAX IV. Considering MAX IV without all those amazing people who are always ready to help sounds more like only an experimental building. I thank all who helped me at MAX IV, especially Dr. Alexei Preobrajenski, Dr. Alexander Generalov, Dr. Nikolay Vinogradov, Dr. Margit Andersson, Dr. Samuli Urpelainen, Dr. Andrey Shavorskiy and Suyun Zhu.

Nano Lund laboratory at physics department in Lund University is one of my favorite places for doing experiments and meet helpful, patient people. I always got full support and help from wonderful staff.

Other people at Lund University Dr. Ola Gustafsson, Prof. Per Persson, Dr. Tao Wang, Dr. Michiel Op De Beeck (Biology Department, Lund University) and Dr. Filip Lenrick are always acknowledged for helping me in my research work.

Collaborating with many groups taught me that one should extend his/her research even beyond the borders to learn new material. I would like to thank all my

collaborators of their help and great scientific experiences during experiments at the SOLEIL synchrotron Dr. Jean-Jaques Gallet and Dr. Fabric Bournel. My research work was a great experience of internationality when I performed some experiments at Gent University in Belgium. I thank Prof. Christophe Detavernier, Dr. Jolien Dendooven and Michiel Van Daele for their help and support during my experiments and fruitful discussions. I always appreciate the help I received during the collaboration with Dr. Roman Tsyshevskiy (University of Maryland in USA). Roman, it was a pleasure working with you. Keep doing your great work!

Last, but not least, I would like to thank my lovely wife Mahsa Pezhman. Mahsa, our first year of married life overlapped with the last year of my PhD. I am sorry for all the times that I could not spend with you, but I can tell that I was highly motivated by the love and support that I received from you continuously during this year.

1. Introduction

The world around us is not in a stationary chemical condition, but it behaves more like a huge chemical batch reactor. Among the continuously ongoing chemical reactions are, e.g., the digestion of food in our bodies, catalysed by enzymes, or the chemical reactions that led to the formation of oil now found under the sea bed or the photosynthesis reaction in trees and other plants. Chemical reactions between reactants in the gas (or liquid) phase can be catalysed by surfaces, and this is why surface scientists are interested in them. Surface science is really a combination of different fields, which provides tools for studying physical and chemical phenomena at the interface between a solid and a gas phase. Two fields that benefit greatly from surface science and which I have dealt with are atomic layer deposition (ALD) and catalysis¹⁻³.

The original aim of my research project was to contribute to the synthesis and, in particular, the characterisation of a new heterogeneous catalyst, i.e. a catalyst in a different physical phase than the starting materials and products of the targeted chemical reaction. The goal was to base this heterogeneous catalyst on a homogenous catalyst material, i.e. a catalytic complex in the same phase as the educts and products. The target chemical reaction was the direct C-H activation reaction, and the aim was to achieve good activity, selectivity and recyclability. The catalyst design approach is schematically demonstrated in Figure 1.1. In this design a catalytically active centre (in this case a transition metal ion in a transition metal complex) is immobilised on a surface. During the immobilisation a template

Commonly used terms in this thesis:

Heterogeneous catalyst: a catalyst is in a different phase than the starting materials and products of the chemical reaction.

Homogeneous catalyst: catalytic complex in the same phase as the educts and products.

Heterogenisation: using an inert support for attaching the catalyst complex to it.

Immobilisation: act of attaching the a complex to an inert, insoluble material.

Molecular imprinting: a method for imprinting a cavity in a polymer matrix that has the same shape as a template molecule for very specific target molecule.

molecule is attached to the active centre of the catalyst. The template has a shape and size that are identical or similar to the desired product. The catalyst complex is encapsulated in a matrix that protects it from the bulk of the reaction environment. After the catalyst synthesis is finished the template molecule is removed so that a catalytically active site in the matrix is left behind. In this way an active nanoreactor has been created⁴. The size of the cavity on the surface depends on the molecule that is used as a template. One particular template molecule that was used when immobilising a catalyst complex designed for the activation of C-H bond in biphenyl (Figure 1.3) was phenyl pyridine. This template molecule leaves behind a cavity in the matrix with a size of around³ 0.7 Å. Hence, the catalyst and template together define the size and shape of the cavity that encapsulates the catalyst complex.

The project was carried out in collaboration with Dr Maitham H. Majeed at the Department of Chemistry at Lund University⁵. In his PhD thesis Dr Majeed focused primarily on the synthesis and catalysis aspects of the project, while I concentrated on the characterisation. The division of the work and the basic ideas are summarised in Figure 1.2.

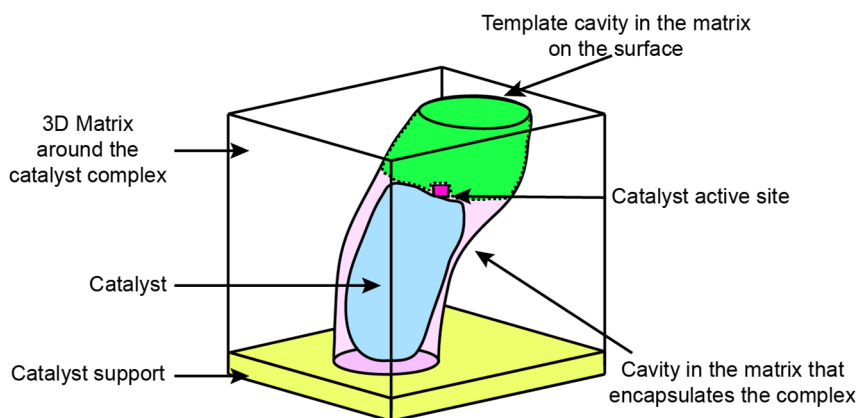


Figure 1.1.

Schematic of the original idea behind my PhD project. A homogenous catalyst is immobilised on a surface and a 3D matrix is grown around the catalyst. The cavity is adapted to the chemical reaction and the desired product. The catalyst is shown as the blue area. The size and shape adaptation is achieved by including a relevant template molecule during the synthesis of the catalyst cavity. It is removed after the synthesis. The size of the cavity depends thus on the size and shape of the template molecule and are thus adapted to the target product.

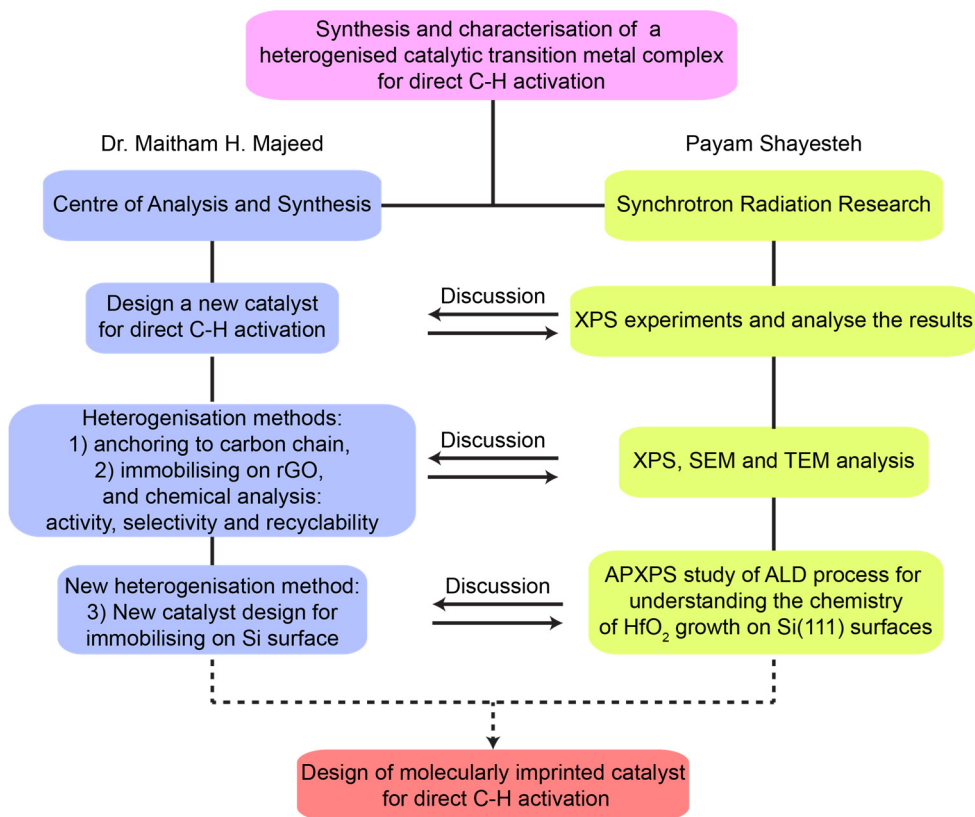


Figure 1.2.

Flow chart of my PhD studies. My PhD work was carried out in collaboration with Dr Maitham H. Majeed at the Department of Chemistry. Our responsibilities are schematically shown here.

Heterogeneous vs homogenous catalysis

As outlined above, the goal of the project was to immobilise a homogeneous catalyst on a surface and to thus heterogenise the homogeneous catalyst. This puts the question what the respective advantages of homogeneous and heterogeneous catalysis are. Heterogeneous catalysts have the following advantages⁶⁻⁸:

- No solvent is required.
- Heterogeneous catalysts are easier to recover and reuse than homogenous ones and, hence, typically less waste is produced. Moreover, the probability of metal contamination of the products is lower in comparison to homogenous catalysts.
- The catalyst can be used in continuous flow mode (cf. paper II).

Homogeneous catalysts have the following advantages^{5,9}:

- All catalyst sites are identical.
- All catalyst sites are accessible because the catalyst is dissolved in solution.
- The activity and selectivity of the catalyst can be tuned rather easily by a modification of the catalyst complex.
- The reaction mechanism can be studied directly in the solution.

The present project aimed at combining the advantages of homogeneous and heterogeneous catalysis. Moreover, the particular design with a cavity that is adapted to the product aimed at further increasing the high selectivity and to provide the best conditions for catalyst stability. For example, dimerisation and agglomeration of the catalytically active sites should be minimised by the design.

It is clear, however, that heterogenised homogeneous catalysts normally suffer from a number of problems, which may make them unsuitable for industrial use⁶⁻⁸:

- the homogenous catalyst may be destabilised by immobilisation,
 - supports may be expensive,
 - the catalytically active metal may leach,
 - the efficiency and selectivity of the catalyst may be much reduced upon heterogenisation,
 - characterisation is typically difficult for a heterogeneous catalyst since a surface needs to be analysed and understood,
 - this also makes it difficult to investigate the exact nature of the active sites.
- Overall, it is more difficult to improve the catalyst system.

Why C-H bond activation?

The C-H bond in arenes, or aromatic hydrocarbons (for some examples of non-functionalised and functionalised arenes see Figure 1.3), is a very stable bond and thus very difficult to activate. For example, the attachment of a new acetoxy group (OAc, CH₃-COO⁻) to a benzene ring to produce a similar substance to aspirin requires activation of a benzene C-H bond. This bond has a bond dissociation energy of¹⁰ 113 kJ mol⁻¹. The example illustrates the importance of C-H activation for, in particular, the fine chemical and medical industry, since the raw material for substances such as aspirin, paracetamol and other medicines is mineral oil⁵. Finding better catalysts for the activation of C-H bonds gives the chance to produce improved products for better medical benefit and to reduce the environmental impact of the production process.

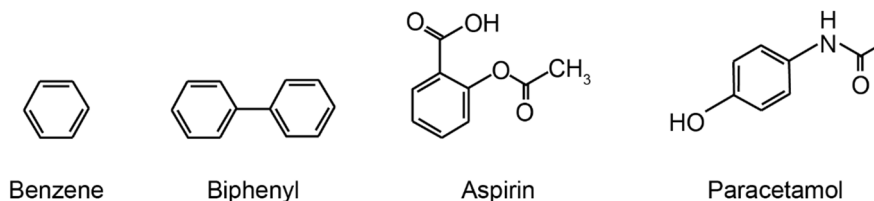


Figure 1.3.

Some examples of arenes. Benzene and biphenyl, here in their unfunctionalised forms, are typical constituents of mineral oil^{11,12}. Aspirin and paracetamol are well-known medical substances.

Molecular Imprinting

Molecular imprinting is a method for imprinting a cavity in a polymer matrix that has the same shape as a template molecule¹³. It is a useful method e.g. for the preparation of polymeric materials for gas sensing, since for such materials a very specific response for very specific target molecules is required. This is achieved by using a “key-lock” approach¹³.

The idea is copied here with the goal of creating a highly selective catalyst (cf. Figure 1.4): A catalyst complex (an organic or inorganic complex) is polymerised into a polymer matrix in the presence of a template. Subsequent removal of the template from the complex imprints a cavity in the polymer matrix that has the same shape as the template molecule. The catalyst will be surrounded by the imprinted cavity, and the matrix around the complex encapsulates and supports the catalyst. This design will improve the selectivity, activity and stability of the catalyst^{4,14}.

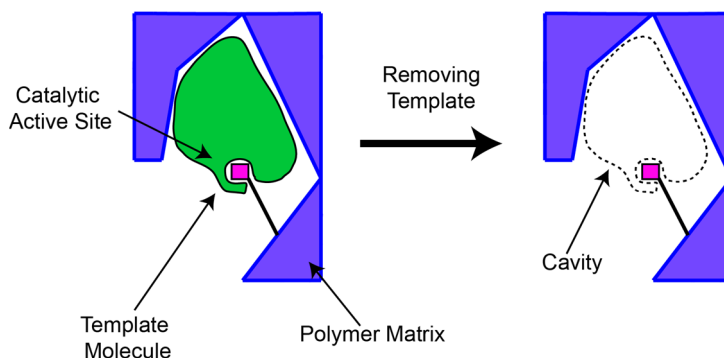


Figure 1.4.

Principle of *molecular imprinting*. The green, blue and pink areas represent the template molecule, polymer matrix and catalytically active site, respectively. After removing the template a cavity is found in the polymer matrix around the catalytically active site.

1.1. Heterogenisation Approaches in this Thesis

As outlined above, the basic idea behind this PhD thesis is the heterogenisation of a homogeneous catalyst, which, in the present case, always is a transition metal complex – a Pd N-heterocyclic carbene (NHC) complex. The chemical structure of the NHC ligand is schematically depicted in Figure 1.5. The heterogenisation may then be combined with the encapsulation of the heterogenised – or immobilised – catalyst in a cavity. In this project three different approaches to heterogenisation were applied.

Approach 1: Heterogenisation of the catalyst on a polymer support using covalent bonds

Papers I and II report the synthesis of a new catalytic transition metal complex^{1,5}, where carbon side chains were added to a complex that allow anchoring the complex to a solid support. This approach uses the same concept as is used in *molecular imprinting*. As discussed briefly above, *molecular imprinting* implies forming selective binding sites that have a shape, size and functional groups that are complementary to a targeted molecule. This is achieved by polymerising the complex together with a template molecule (printing molecule)¹⁵ and other polymer constituents in a block copolymer approach to provide the final and stable solid catalyst^{5,16,17}.

The approach was quite successful in that an efficient catalyst was produced. However, it also needs to be said that the encapsulation and formation of the selective cavity could not be achieved. As it is shown in papers I and II catalyst complexes designed by this approach anchored to the carbon chain and polymer can

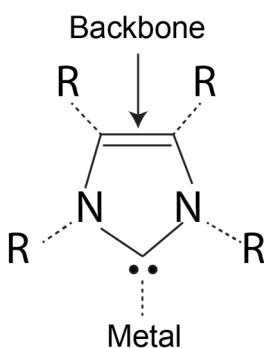


Figure 1.5.

Chemical structure of the NHC ligand. Dashed lines that end in an R show that different ligands can be placed in each of these places. In this study a Pd ion is placed in the location that is indicated by "metal" in the picture. NHC ligands are two-electron σ -donors with little π -accepting ability. The σ -donor strength can vary depending on the structure of the complex. N-heterocyclic carbenes can form strong bonds to metal centres and have little dissociation tendency¹⁸.

successfully act as a solid support. Anchoring arm/arms are designed on one side of the catalyst complex. This design allows the catalyst to be attached to the support but omits the possibility of encapsulation of the catalyst complex. In addition production of the cavity is not possible since the polymer chain cannot cover the complex and encapsulate it.

Approach 2: Heterogenisation of the catalyst on a reduced graphene oxide support using non-covalent interactions

The second approach to heterogenisation, reported in papers III and IV, was to immobilise a similar catalytic transition metal complex as above on reduced graphene oxide (rGO) using π - π interactions, i.e. using a non-covalent bond (cf. Figure 1.6). Here, the complex was functionalised with anthracene groups, which provide the required sticking force. In comparison to approach 1 this method decreases the need for chemical modification of the homogenous catalyst and of the support, but still provides a stable heterogeneous catalyst material, since the dissociation energy¹⁹ for π - π or CH- π bonds on graphene is 50 kJ mol^{-1} .

Approach 3: Immobilisation of the catalyst on an inorganic surface using covalent bonds and encapsulation in an inorganic matrix

Here, immobilisation of the catalytic transition metal complex together with a product template was planned to be done onto an inorganic surface such as Si or SiO_2 . Then it was planned to grow an oxide matrix around the complex and template using ALD, i.e. a form of chemical vapour deposition (see chapter 3). The template molecule would have been removed after oxide deposition and thus a nanoreactor cavity be created as outlined above. In this way a highly selective catalyst should have produced, which also was expected to retain the high activity of the catalytic transition metal complex. Indeed, such an approach has already been reported in

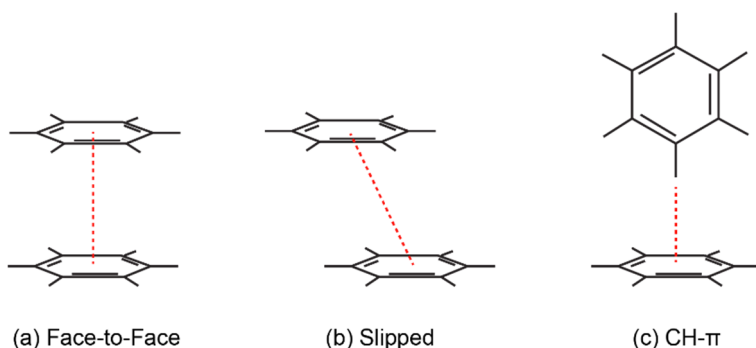


Figure 1.6. Three different types of non-covalent π - π interactions between two aromatic rings. Figure is redrawn from reference 19.

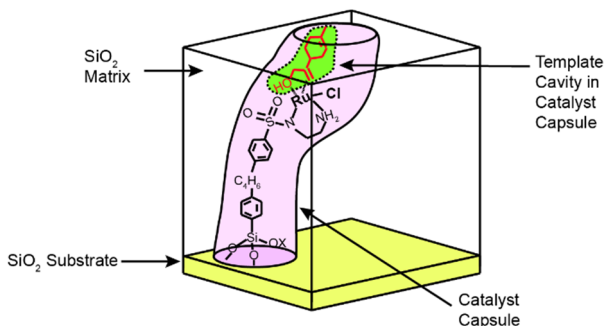


Figure 1.7. Ru catalyst complex immobilised on a SiO₂ surface and encapsulated in a SiO₂ matrix. The figure is redrawn from reference 4.

literature⁴: Figure 1.7 shows the structure of the Ru catalyst complex that was immobilised on SiO₂ and encapsulated by a SiO₂ matrix.

Immobilising the catalytic transition metal complex on a solid surface using covalent bonds as in the present approach has some advantages with respect to the other two approaches⁴:

- 1) The cavity, which matches the size and shape of the product, is expected to significantly improve the selectivity.
- 2) The cavity is orientated correctly with respect to the catalytic complex.
- 3) The matrix wall around the complex protects the catalytic complex and regulates the mobility of the metal complex.

The first step towards this approach was to study the growth of HfO₂ on a SiO₂ surface. More specifically, I studied the HfO₂ growth on *in situ*-oxidised SiO₂/Si(111), and I did this using *operando* conditions in order to learn about the surface chemistry during the precursor/surface interaction. In the meantime, my collaborator at the Department of Chemistry synthesised a new catalytic transition metal complex, and the plan would be to continue my research by immobilising this catalyst on a surface and investigate its structure, before combining the immobilisation with oxide growth around the catalyst.

Catalyst design, synthesis and heterogenisation

In all three approaches the design, synthesis and heterogenisation of the catalysts were done at the Department of Chemistry by Dr. Majeed^{1,5}. Approaches 1 and 2 were used successfully to synthesise new catalysts. Regarding approach 3, I started to study the ALD growth process to gather detailed information about the reaction

mechanism, while the entire approach has not yet been realised. As stated above, this endeavour is left for the future.

My goal in this research was to characterise the different samples with respect to their surface structure by spectroscopy and microscopy techniques such as X-ray photoelectron spectroscopy (XPS), scanning electron microscopy (SEM) and transmission electron microscopy (TEM). The results from the characterisation together with the chemical analysis formed the basis to understand the performance of the catalyst^{1,5}. In order to employ the third approach proper surface and overlayer materials needed to be chosen. Therefore, studying ALD in atomic-scale detail became part of my research project and turned out to be very interesting in itself.

Employing ALD in my thesis

ALD is a thin film deposition technique with Ångström thickness precision. In the third approach to the heterogenisation of catalytic transition metal complex deposition of an inorganic matrix is part of the process that needs to be done with good control^{3,4}. In particular, it is important to make sure that the right amount of matrix material is deposited so that the catalytic complex is encapsulated, but not completely buried under the solid matrix. ALD is, obviously, a technique of choice. It has been used widely to produce materials for electroluminescent displays, semiconductor devices, photochemistry sensors and catalysis^{4,20,21}. It also turns out that, although ALD has widely been studied before, there are not many studies that use *operando* conditions, which allow to follow the ALD deposition while it is ongoing and during the important early stages of the process²². This motivated me to put focus on investigating the chemistry of the initial ALD process using an *operando* technique: ambient pressure X-ray photoelectron spectroscopy.

A Si(111) surface was chosen as the substrate, and deposition of HfO₂ using ALD was targeted. The combination of the particular substrate and deposited oxide layer is suitable not only for the catalyst immobilisation strategy aimed at here, but has also been studied widely for application in electronics in general and gate dielectric production in particular^{23–26}.

It is vital to know and understand the state of the substrate surface during the ALD process and to be able to follow the surface chemistry during ALD deposition. In particular, the early stages of the process will be decisive for the structure and quality of the films grown. Thus, any interfacial layer during HfO₂ growth has an impact on the electrical properties of the designed device. As has been shown in several studies^{27–30}, the interfacial layer between HfO₂ and Si substrate surface causes an increase in permittivity with respect to SiO₂, which might be undesired in many applications^{31,32}. Controlling the interfacial layer and avoiding undesired atom incorporation or the presence of contaminations in the film is doable by means of better understanding the reaction mechanism of the ALD process³³.

In this thesis I worked on characterising the ALD of HfO₂ on Si surfaces in order to gather fundamental information about the surface chemistry for optimum film deposition. In my research I employed ambient pressure XPS in order to cover the pressure gap and time delay between the ALD and XPS measurements. I used snapshot mode of the analyser for faster measurements. In this mode a snapshot image of the detector will be provided for each core level during the measurement intervals. In this way, a time resolution of 0.08 Hz was achieved. This implies that measurement of five core levels (Hf 4f, N 1s, C 1s, Si 2p and O 1s) took only 13 s. In comparison to the normal “swept mode” measurement of electron energy analysers, which can take about two minutes to perform, the time resolution in my study has considerably improved. In addition, a comparison to a recent study by Timm *et al.* shows that I was capable of measuring five core levels with snapshot mode, while in their ALD study only one core level was monitored in swept mode²².

1.2. Surface Science

The surface chemical reactions in ALD and heterogeneous catalysis need to be understood and improved to find optimum conditions for different applications. Choosing new materials and controlling the reaction conditions allow developing higher quality materials. Modern society requires better quality electronics at a high pace (for examples computers and mobile phones etc.), but also an improved environmental friendliness. Surface science can help to address these challenges.

In order to better understand ALD and catalysis, new experiments are required. Data collection and analysis of the results from the experiments cannot be done without proper tools. Tools that are provided by surface science give the opportunity to monitor surface chemical reactions closely. From an improved understanding of the reaction mechanism, production quality can be improved, and energy waste and material consumption can decrease in many production processes^{34–36}. Several analysis techniques have been developed and are useful for surface science to provide information about the nature of the reactions. This includes spectroscopy and microscopy techniques such as XPS, infrared spectroscopy, low energy electron diffraction, electron energy loss spectroscopy, atomic force microscopy, scanning electron microscopy (SEM), transmission electron microscopy (TEM), etc. Here, I used ultrahigh vacuum XPS (UHV XPS) and ambient pressure XPS as two main spectroscopy techniques for conducting my research. SEM and TEM were microscopy techniques that I used for sample characterisation³⁷. In the next chapter I describe the techniques that I used in my research in more details.

In order to interpret the reaction and understand the mechanism of a reaction on a surface during ALD it is necessary to understand the interaction between the solid

surface and the gas/liquid phase molecules³⁸. I used ambient pressure XPS, which allowed me to measure surface chemical processes in real time. The resulting data on the ALD of the HfO₂ on the clean and oxidised Si(111) surface are discussed in the ALD section and in papers VI. In addition, paper V reports an ambient pressure XPS gas phase analysis of the precursor molecule that I used for the ALD study. The ambient pressure XPS data are combined with density functional theory (DFT) calculations (cf. chapter 2.4) to obtain a better understanding.

1.3. This Thesis: Organisation of the Work

My PhD project is summarised in the chart in Figure 1.8. The three approaches for the heterogenisation of a homogeneous catalyst are divided into two main categories: covalent and noncovalent immobilisation. Immobilisation using covalent bonds is further divided into an approach using an organic matrix and one using an inorganic matrix. The noncovalent bond immobilisation only comprised immobilisation on rGO. In the green boxes of the chart a future outlook of my PhD work is also presented. This outlook is discussed in more detail in Chapter 6.

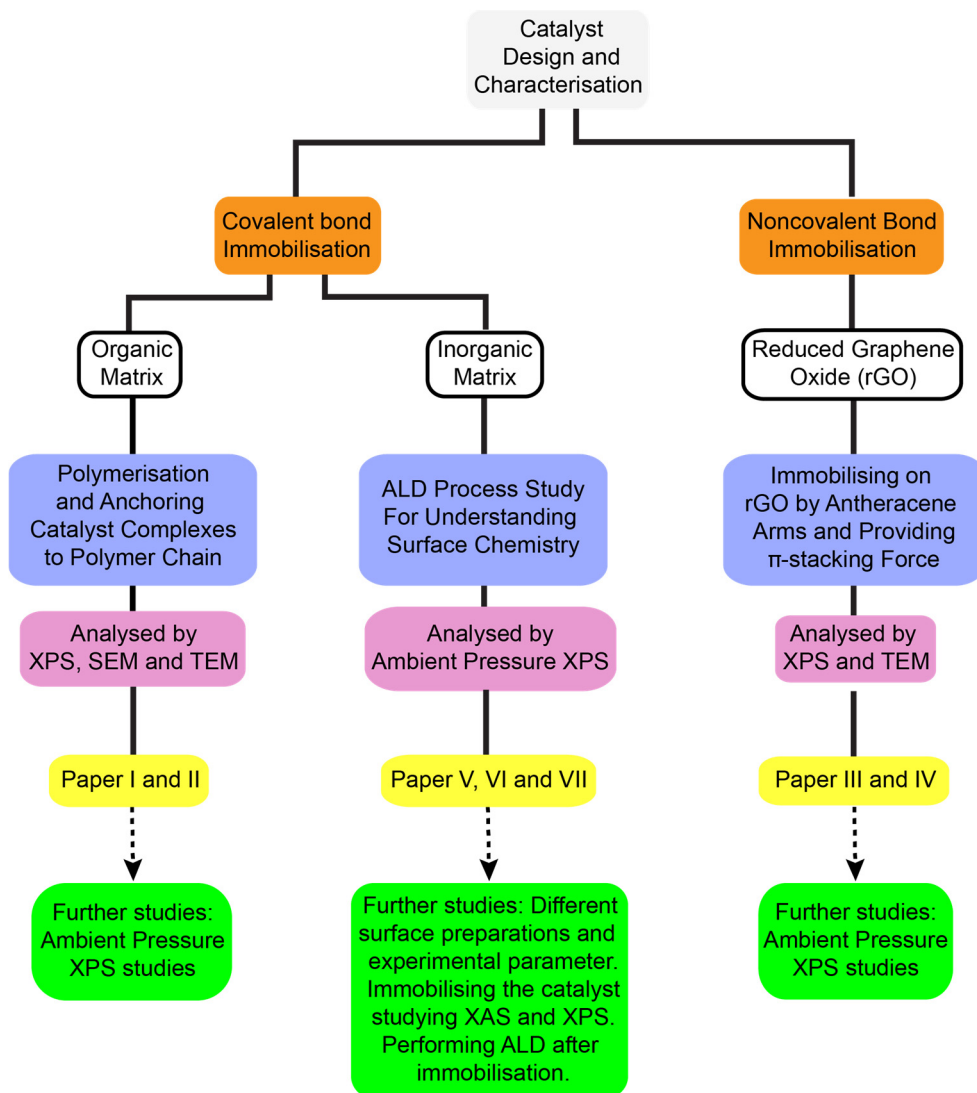


Figure 1.8. Schematic of the work this thesis has conducted and summary of outlook.

2. Analysis Techniques

2.1. X-ray Photoelectron Spectroscopy

2.1.1. Principle and Theory

XPS technique is a powerful technique for studying the electronic properties of a material. In particular, it is very useful for investigating the chemistry at a material's surface and near-surface region and for monitoring chemical phenomena occurring at the surface³⁹. The XPS technique is based on the photoelectric effect, which was discovered by Heinrich Hertz in 1887. Einstein was awarded the Nobel Prize for explaining the basic law of photoelectric effect theoretically in 1921. Kai Siegbahn was awarded the Nobel Prize in Physics for developing the electron spectroscopy for chemical analysis (ESCA) method in 1981⁴⁰. Today, ESCA is normally referred to as XPS, and it has become a technique that plays an important role in many scientific fields. XPS as a technique has some features that make it a reliable technique for organic and inorganic material analysis^{41,42}:

- 1) this technique is non-destructive for most compounds,
- 2) all elements in the periodic table can be measured using XPSⁱⁱ,
- 3) the depth sensitivity can vary within certain limits,
- 4) the method is sensitive to minute amounts in the range of a fraction of a monolayer,
- 5) the theoretical background of the technique is well understood.

XPS is based on the interaction of X-ray photons with atoms, molecules or solids and subsequent emission of electrons that originate from either a core or valence level, i.e. in short XPS is a “photon in, electron out” method. Measurement of the emitted electrons' kinetic energy provides information on the occupied electronic states of the sample.

ⁱⁱ For hydrogen the gas phase spectrum can be measured. See reference 42.

One important characteristic of XPS is its surface sensitivity. The surface sensitivity of this technique derives from the very limited distance that an electron with a kinetic energy of up to some hundred eVs can travel within a solid without being scattered inelastically. The characteristic average travel distance, assuming an exponential decay law, is called the electron inelastic mean free path (IMFP). In solid samples the IMFP depends mostly on the kinetic energy of the electron travelling through solid rather than the nature of the material. The shortest IMFPs occur for electrons within the kinetic energy range of 20-100 eV. Then the IMFP is about 2-5 Å, which corresponds to the maximum surface sensitivity. Figure 2.1 illustrates this phenomenon by providing the IMFP as a function of kinetic energy⁴³. This curve is often called the *universal curve of surface science*. The electron IMFP has to be distinguished clearly from the penetration depth of X-rays, which for soft X-rays is in the range of microns, i.e. the escape depth of electrons in solid materials is much smaller than that of X-rays. Hence, the surface sensitivity of XPS technique arises from the large probability of inelastic scattering of the photoelectron⁴⁴.

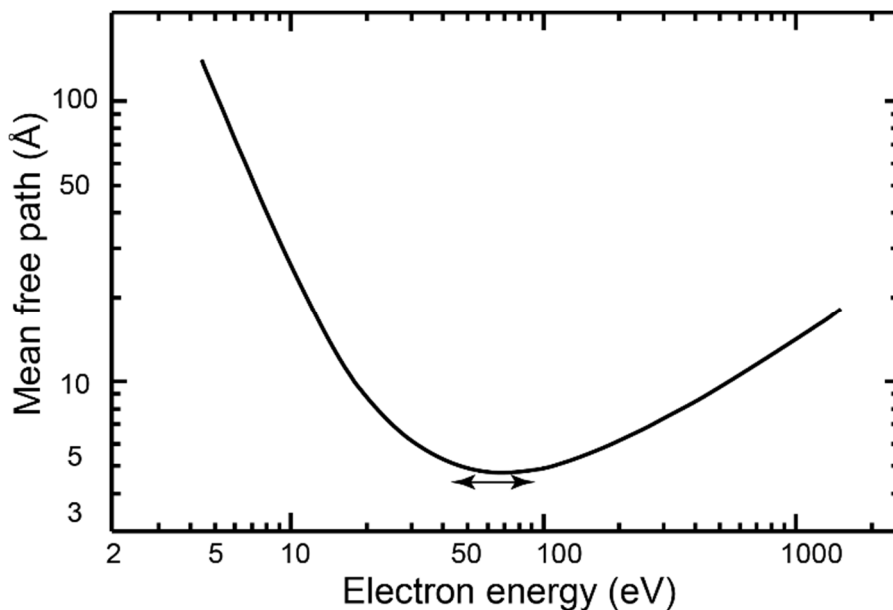


Figure 2.1. The *universal curve of surface science*: the electron IMFP as a function of kinetic energy. The minimum of the escape depth is 2-5 Å and is found at a kinetic energy of around 50-100 eV. This figure has been redrawn from references 48 and 49.

Process description:

In order to describe the XPS process two models are commonly used: the one-step and the three-step model. The three-step model is more intuitive. Here the photoelectric process is divided into three steps⁴⁵⁻⁴⁷ (cf. Figure 2.2):

- 1) photoelectron excitation,
- 2) photoelectron travel to the surface,
- 3) escape of the photoelectron through the surface into vacuum.

Figure 2.3 provides a simple photoelectric scheme for an atom. In this diagram, which depicts the electronic orbitals, only the first step of the three-step model is considered. The X-ray light with energy $h\nu$ interacts with the atom, which leads excitation of an electron from a core level and to emission of a photoelectron with kinetic energy E_k . This energy is measured in the electron energy analyser (cf. section 2.1.3). From energy conservation it is clear that the binding energy – or rather ionisation potential – of the electron E_b is $E_b = h\nu - E_k$. For metallic samples, another parameter adds to the equation since E_b here by convention is referenced to the Fermi level. This is the work function of the sample, i.e. the difference between the Fermi and vacuum levels. Hence, for metallic samples the equation can be written as⁴² $E_b = h\nu - E_k - \phi_s$.

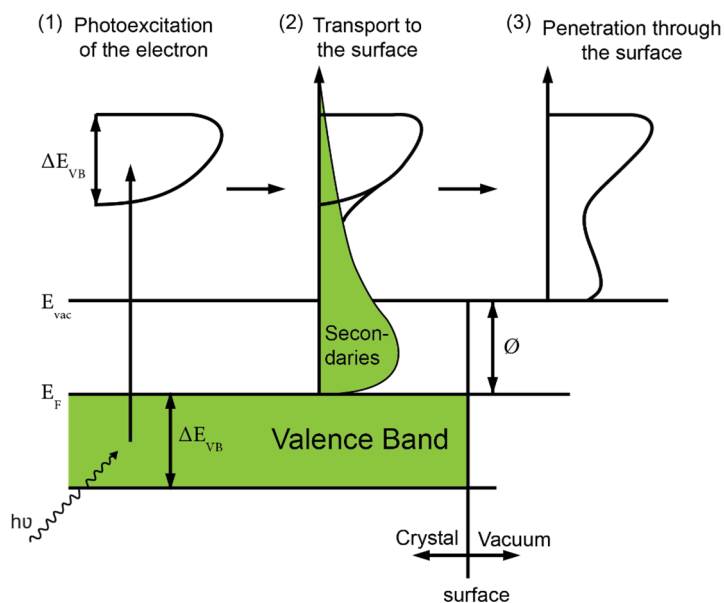


Figure 2.2.

Schematic illustration of the XPS three-step model. (1) Photoexcitation of electron. (2) Photoelectron travel to the surface together with production of secondary electrons (green area). (3) Penetration through the surface and escape into vacuum. Figure is redrawn from reference 42.

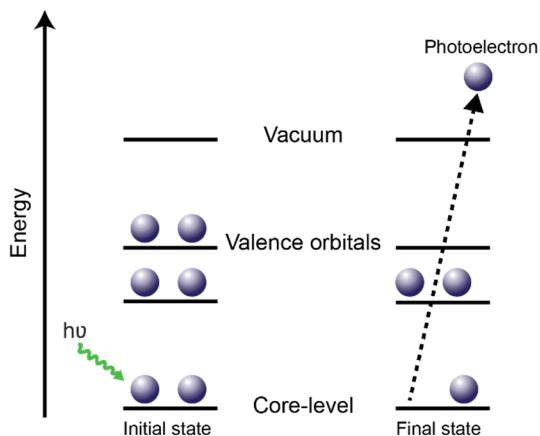


Figure 2.3.

Schematic illustration of core level photoemission. An X-ray photon with energy $h\nu$ interacts with a core level electron, and a photoelectron is emitted from the atom.

In order to calculate E_b , both $h\nu$ and ϕ_{sample} need to be calibrated. A schematic energy level diagram for a conductive sample is shown in Figure 2.4. In metallic samples, due to the electrical contact between the sample and the analyser, the Fermi levels are aligned. Therefore, the equation $E_b = h\nu - E_k - \phi_{\text{sample}}$ can also be written as $E_b = h\nu - E'_k - \phi_{\text{analyser}}$, and it stands clear that the measured kinetic energy is not that of the photoelectron just outside the sample, but it is that inside the analyser. Knowledge of the analyser work function thus provides the binding energy with respect to the Fermi level. For laboratory XPS machines a correct energy calibration is achieved easily since the energy of the photons provided by the anode source is exactly known. This allows proper calibration of the analyser work function by measurement of the Fermi level of a metallic reference sample. The calibration has to be redone once in a while.

For a synchrotron light source the measurement of the Fermi level has to be redone much more frequently – essentially for each spectrum. This is because the photon energy is not exactly known (although it can be measured, but this is time-consuming) and since the photon energy changes with slight changes in the position of the electron beam inside the storage ring. For slightly insulating samples it is often enough to measure the Fermi level on a metal in good electrical contact with the sample.

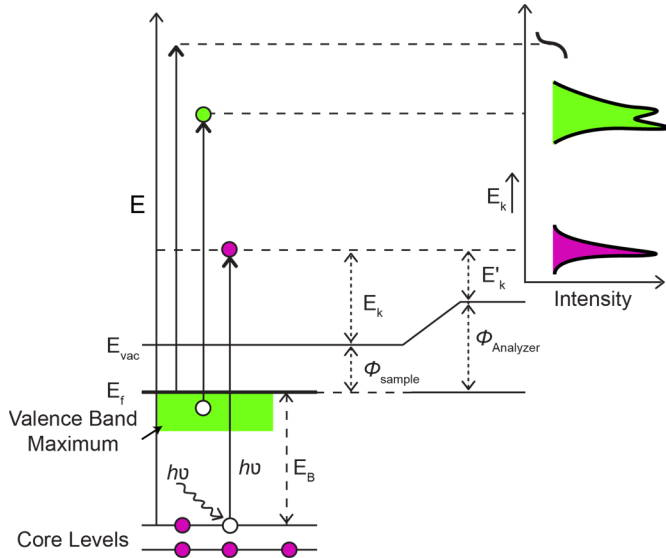


Figure 2.4.

Energy level diagram for a metal sample. The sample is in electrical contact with the analyser. Therefore, the Fermi levels E_f are aligned. Interaction of a photon with energy $h\nu$ with the atom leads to emission of a photoelectron with a kinetic energy above the vacuum level E_{vac} . Both the localised core level electrons and the delocalised valence electrons can be measured.

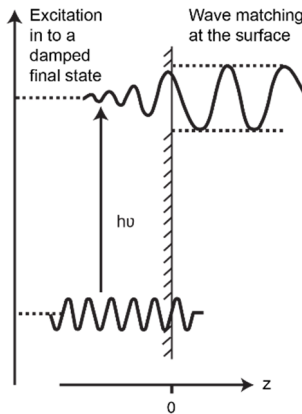


Figure 2.5.

Illustration of the one-step model of photoemission. In the one-step model, a Bloch wave electron is excited into a wave that propagates freely in vacuum. This wave decays away from the surface into the solid Figure is redrawn from reference 42.

In the three-step model there are several simplifying assumptions that ignore some phenomena happening in the photoelectron creation process. This model neglects the bulk and surface emission interference, interaction of the photoelectron with other atoms during the transport step and the surface and finally applying a simple

transition factor for escape of the electron. However, the photoemission process is described more accurately by the one-step model illustrated in Figure 2.5. In this model, the excitation from an initial state, a Bloch wave in the crystal, is to a final state, which outside the crystal propagates freely while it is dampened from the surface into the solid's bulk. Within the one-step model of photoemission, Fermi's golden rule describes the transition probability W_{fi} between the initial and final state:

$$W_{fi} = \frac{2\pi}{\hbar} |\langle f | -e\vec{r} | i \rangle|^2 \delta(E_f - E_i - h\nu), \quad \text{Eq. 2.1}$$

where $\langle f | -e\vec{r} | i \rangle$ is the transition matrix element between the initial and final states, $-e\vec{r}$ is the dipole operator that describes the electromagnetic wave in the electric dipole approximation, δ is the delta function, E_f and E_i are the final and initial states energies of the system, respectively, and $h\nu$ is the photon energy.

From equation 2.1 it is obvious that a description of the non-orthogonal initial and final states $|i\rangle$ and $|f\rangle$ in the matrix element is required for a derivation of W_{fi} . Typically one applies the Hartree-Fock method, i.e one considers multi-electron states that are built up from one-electron orbitals. The approximation implies that the initial state single-electron orbital of the electron that is photoemitted can be singled out and be separated from the orbitals of the remaining $N-1$ electrons. The transition matrix element can then be written as a product of the dipole operator matrix element between the one-electron orbital of the electron to be emitted and a free-electron wave function times the $N-1$ -electron overlap integral:

$$M_{fi} = \langle \Psi_f | r | \Psi_i \rangle = \langle \phi_{f,E_k} | r | \phi_{i,k} \rangle \langle \Psi_{f,R}^k(N-1) | \Psi_{i,R}^k(N-1) \rangle, \quad \text{Eq. 2.2}$$

In order to calculate (or understand) the binding energy measured in XPS it is necessary to make some approximations. One approximation is the *frozen-orbital approximation*, in which the single-electron orbitals of the $N-1$ electrons left in the atom after photoemission are considered to be the same as in the initial state. This means that the $N-1$ -electron overlap integral is unity and only the single-electron matrix element (the first element on the right-hand side in equation 2.2) remains. In this approximation XPS measures the negative Hartree-Fock orbital energy, also known as Koopmans' binding energy. The approximation is, however, inaccurate because the removal of one electron will force the remaining electrons and hence the orbitals in the atom to rearrange themselves in order to minimise the total energy. This reaction is called *relaxation*.

In the *sudden approximation* the photoemission process occurs much faster than the time requires for valence electrons readjustment. Therefore, a response of the valence electrons to the change in core potential due to the creation of the photohole is not possible. In this approximation multiple final states with the same core hole

are allowed, since the Hamiltonian in the final state has changed. The final state wave function for the (N-1) electrons is not an eigenstate of the initial state Hamiltonian. In this approximation the negative of Koopman's energy is equal to the first moment of the total intensity⁵⁰.

2.1.2. Core Level Shifts

The core level binding energies measured in XPS depend on the chemical environment of the photoemitting atom. The difference between the binding energies observed for an atom of the same element in different environments is known as core level shift. One particular core level shift, related to a particular geometrical configuration, is the surface core level shift: there is a difference between the binding energy of the electrons in surface and bulk atoms. To illustrate the surface core level shift Figure 2.6 shows the Ir $4f_{7/2}$ XP spectrum of a clean Ir(100) surface. Curve fitting shows that there are two different peaks at 60.08 and 60.85 eV binding energy, which are related to the bulk (Ir_B) and surface (Ir_S) atoms, respectively⁵¹.

Another type of core-level shift is illustrated in Figure 2.7, namely a core-level shift due to different oxidation states. The spectrum represents a Si 2p core level and was measured on a native oxide-covered Si(100) surface. It is seen that the spectrum contains a number of different components. The Si^0 bulk peak at 99.3 eV is, as expected and like all other components, a doublet due to spin-orbit splitting. In addition to the Si^0 bulk peak one sees four other doublets related to the Si^+ , Si^{2+} , Si^{3+} and Si^{4+} oxidation states. Between these components a shift of ~ 0.9 eV toward higher binding energy is found⁵².

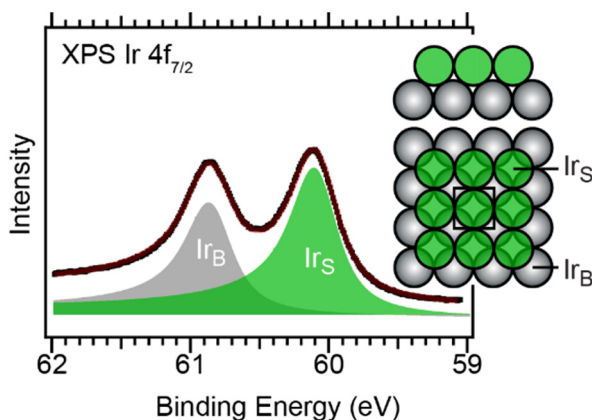


Figure 2.6. Ir $4f_{7/2}$ XP spectrum of an Ir(100) single crystal. Ir_B and Ir_S are the bulk and surface components. The image is modified from reference 51.

It can be mentioned that I frequently used the Si 2p bulk peak to calibrate XP spectra of other core levels such as the N 1s, Cl 2p and Pd 4f levels. In order to calibrate the Si 2p bulk peak of Si(100) itself, I typically used an Au 4f peak on an Au foil which was in good electrical contact with the Si sample. For applying fit I used IGOR PRO software and I used Gaussian line shape for fitting spectra in my thesis. Yet another example of a core-level shift, namely that due to different bonding partners, is found in the Cl 2p XP spectra on the samples studied in paper I (cf. Figure 2.8 for their

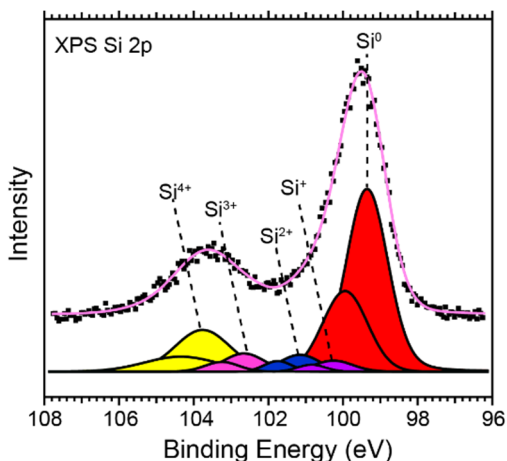


Figure 2.7. Si 2p XP spectrum of native oxide-covered Si(100). The Si surface was e.g. used for supporting MIP particles in UHV XPS experiments.

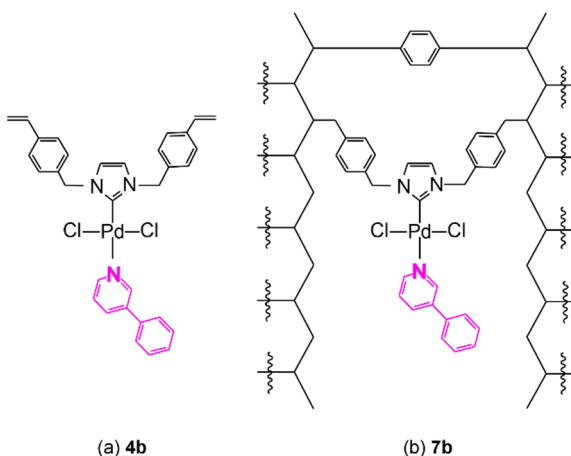


Figure 2.8. (a) Catalytic transition metal complex of catalyst complex (compound **4b** in the paper I) and (b) Polymerized catalytic transition metal complex (compound **7b** in paper I). Figure is redrawn from references 1 and 5.

structures). The XPS results in the same figure are for a catalytic transition metal complex, labelled **4b**, sample **4b** after polymerisation (**7b**) and sample **7b** after being used for four cycles in acetoxylation reaction of biphenyl (cf. chapter 4.2).

The Cl 2p XP spectra of these compounds are presented in Figure 2.9. In the spectrum of sample **4b** one can see the Cl 2p_{3/2} and Cl 2p_{1/2} components at 199.8 and 201.4 eV, respectively. Only a single doublet is observed and, hence, only one type of Cl species in agreement with the structure of **4b** in Figure 2.8. Copolymerisation to form **7b** and thus embedding **4b** in a polymer matrix leads to the appearance of a new species with a characteristic lower binding energy. Even the original doublet is retained. The difference in binding energy between the two species is related to a difference in chemical environment. Sample **7b** was then used as catalyst in acetoxylation of biphenyl. After each cycle a new XP spectrum was measured. Already after the first catalytic cycle a new doublet appears at higher binding energies: 201.9 and 203.5 eV. A Cl 2p components with such a high binding energy can be related to C-Cl bonds^{53,54}. It is noted that a doublet at even high binding energy, 204.5 and 206.1 eV, had to be added in order to reach a proper fit. Literature does not provide any assignment for such a high binding-energy Cl 2p peak¹.

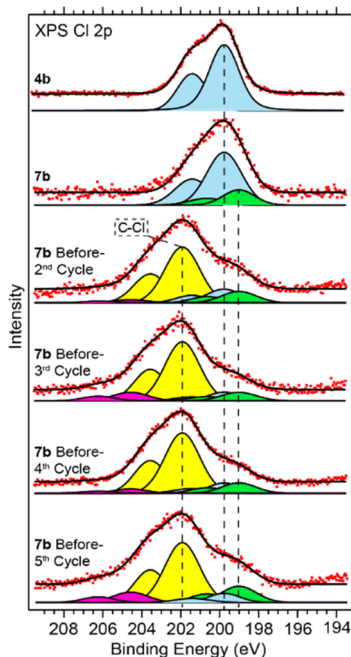


Figure 2.9.

Cl 2p core level analysis in catalytic transition metal complex, polymerised catalyst and polymerised catalyst after four cycles in the reaction condition. The figure is adapted from reference 1.

2.1.3. XPS Instrumentation

X-ray light sources used for XPS comprise synchrotron radiation sources, lasers and anode sources. Among the anode sources the most prominent ones are based on Mg and Al: they make use of the Mg K_{α} (1253.6 eV) and Al K_{α} (1486.6 eV) emission lines. In the work presented in this thesis XPS measurements were performed using Al K_{α} and synchrotron radiation at the SPECIES^{55,56} and HIPPIE beamlines of the MAX IV Laboratory in Lund. In addition, I used synchrotron radiation at the TEMPO beamline⁵⁷ of the SOLEIL synchrotron in St-Aubin, France.

In an X-ray anode, a high voltage between an anode and a hot cathode accelerates the electrons emitted by the cathode towards the anode, leading to inner-shell ionisation. Outer-shell electrons fill the created holes and X-rays are emitted. The X-ray energy is characteristic for the material. Anode sources are simple, cheap, and easy to operate and small, but one is limited to one photon energy and a limited flux. As an example, the photon flux at the HIPPIE beamline at MAX IV is $>10^{12}$ photons s^{-1} , while for an anode source it is around⁵⁸ 10^6 photons s^{-1} . Thus, often synchrotron radiation is often preferable, but it is also clear that a synchrotron radiation source is a much larger and much more costly facility. Beamtime at a synchrotron radiation source is also limited, and it can be difficult to obtain beamtime.

In order to create synchrotron radiation, electrons are accelerated to almost the speed of light. A synchrotron radiation source is typically made of four different parts: an electron gun, linear accelerators, an electron storage ring and beamlines. In the straight sections of modern electron storage rings, insertion devices are put into place: wigglers and undulators. Wigglers and undulators are arrays of periodically alternating polarity. The magnetic field provided by the magnets is perpendicular to the electrons trajectory and causes a sinusoidal variation of the electron path. The electrons are thus radially accelerated and emit light. The X-ray energy depends on the magnetic field strength; adjusting the gap between the two magnet arrays in a wiggler or undulator thus tunes the energy of the radiation. The X-ray produced in the storage ring will be guided toward the experimental station through the "beamline". In a beamline several components are found, and most important are the monochromator containing a dispersive element, focusing and collimating mirrors, adjustable slits and baffles. Synchrotron radiation delivers a very high flux of photons, which makes the data acquisition time shorter and allows much higher resolution than what is possible with X-ray anodes. Another advantage is that the photon energy is tuneable, and thus it can be tuned to reach the maximum subshell photoionisation cross section. One can also tune the photon energy to achieve high surface or high bulk sensitivity⁴².

In order to measure the kinetic energy of an electron, an electron energy analyser is employed (cf. Figure 2.10). Nowadays, the predominant type of electron energy analyser is the hemispherical electrostatic type. Such a hemispherical analyser is composed of an electrostatic lens system and a hemispherical electrostatic band pass filter. The electrostatic lens system focuses the electrons onto the entrance slit of the hemispherical section and retards (some analysers can also accelerate) the electrons. Only electrons that after passing through the electrostatic lens system are within the right energy interval $E_{pass} \pm \Delta E$ pass the hemisphere. E_{pass} is called the pass energy. To allow this behaviour, the hemispherical analyser is kept at a constant potential difference (ΔV) between its inner and outer hemispheres. This ΔV sets E_{pass} . The potential difference selects electrons with a desired kinetic energy, while electrons with lower or higher kinetic energy than $E_{pass} \pm \Delta E$ hit the inner or outer hemisphere, respectively. In order to detect the electrons that pass through the analyser a combination of microchannel plate (MCP) detector, phosphorous screen and charge-coupled device (CCD) camera are employed.

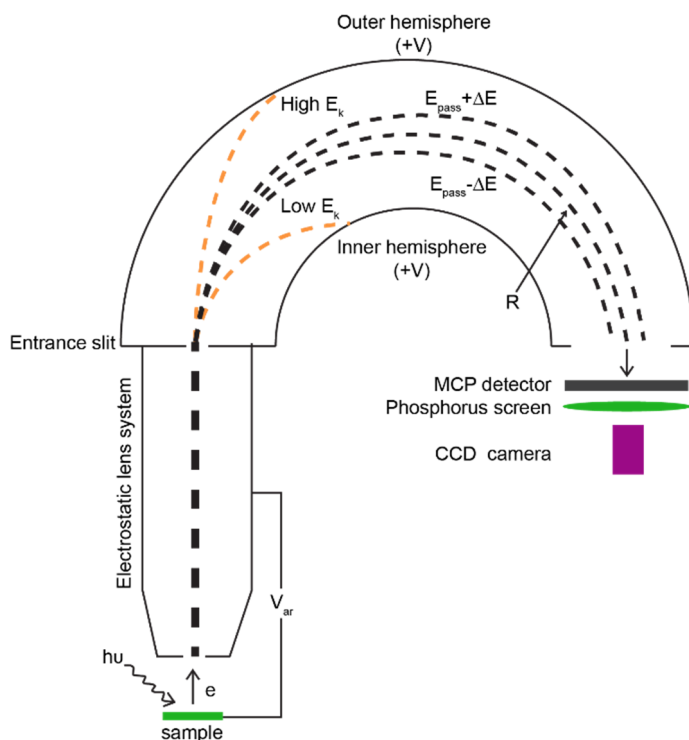


Figure 2.10.
Schematic illustration of a hemispherical electron energy analyser.

2.2. Ambient Pressure X-ray Photoelectron Spectroscopy

XPS instruments typically work under high vacuum or ultrahigh vacuum (UHV) conditions, i.e. in the pressure range between 10^{-11} and 10^{-6} mbar. UHV, i.e. 10^{-11} to 10^{-10} mbar, is appropriate for samples that must be kept atomically clean before and during the experiment; this is the normal range for standard surface science experiments. In addition, a controlled environment permits the measurement of the interaction of a solid surface with a gas/vapour pressure in the 10^{-6} mbar regime. However, in real life, or in industrial and similar applications, interface chemical reactions at the solid-gas, liquid-gas and solid-liquid interfaces occur at higher pressure than UHV. Relevant information on the surface state and reaction mechanism are required for surfaces under realistic conditions. It is, however, impossible, to use conventional XPS instrumentation in studies using such realistic conditions due to the strong inelastic scattering of electrons in the gas or vapour.

One consideration that one has to bear in mind when going from UHV to more realistic pressure conditions is, thus, the electron IMFP in a gas⁵⁹. An increase in pressure will decrease the IMFP. As an example, at a pressure of 1 mbar of water the IMFP for electrons with 100 eV kinetic energy is around one millimetre⁶⁰, and, thus, the travel distance that the electrons approximately can travel through a gas or vapour with acceptable attenuation is of the same order of magnitude. This means that the instrumentation design requires an aperture (or “nozzle”) close to the sample and a differential pumping stage in the analyser in order to reduce the distance that the electrons have to travel through the gas or vapour to a suitable value (see below) and thus make the measurement feasible.

Figure 2.11 provides a layout of the ambient pressure XPS instrument used at the TEMPO beamline at the SOLEIL synchrotron⁶¹. The ambient pressure XPS instrument at TEMPO has a front aperture with a diameter of 0.3 mm. This aperture separates the SPECS Phoibos 150-NAP hemispherical analyser from the ambient pressure environment in the analysis chamber. Four differential pumping stages reduce the pressure from 5×10^{-4} mbar in the analysis chamber to below 5×10^{-8} mbar at the electron detector, i.e. there is a pressure drop of four orders of magnitude. The differential pumping stage is combined with an electrostatic lens system. It focuses the electrons first onto an aperture of 2 mm size between the “prelens” pumping stage and the second pumping stage, then onto an iris aperture between the second and third pumping stage and finally on the analyser entrance slit⁵⁵.

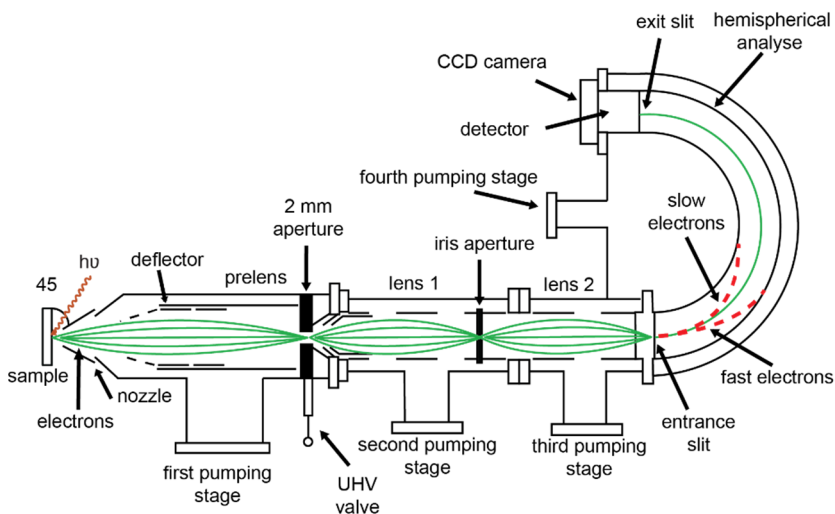


Figure 2.11. Schematic drawing of the hemispherical electron energy analyser with separate differential pumping stage of the ambient pressure XPS instrument at the TEMPO beamline. The figure is redrawn from reference 49.

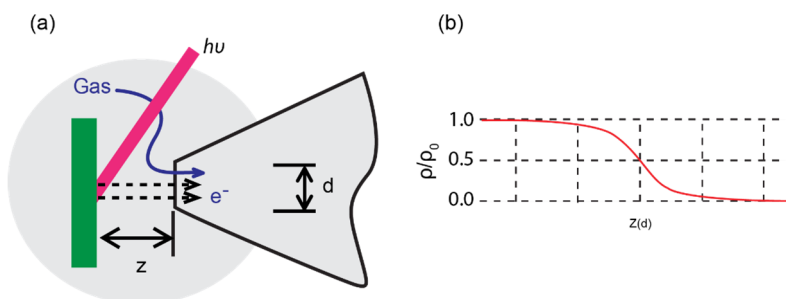


Figure 2.12. (a) Sample-nozzle region demonstration in ambient pressure XPS setup. Sample surface and the gas phase are irradiated. The gas phase irradiation can lead to a gas phase peak at XP spectra. (b) Pressure distribution along the optical axis as a function of distance z from the nozzle plane in units of background pressure p_0 . At the distance d (d is aperture diameter) the pressure at the sample surface is $0.95p_0$. Increasing the distance to $2d$ causes an increase in pressure at the sample surface up to $0.98p_0$. The pressure at the nozzle plane is $0.5p_0$. Picture is redrawn from reference 62.

The question what the distance between the sample and first aperture should be justifies some more discussion. Figure 2.12 shows a schematic picture of the sample-first aperture arrangement and the calculated pressure along the optical axis of the lens system⁶². It is seen that the distance should be approximately one aperture diameter, if the pressure at the sample surface should be retained at around 95% of the measured pressure. Bluhm *et al.* suggested the distance of two aperture diameter in order to have 98% of the measured pressure on the sample surface. On the other

hand other studies also suggest that one to two aperture diameter distance between sample surface and the nozzle can be used for measurements⁶²⁻⁶⁴.

By employing a differential pumping stage reaching pressures up to 130 mbar during reaction was possible^{65,66}. Another consideration in doing ambient pressure XPS measurements is the aperture size, which should be small in order to lower the pressure in the analyser and differential pumping stage. The effect of the aperture size is discussed by Ogletree *et al.*⁶⁷. A small aperture size decreases the effective sample area and the solid angle contribution to XPS signal. Using smaller aperture on the other hand thus also requires a smaller spot size of the incoming X-rays⁶⁷.

Performing ambient pressure experiments means inserting vapour or gas into the experimental chamber. This simple act of dosing gas into the chamber will make the chamber dirty from the surface-science point of view. Reactions in ambient pressure conditions will thus cause an increase in the base pressure inside the reaction cell. This is due to the residual starting materials or byproducts. These materials are sometimes hard to remove from the surface in the chamber, and it may be difficult to achieve a clean environment in the reaction cell. Therefore, different designs have been introduced in order to make it easier to clean the reaction cells and avoid cross contamination between different reactions and experiments. In Figure 2.13 three different designs are schematically shown. Figure 2.13a shows a case in which the vacuum chamber is filled with gas to the desired pressure. In Figure 2.13b the ambient pressure cell is combined with the UHV chamber such that it can be exchanged and removed from the analyser chamber. In this case the instrument does not have any UHV chamber for XPS experiments. This design helps to avoid cross-contamination between different experiments. The third design, Figure 2.13c, is similar to the design in Figure 2.13b. However, in the cell-in-cell design there is a UHV chamber surrounding the ambient pressure cell during the experiment. This design will help to avoid cross contamination between ambient pressure and UHV environments. In addition, this configuration allows the design of cells with minimal volume and wall area^{60,61,68}.

For the ALD experiments I used the TEMPO beamline⁶⁹ at the SOLEIL synchrotron, which provides a setup with the configuration of Figure 2.13a. The chamber can also be used for UHV experiments. The HIPPIE and SPECIES beamlines at MAX IV laboratory provide the cell-in-cell concept for ambient pressure experiments^{56,61}.

Today, there are around 15 ambient pressure XPS instruments at synchrotrons around the world^{61,68,70}. There are still efforts for improving the ambient pressure XPS technique including accessing higher pressure even up to atmospheric or higher pressures, involving liquid to study homogenous systems and solid-liquid or liquid-gas interface and achieving higher time resolution⁷⁰.

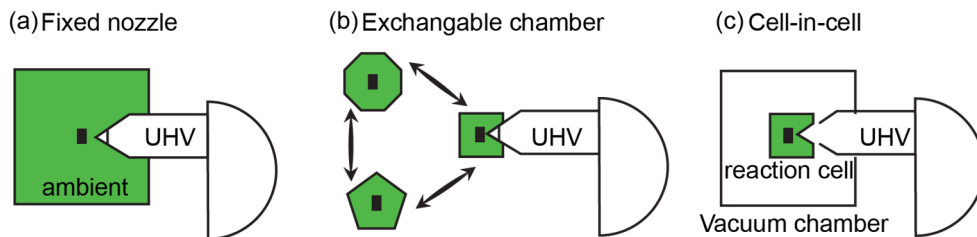


Figure 2.13.

Different configuration for designing ambient pressure XPS cell. (a) Setup in which the vacuum chamber is backfilled with the gas or vapour. (b) Setup without a UHV chamber. This setup is good for liquid jet experiments due to possibility of installing big setups. (c) A detachable an exchangeable ambient pressure cell inside a UHV chamber. Ambient pressure cell can retract into vacuum cell and this provides possibility of UHV experiments. Figures are redrawn from references 61 and 68.

2.3. Microscopy Techniques

Surface analysis can gain a lot from detailed images of the surfaces' structure. For example in catalysis, scientists would like to relate the overall surface morphology as well as its structural details, in particular in terms of the structure of the catalytic sites, to the catalytic reaction mechanism. Here, imaging may give very important input on how to improve the surface properties for better catalysis. Microscopy techniques provide images of surface and are thus often the tools of choice in surface analysis. However, optical microscopes are not useful to detect small objects since the wavelength of the light is too long to resolve any details below approximately 400 nm. Electron microscopy comprises a range of experimental tool that fill this gap. In electron microscopy, electrons with shorter wavelength are used by increasing the power of the electron beam used for analysis. Typically, smaller objects in the size range down to approximately 0.1 nm can be detected. For example, imaging of surface reactions sites helps to understand the interaction of a gas or liquid molecule with the surface. Electron microscopy can make use of a variety of effects that can be used for imaging as is illustrated in Figure 2.14. Each of these interactions can be detected and analysed in order to understand the sample geometry and chemistry⁷¹. Many different electron microscopes are available today and can be used depending on the type of necessary analysis and the sample. A few examples of microscopy techniques are: SEM, TEM, scanning tunnelling microscopy, photoemission electron microscopy (PEEM), low energy electron diffraction (LEED). Among all these available microscopy techniques I used SEM and TEM in my thesis work.

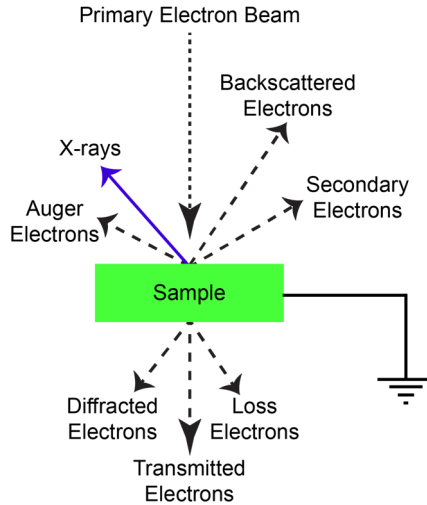


Figure 2.14. Interaction events between the primary electron beam and sample in an electron microscope. Figure is redrawn from reference 71.

2.3.1. Scanning Electron Microscopy

In SEM, the surface is scanned using an electron beam. This technique can be applied to a wide range of materials, including both conductive and insulating materials. In case a sample is not conductive, a metal coating can provide a sufficient conductivity to avoid charge accumulation on the surface. The images provided by this technique represent primarily the sample topography, but also other information can be gained.

In SEM thermionic emission creates the “primary electron beam”. The signal is analysed in a backscattering geometry, and this signal includes secondary electrons, back-scattered electrons, Auger electrons, characteristic X-rays and bremsstrahlung, cf. Figure 2.15. As the figure illustrates, the signals originate from different depths of the sample, and for low-Z elements the interaction volume has a characteristic pear shape. Thus, depending on the combination of detectors one can obtain quite different information on sample topography, morphology and sample composition with 1 nm spatial resolution. Image formation in SEM is done by scanning a focused electron beam across several lines and construct a pixel-by-pixel image and according to the scanned position⁷². In SEM resolutions down to ~0.4 nm at 30 kV acceleration voltage can be achieved⁷³.

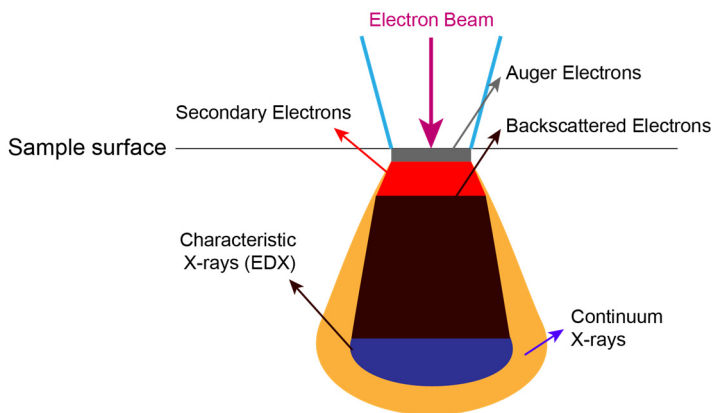


Figure 2.15.

“Pear” effect in SEM analysis. Electrons interact with the sample and create different signals that can be detected for different analysis purposes. This graph is modified from reference 72.

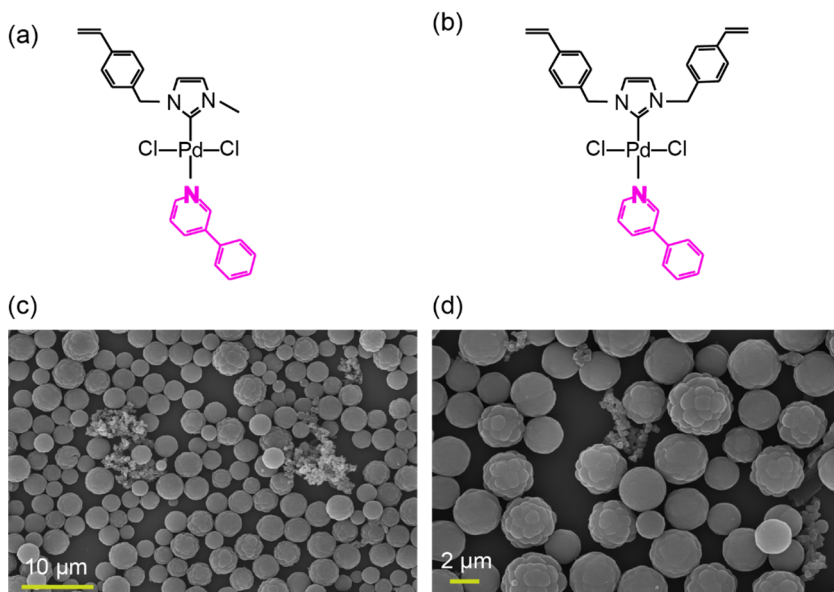


Figure 2.16.

(a), (b) Schematic illustration of catalytic transition metal complexes. (c), (d) SEM images of polymers containing the complexes in (a) and (b). The figure is redrawn from references 1 and 5.

In my thesis I have primarily used the detection of backscattered electrons for topographical analysis⁷⁴ and the detection of characteristic X-rays in energy-dispersive X-ray spectroscopy (EDX), which provides chemical information on the studied surface⁷⁵. Thus, I used high-resolution SEM (papers I and II) analysis to image heterogenised catalytic transition metal complexes particles after

polymerisation. Figure 2.16a and b show two catalytic transition metal complexes, and Figure 2.16c and d are SEM images of these catalytic transition metal complexes after polymerization. As can be seen in the Figure 2.16c and d, the size distribution of the catalytic polymer samples varies greatly. A dominant particle size can, however, be identified; it is around 4 μm .

2.3.2. Transmission Electron Microscopy

TEM is an important high-resolution microscopy technique for the analysis of nanostructures and nanostructured materials. In TEM the image is produced by transmitting electrons through a thin sample. Information about the particle size, morphology of particles, crystalline structure and chemical composition of the sample can be obtained. TEM has a number advantages such as: high spatial resolution below one nm, powerful magnification potentially over one million times, wide range of applications for analysing different samples in biology and material science, the ability to provide insight of surface features, their shape, size and structures and easy operation after proper training. TEM has some disadvantages such as: TEM is an expensive instrument, sample preparation is laborious work, the TEM instrument needs to be hosted in a vibration-isolated building free from strong magnetic fields, samples must be electron transparent and able to tolerate vacuum chamber, they must be small enough to fit in the chamber and finally sample preparation may add artefacts to the sample⁷⁶.

Two different modes are employed: the TEM and scanning TEM (STEM) modes. The difference between both modes is that in STEM mode, in contrast to standard mode, a focused beam (spot size 0.2 nm in diameter at 200 kV acceleration voltage⁷⁷) is scanned across the sample. The advantages of STEM over standard TEM are the possibility of collecting both bright and dark field images simultaneously for inhomogeneous samples, that the alignment of the detector is very easy and quick, that the electron beam can be stopped on any desired point on the sample and that diffraction or spectroscopy can be performed at that point with atomic or nanometre-scale spatial resolution⁷⁸.

As in SEM, different signals are produced by the electron-matter interaction and can be used for different types of analysis. Images produced by TEM are real images formed on the screen. The electrons accelerate toward the sample and go through the sample to hit to a screen and convert to light where they can make an image. The brighter areas of the image represent areas where more electrons were able to pass through the sample and the darker areas represent the dense areas of the sample. These differences in contrast provide information on the structure, texture, shape and size of the sample. The spatial resolution of TEM is $\sim 0.5 \text{ \AA}$ at 300 kV of electron acceleration energy⁷⁹. In addition to the standard imaging mode

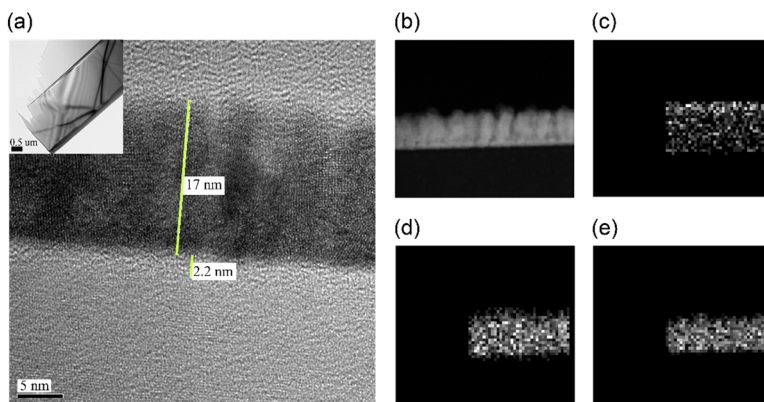


Figure 2.17.

(a) TEM image of the cross section of the laminate from the oxidised $\text{SiO}_2/\text{Si}(111)$ surface after three cycles of deposition of HfO_2 from TDMAHf and water in UHV XPS chamber. (b) Dark field image of the sample. (c), (d) and (e) Are EDX signals related to C, O and Hf, respectively.

of TEM, one of the standard tools is EDX for chemical analysis of the sample. Both TEM imaging and EDX have been used in my thesis.

Figure 2.17 shows measurements of the *in situ*-oxidised $\text{SiO}_2/\text{Si}(111)$ interface after depositing HfO_2 in a three-cycle ALD process. Figure 2.17a shows a cross-section TEM image obtained on a lamella of the surface prepared using a focused ion beam (FIB)⁸⁰, (b) dark field image of the sample and (c-e) EDX analysis of the same portion of the surface. In the HfO_2 deposition region C, O and Hf are detected. Carbon is found at higher density at the top of that region; this is because a permanent marker was used to deposit a polymer-like material on top of the surface prior to preparation by FIB to protect it from getting damaged.

2.4. Density Functional Theory

DFT is a computational quantum mechanical method to study the ground state electronic structure of atoms, molecules and the condensed phase and is widely used in chemistry, physics and materials science. In the context of my thesis, DFT helped to understand the experimental results. The calculations were not carried out by myself, but by a colleague.

For the investigated samples DFT provides a precise quantitative description of the geometric structure and the chemical properties^{81,82}. DFT is built on two fundamental mathematical theorems proved by Kohn and Hohenberg and the derivation of a set of equations by Kohn and Sham. The first theorem, proved by Hohenberg and Kohn, is: “*The ground-state energy from Schrödinger’s equation is*

*a unique functional of the electron density*⁸³. A functional acts like a function, but while a function takes a number as the argument and returns a number as the outcome, a functional takes a function as the argument and provides a number. A second important theorem is also given by Hohenberg-Kohn: “*The electron density that minimises the energy of the overall functional is the true electron density corresponding to the full solution of the Schrödinger equation*”⁸³. This theorem provides the possibility to change the electron density functional until the energy reaches its absolute minimum. This energy density is then the true electron density.

The main advantage of using DFT instead of other electron-correlated wave function-based methods is the good price/performance ratio. In DFT one deals with the electron density as a fundamental quantity instead of dealing with the wave functions. Therefore, DFT requires less computing time than wave function-based methods, or, inversely, using DFT one can reach increased calculation accuracy or calculate larger systems without an increase in computing time. Large molecular systems can be investigated with good accuracy in a reasonable amount of time^{84,85}.

In this, the Kohn-Sham equations provide an important tool because they include the effects of electron correlation at a reduced computational cost. In Kohn-Sham DFT the model molecular orbitals are treated as mathematical objects and the electron density of the chemical system can then be constructed. Combining the density calculated using the Kohn-Sham equations with the theorems by Hohenberg and Kohn implies that chemical properties of interest can be calculated⁸⁶.

2.4.1. How Accurate is DFT?

With the help of improvements in computer performance DFT is more computationally effective. This helps to deal with more complicated and realistic systems and more accurate electronic structure can be predicted⁸⁴. DFT can accurately calculate structures, energies, binding energy shifts and vibrational frequencies of systems in electronically excited states^{87,88}. However functional does not always have a full picture model for the excited state and in this situation DFT can only calculate valence and Rydberg states in which there are no charge transfer excited states⁸⁸.

Nowadays, DFT calculations are often combined with experiments in order to predict the mechanisms of surface reactions and to test and describe the electronic structure of the samples in different configurations and chemical environments. I would like to use an example to exemplify the strength of a combination of DFT and experiment: In a recent study Head *et al.*⁸⁹ studied the adsorption and decomposition of dimethyl methylphosphonate on MoO₂ using APXPS and DFT calculations. In this study, the ambient pressure XPS measurements provide information on the presence of different species due to the reaction between

dimethyl methylphosphonate and the MoO₂ surface. This experimental results show the appearance of different species at the surface, but the observation provides only indirect information on the relevant reaction mechanisms. Here, DFT could help by identifying different decomposition reaction pathways that could be correlated to the XPS data. Binding energy shifts calculated differ from the experimental values. These differences can be due to that DFT was performed using a pristine MoO₂ model surface, while other surface properties, such as defects or facets, can contribute to the decomposition pathway of dimethyl methylphosphonate. This would introduce shifts in the binding energies that differ from the modelled ones⁸⁹. This study is an example that shows that DFT has a good accuracy and is capable of predicting mechanism of reactions. The accuracy of DFT in calculating binding energy shifts and its ability in predicting reaction mechanisms can improve the understanding of the experiment and decrease the number of necessary experiments^{87,89}.

2.4.2. DFT and Relation to Experiment

DFT can provide structures, energies and spectroscopic properties, and, hence, theory and experiment can complement each other in order to give a more complete understanding of the system. Detailed mechanistic questions can be addressed using the techniques of quantum computations. DFT has provided a route to the study of chemical processes which may be difficult to study experimentally⁸⁵.

The DFT calculations in my thesis were carried out by Dr. Roman Tsyshevskiy from the University of Maryland. In my experiments I deal with solid-gas interactions. Both the solid and the liquid phase were subject to DFT calculations and an elucidation of the geometric and electronic structure. DFT contributed in paper V to the investigation of the electronic structure of two ALD precursors, namely TDMAHf and tetrakis(dimethylamido)titanium (TDMAT). In paper VI the reaction mechanism of TDMAHf on an oxidised SiO₂/Si(111) surface is studied by a combination of DFT and *operando* APXPS. I analysed the ALD process using X-ray techniques to cast light on the surface chemical reactions. Understanding the chemistry of the surface can be more accurate and reliable by considering possible pathways for the precursor adsorption and decomposition on the surface. This is made possible by DFT. Overall, combining experiment and DFT can help to optimise ALD processes so that better final products can be achieved.

3. Atomic Layer Deposition

ALD is a technique for the growth of thin material layers with Ångström thickness precision, which is closely related to the method of chemical vapour deposition (CVD). While in CVD all precursor materials for the reaction flow at the same time and an energy source (high temperature or plasma) provides energy to help the reaction, in ALD the cyclic flow of typically two precursors is separated into two half cycles. The two half cycle are separated by an inert gas flow to purge the chamber and to separate two or more different reactions. ALD was introduced as atomic layer epitaxy by Suntola and Antson in 1977. Before that the concept had already been used in the 1960s by Aleskovskii and Koltsov^{36,49,90}. At that the technique was called “molecular layering”.

The ALD process relies on separate (typically two) self-limited gas-solid reactions. The self-limiting nature of the ideal ALD process avoids any contribution of the excess of precursor dose to film growth. Important properties of ALD are that the films produced using ALD have a high degree of uniformity and conformity and that ALD can be performed on any surface irrespective of substrate shape. Therefore, ALD has become a major thin-film growth method in many fields of materials technology, for example in semiconductor technology and other nanotechnology, catalysis, and solar photovoltaics⁹¹⁻⁹⁴. A wide range of materials can be deposited using ALD, such as oxides (SiO₂, TiO₂, HfO₂ etc.), nitrides (TiN, BN, Cu₃N etc.), chalcogenides (a compound that is made of at least one chalcogen anion (group 16 in periodic table) and at least one more electropositive element, e.g. ZnS, CaS, TiS₂ etc.), elements (Si, Ti, Cu etc.) and organic materials⁹⁴. The focus in my thesis is on oxide film deposition and more specifically on growing HfO₂ on Si surfaces.

3.1. Ideal ALD Process

The ideal ALD process is shown schematically in Figure 3.1(a-f). It is composed of sequential alternating pulses of gaseous precursors to which the substrate is exposed. The process starts out with a functionalised surface as shown in Fig 3.1a. The type of functionalisation is adapted to the particular ALD process. The surface

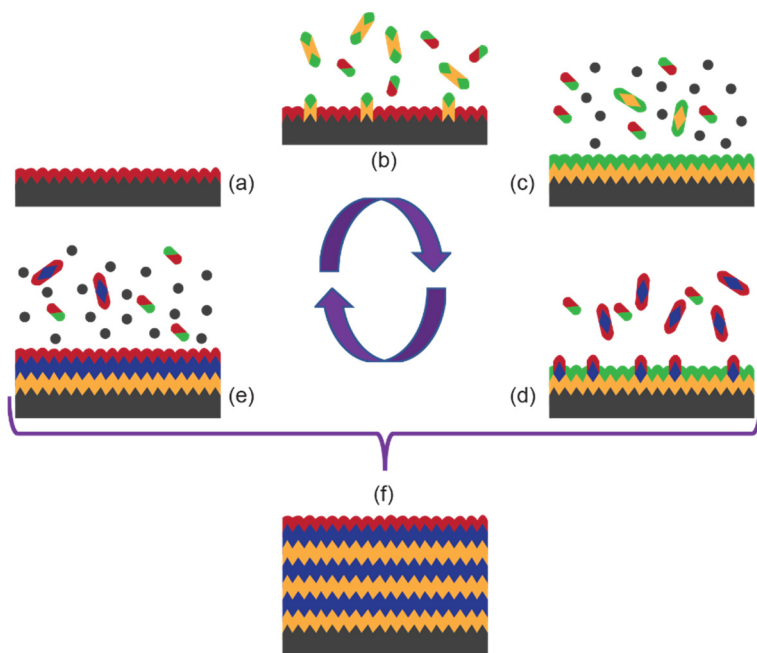


Figure 3.1.

Ideal ALD process using two precursors. (a) The surface is functionalised either naturally or from a pre-treatment. (b) The first precursor is dosed and reacts with the substrate surface. (c) Reaction by-products and excess of the precursor are removed from the growth chamber in a purge and/or pump-down step. (d) The second precursor is dosed, which reacts with the substrate that is covered with the first precursor. (e) Another purge/pump step removes reaction by-products and second precursor excess. (f) By repeating steps (b)-(e) the desired material thickness is achieved. This picture is redrawn from reference 93.

reacts partly or fully with the precursor during the first half cycle of the reaction. In this reaction the precursor might e.g. loose one or more ligands or dissociate (Figure 3.1b). The reaction is self-limiting, and only a single (molecular) layer of material is adsorbed on the surface (Figure 3.1c). The growth chamber is then purged with a neutral carrier gas and/or pumped down before the second precursor is introduced to the substrate in the second half-cycle (Figure 3.1d). The irreversible chemical reaction with this second precursor finalises the desired reaction and leads to a new functionalised surface, which can be used to start the process from the beginning. Another purge-pump down step will clean the residual gases inside the chamber. At this point, the surface is covered with the first layer (Fig 3.1e). Repeating the same process for several times will give the desired thickness of the aimed material on the surface (Fig 3.1f)^{94,95}.

A key feature of ideal ALD process is, as mentioned earlier, the automatic control of the amount of deposited material in each half cycle. This is achieved by saturation/self-limitation/self-termination of the adsorption process. Even the partial pressure of the reactant does not affect the amount of material during adsorption. This key features leads to a uniform amount of adsorbates on the entire surface,

irrespective of the substrate's shape⁹⁴. Chemical reactions involved in ALD can, like in any other chemical process, lead to the incorporation of unwanted impurities in the film. However, ideal ALD only results in the deposition of the desired material⁹⁶.

3.1.1. Adsorption Mechanisms in ALD

This simple idea, which really is at the core of the utility of ALD, hides, however, that adsorption processes can proceed very differently and that they often do not follow the ideal scheme. The basic types of adsorption processes that can occur are categorised in Figure 3.2. In the figure dashed lines indicate the end of precursor dosing. Figure 3.2a exemplifies the ideal ALD process with irreversible saturation. The amount of the adsorbate on the surface increases during the precursor dose until it reaches a plateau and the precursor fully covers the surface. Additional dosing of the precursor will not change the amount of adsorbate on the surface. Figure 3.2b illustrates *reversible* saturation of the adsorbate. Here the precursor can desorb again from the surface. Reversible and irreversible adsorption can occur together as is demonstrated in Figure 3.2c, and the true saturation coverage lies below the coverage obtained during the precursor pulse. Adsorption might also be non-saturating with a behaviour that is shown in Figure 3.2d: the precursor continues to adsorb on the surface as long as the precursor molecules are available in the chamber. This behaviour is very similar to CVD where precursors adsorb on the surface continuously and grow a film. After dosing is stopped, there is no change in the amount of adsorption. Finally, Figure 3.2e demonstrates that the irreversible saturation of Figure 3.2a might not lead to full coverage of the surface at the time that dosing is stopped. On complex and large substrates only irreversible and saturating reactions lead to homogeneous adsorption of the material on the whole surface irrespective of available amount of reactant, precursor's partial pressures and exposure and purge times. This is a key factor in ALD that the adsorbate amount is automatically controlled all over the surface⁹⁴.

ALD film growth is a result of exchange reactions between precursors and surface active sites. Reversible reactions and irreversible reactions in precursor decomposition or reaction by-products may also involve in the reaction mechanism. Layer growth can be blocked by adsorption of by-products on the surface⁹⁷. Therefore, if gaseous by-products that are produced on the surface due to the surface reaction participate in more reactions on the surface active sites the surface can be poisoned. This results to deactivation of reaction sites for precursor adsorption, incorporation of undesired elements into the grown film and ununiformed film growth⁹⁷.

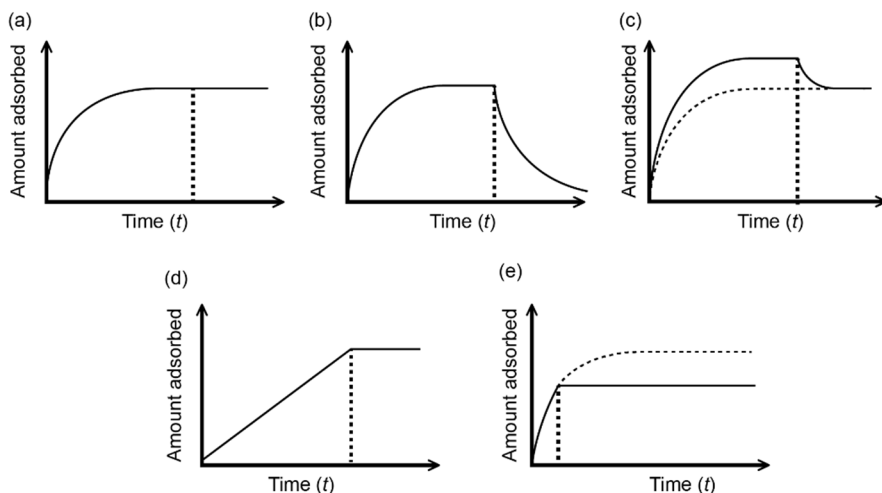


Figure 3.2.

Different adsorptions schemes. (a) Irreversible saturation. (b) Reversible saturating adsorption. (c) Combined reversible and irreversible saturating adsorption. (d) Irreversible non-saturating adsorption. (e) Irreversible saturating, but non-complete adsorption. Dashed lines illustrate the end of the reactant pulse and the beginning of the purge step. The image is redrawn from references 94 and 95.

3.1.2. Temperature Dependency in ALD

While CVD processes are strongly temperature dependant, especially if the growth rate follows an Arrhenius-type relation, a characteristic feature of ALD is its low temperature dependency. This is illustrated in Figure 3.3 which shows different types of temperature dependency of the growth per cycle or *growth rate*. Each ALD process has its optimum temperature window, typically in the range below 350 °C. Temperatures outside of the window will move the process to a non-ALD mode, poor growth rates, slow reaction kinetics or precursor condensation (at low temperature) and thermal decomposition or rapid desorption of the precursor (at high temperature). Therefore, each ALD process should be performed within the designated ALD temperature window^{93,94,98}. The ALD temperature also has impact on the precursor. For example it can lead to the decomposition of the precursor on the surface in an undesired fashion and result in the incorporation of undesired elements in the film. The decomposition process is typically a slow reaction and it is difficult to recognise. Depending on the precursor and the surface, the ALD temperature varies, although growth of the same material is targeted. Some surfaces can even act as catalyst and trigger the decomposition of the precursor⁹⁹. Some precursors such as metal halides (ZrCl₄, TiCl₄, TiI₄ and TaCl₅) are more stable at higher temperature, which leads to better film growth. Therefore, depending on the surface and precursor type the ALD temperature can change the chemistry of the surface⁹⁷.

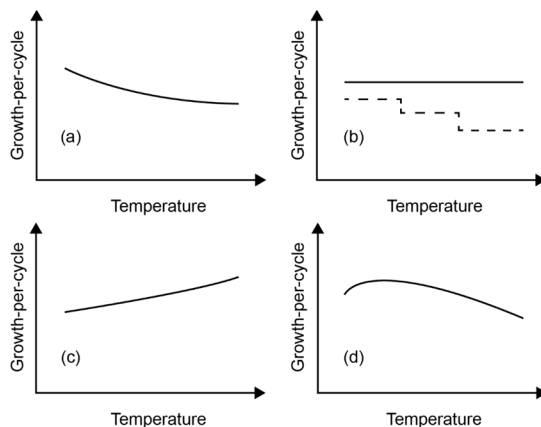


Figure 3.3.

Schematic illustration of growth per cycle change with temperature change within the ALD window. (a) Decrease in growth per cycle by temperature increase. (b) Constant growth per cycle over all temperatures or with different values at different temperatures. (c) Growth per cycle increase as temperature increases. (d) Growth per cycle has a maximum point when temperature increases. Figure redrawn from reference ³⁶.

3.2. ALD Precursors

Impurities affect the properties of the final product especially in electronics where purity is vital. Efforts have been done on different precursors and different surfaces in order to achieve better properties. Choosing a proper precursor is a challenge because a precursor can participate in undesirable reactions on the surface, which lead to deposition of impurities in the film. Choosing a precursor in ALD requires consideration. The basic requirements on an ALD reactant are³⁶:

- 1) It should be gaseous or vaporisable at lower temperature than that of the ALD reaction.
- 2) Its chemical reaction with the substrate should be fast, aggressive, irreversible and saturating.
- 3) The gaseous by-products of the ALD reaction should be inert and they should not dissolve into the film.
- 4) It should be safe and easy to handle, i.e. it should be non-toxic and non-corrosive.
- 5) It should have a reasonable price for industrial use.
- 6) For certain ALD processes the precursor needs to have a high purity.

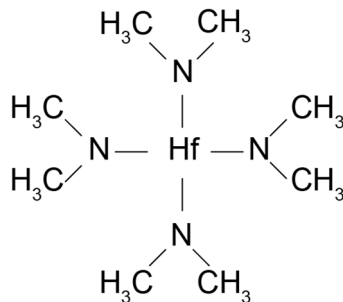


Figure 3.4.
TDMAHf precursor schematic structure.

In my thesis the ALD of HfO_2 on a Si(111) surface is studied. I chose $\text{SiO}_2/\text{Si}(111)$ as substrate and HfO_2 as the deposited layer because it is suitable for the design of an encapsulated catalytic transition metal catalyst immobilised on the surface (as was discussed in the introduction). There is also a wide range of application of this material combination in electronics, for example for gate dielectric applications production. Figure 3.4 illustrates schematically a metal alkylamides precursor, tetrakis(dimethylamido)hafnium ($\text{Hf}[\text{N}(\text{CH}_3)_2]_4$), also known as TDMAHf. This precursor has attracted significant attention for the deposition of HfO_2 films due to the relatively weak Hf-N bond and high volatility which enables efficient deposition at lower temperature^{23,100,101}. The precursor has been used in many studies, and the ideal growth scheme for HfO_2 from TDMAHf and water is as follows: in the first half cycle the intact precursor (TDMAHf or $\text{Hf}[\text{N}(\text{CH}_3)_2]_{4(\text{g})}$) reacts with the functional groups on the surface (in this case OH groups). By removing dimethylamide ligands $(-\text{O})_x\text{Hf}[\text{N}(\text{CH}_3)_2]_{4-x(\text{s})}$ is produced. In the second half cycle, the water dose causes loss of all remaining ligands on the Hf precursor and production of HfO_2 ^{98,102}. The ideal growth scheme of HfO_2 from TDMAHf and water does not predict any inclusion of impurities in the HfO_2 film. However, in reality, literatures show varying impurity levels. It is also clear that the growth chemistry is largely unknown, and, so far, no information is available on the growth chemistry of the type that could be obtained in an *operando* experiment.

3.3. HfO_2 Growth on Si Surface Employing ALD

The combination of metal oxygen precursors has gained considerable attention for applications and research into microelectronics since the miniaturisation of transistors and capacitors requires high- κ oxides to solve the current leakage problem of traditional SiO_2 capacitors in small sizes. Therefore, the ALD of these materials and their electrical properties are particularly interesting^{103–106}. Group 4

metal oxides (HfO_2 and ZrO_2) are the primary candidates for thermally stable ultrathin films with high κ value¹⁰⁷. For example, HfO_2 has a permittivity of about 20. Together with a good transparency to light, between mid-infrared and ultraviolet range due to the wide band gap (~ 5.5 eV), the high- κ value makes HfO_2 interesting for semiconductor nanotechnology, but also for antireflection coatings for mirrors and beam splitters⁹⁸.

Basically, the ALD reaction mechanism relies on a ligand exchange reaction. Although many ALD reactions follow this mechanism, other reaction pathways compete with this reaction. Several research studies suggest different pathways for the reaction of alkylamide precursors on a surface leading to the production of HfO_2 . It is suggested that reaction pathways involve the decomposition of the alkylamide ligands and formation of reactive products such as methyl methyleneimine [$\text{CH}_3\text{N}-\text{CH}_2$] (MMI). Such a pathway is initiated by the reaction between the lone pair electrons on the N atom and electron-deficient sites on the surface. Several studies suggest β -hydride elimination reaction to occur for TDMAHf or TDMAT deposited on Si surfaces. In addition, ligands can also participate in the adsorption process and be the reason for dissociation of the precursor. Hence, different pathways occur other than ligand exchange¹⁰⁸.

Many studies were performed on the structure and properties of HfO_2 film grown on SiO_2/Si surfaces. The choice of ALD precursors is an important focus of research, so that a better quality of films grown by ALD can be achieved. One particular issue is that of poor interface quality. This is a very fundamental issue and needs to be solved by improved surface preparation and optimised ALD conditions. Having better control over the interfacial layer requires better understanding of the chemistry of the surface during the surface reactions^{24,109}. In the ALD process, choosing the proper precursor is essential for gaining a superior thin film. Different precursors can cause creation of different interfacial layers and introduce different impurities, which can e.g. change electric properties¹¹⁰⁻¹¹².

“*In situ*” techniques have previously been employed to investigate the HfO_2 ALD on SiO_2 . These studies still separate the ALD cycles or half cycle from the measurement, and the ALD is carried in a separate chamber from the characterisation chamber. For example, XPS is typically carried out in a UHV chamber connected to the ALD reactor. Therefore, in none of these studies ALD has been studied using *operando* conditions^{23,27,100,109,113}. My research goal was to collect data while the initial ALD was proceeding. This should provide highly interesting information on the surface chemistry of ALD.

3.4. Gas Phase Study of TDMAHf and TDMAT

In Paper V the electronic structure of TDMAT and TDMAHf was studied. Further insight was gained from DFT. TDMAT and TDMAHf are widely used as precursors in the ALD of ultrathin films for nanoscale devices^{114,115}. Using these precursors can cause the incorporation of undesired residual elements in the film due to side reactions that can happen between the surface and the precursor^{24,34}. In order to minimise the side reactions on the surface during ALD it is crucial to have a good understanding of the electronic structure of these precursors. This is a necessary step for improving the ALD process, because it is the electronic structure that in the end is responsible for all chemical reactions between precursor and surface¹¹⁶. Ambient pressure XPS provided the possibility to study both valence band and core levels of the precursor vapour phase.

TDMAHf and TDMAT have very similar structures and thus similar valence bands. The reason for the similarity between these two compounds is that Hf and Ti belong to the same group in the periodic table, which results in similar chemical properties. The prime difference is that Ti has a higher electronegativity than Hf; 1.30 for Hf in comparison to 1.54 for Ti. The atomic radii of Hf⁴⁺ and Ti⁴⁺ are 72 and 56 pm, respectively¹¹⁷. In a simplified picture these parameters lets one expect that Hf has a lower ionisation energy than Ti. The reasoning also holds for TDMAHf in comparison to TDMAT. Literature shows a reversed trend, however. In Paper V the reason is found to be that the higher electronegativity and smaller ion size of Ti cause a shorter length of the Ti-N (1.90 Å) bond in comparison to the Hf-N bond (2.04 Å). Nitrogen atoms in the ligand donate lone pair electron density to the d-orbitals of the metal centre. In TDMAT the higher electronegativity of Ti causes a stronger interaction with these electrons. This stronger interaction causes a stronger delocalisation of the nitrogen lone pair. Therefore, TDMAHf has a higher ionisation energy than TDMAT.

This study shows that the interaction between the lone pair of electrons on the amido ligands and the empty metal orbitals influences the core level ionisation energies, which has also direct impact on the chemistry of the precursor on the surface. Dissociation pathways and mechanisms can be more precisely studied using this information about the electronic structure of the precursors. The vapour study can therefore be used as one of the puzzle pieces when dealing with DFT calculations and experiments for finding the reaction mechanism of TDMAHf during the ALD of HfO₂ on Si(111), which is the studied in paper VI.

3.5. *Operando* Study of ALD Employing Ambient Pressure XPS

In many ALD studies the word *in situ* refers to a measurement technique in which the sample after ALD growth in an ALD reactor is not composed to air, but directly introduced into a vacuum chamber for characterisation, e.g. by XPS. In my measurements, APXPS was instead performed *during* the gas dosing and evacuation stages. It is important to note that my experimental setup is not an ALD commercial reactor. In commercial ALD reactors, the process of dosing precursor and evacuating the chamber is carried out using rather short timescales. The short pulse duration followed by a quick purge step make it difficult to gain sufficient intensity in an APXPS measurement²². Moreover, an APXPS setup is typically not ideally suited for ALD: longer pipes and a bigger volume and larger wall surface area in comparison to an ALD reactor cause a slow and delayed reaction. I also did not have the possibility to purge the chamber quickly with a neutral gas between precursor pulses. Still, the APXPS measurement could be carried out rather quickly by using the “snapshot” rather than “swept” mode of the electron energy analyser. In swept mode the measurement is done by scanning through all the channels of the detector to obtain a spectrum without dependence on the varying detector sensitivity. In contrast, in snapshot mode an image of the detector is measured and the resulting spectrum will show signs of the influence of detector sensitivity on the line shape. Calibration measurements can help to alleviate this issue. In snapshot mode, the total acquisition time for the measurement of five core levels (Si 2p, C1s, N1s, Hf 4f and O 1s) and instrumental overhead was 13 s. Employing ambient pressure XPS experiment at high temporal resolution gave me thus the chance to collect evidence of the reaction at 0.08 Hz and identify surface species during the reaction. Thus, APXPS enabled me to cast light on the surface chemical reaction in the initial stages of ALD. This provides input on the evolution of surface species, adsorption and desorption on the surface, and reaction mechanisms. Paper VI discusses the APXPS study of ALD of HfO₂ on SiO₂/Si(111). Here, APXPS was combined with DFT.

In the experiment pieces of a highly phosphorus-doped n-type Si(111) wafer with a resistivity of 10⁻³ Ohm cm ($ND \approx 2 \times 10^{19}$ atom cm⁻³) were used as the substrate. For cleaning, the surface was heated up to 600 °C for 11 hours to make sure that it was fully degassed. A pyrometer was used to monitor the surface temperature. The sample was cleaned from native oxide by flash annealing to 1050 °C while the chamber pressure was kept below 6×10⁻⁹ mbar. The Si(111) surface was then oxidised at room temperature using an oxygen pressure of 5×10⁻⁸ mbar for 20 minutes¹¹⁸.

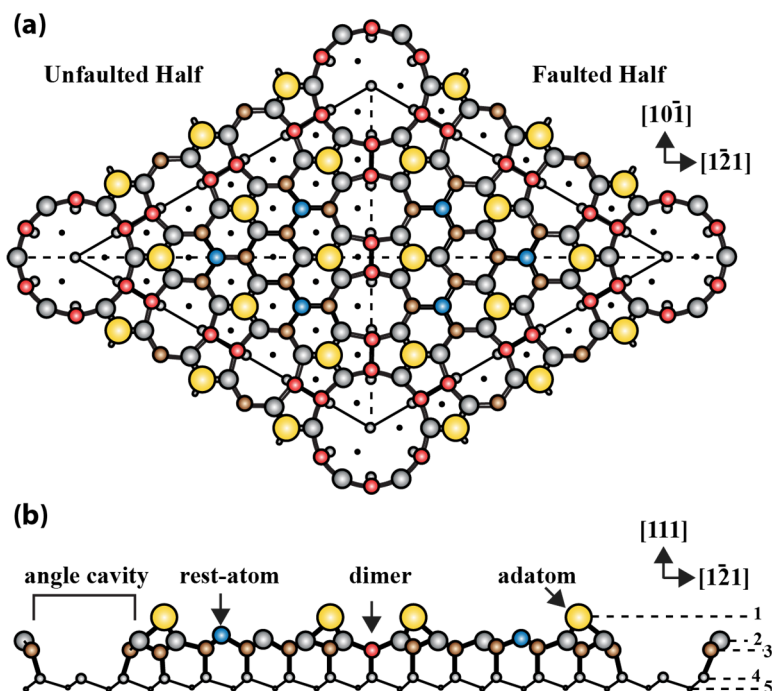


Figure 3.5. Schematic diagram of the Si(111)-(7 \times 7) surface. (a) Top view and (b) side view. The figure is redrawn from reference 119.

A model of the clean reconstructed Si(111)-(7 \times 7) is shown in Figure 3.5. The top layer contains the so-called Si adatoms, the second layer contains the so-called rest atoms with unsaturated dangling bonds, corner holes, two different stacking patterns and dimers¹²⁰. In total, the (7 \times 7) unit cell contains 12 adatoms and 6 rest atoms and one corner hole. Further, it contains nineteen dangling bonds: twelve on the adatoms, six on the rest atoms and one in the corner hole. The unit cell is 2.7 \times 2.7 nm². Deeper atoms are also shown in Figure 3.5 as black dots. Figure 3.5b shows a side view of the Si(111)-(7 \times 7) reconstruction¹¹⁹.

For a better understanding and discussion of the oxidation process of the clean Si(111), Figure 3.6 presents the local atomic structures around that Si adatoms that occur upon oxidation. Up to four O atoms react with the Si adatom, which is the primary oxidation site of the surface. Each of the structures has a name that represents the chemical character of the model^{121,122}: O atom bonded on top of the Si adatom is called “ad”, “ins \times n ” means that n O atoms are singly inserted into n Si adatom backbonds, and the three-fold-coordinated subsurface O atom is named “tri”.

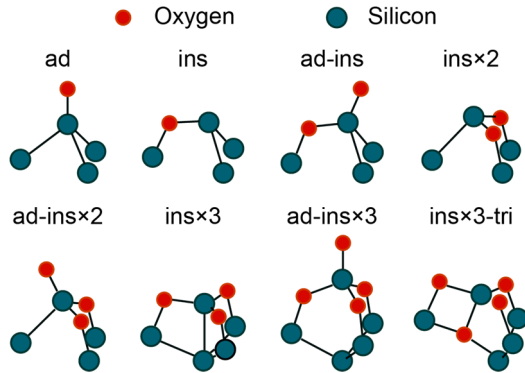


Figure 3.6. Optimised possible structures for Si(111) oxidation models. Figure is redrawn from reference 121.

The oxidation pathway of the clean Si(111) surface is shown in Figure 3.7: the O_2 molecule adsorbs on Si adatoms and dissociates without any barrier. An ins×2 structure is produced. Alternatively, also an “ad-ins” could be formed, which decays with a very low energy barrier (-0.15 eV) into the ins×2 structure. Addition of another O_2 molecule leads to formation of a stable ins×3 or ad-ins×3 structure, which is metastable up to ~400 K. The initial oxidation stage is completed by conversion of the ad-ins×3 structure into a ins×3-tri configuration, which does not have any adatom dangling bond. At this stage a thin layer of SiO_4 units on the surface has been created. Further oxidation of the surface requires diffusion of the O(tri) atoms, which is an endothermic reaction. This step is only possible at higher temperature¹²¹.

In the SiO_4 units Si is in an +4 oxidation state, which results in an Si 2p XPS binding energy that is by 3.6 eV higher than that of Si^0 . Lower oxidation states can also be observed in XPS with binding energies intermediate between the Si^0 and the Si^{+4} peak. Their characteristic Si 2p binding energies are by ~+0.9 eV per O ligand higher than that of Si^0 . Figure 3.8 illustrates the appearance of the Si 2p line before and after starting the ALD process.

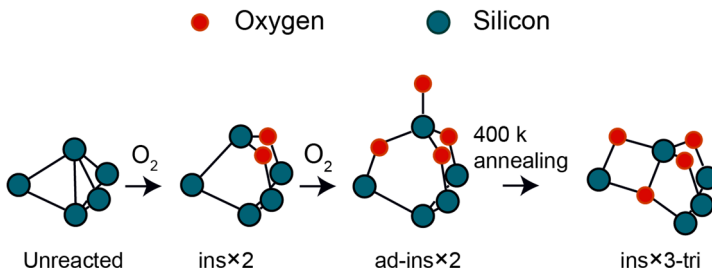


Figure 3.7. Oxidation pathway model of Si(111). Figure is redrawn from reference 121.

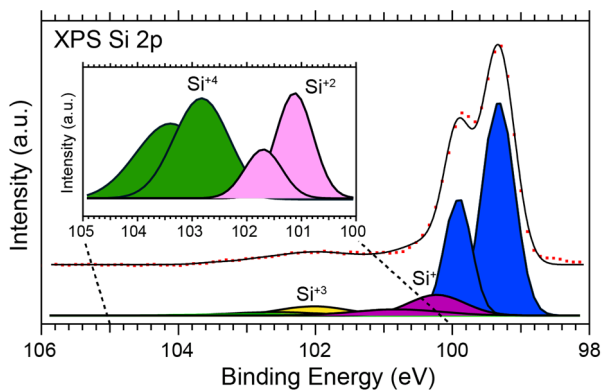


Figure 3.8.

Si(111) surface after oxidation. The main peak is located at 99.3 eV and oxide peaks are 0.9 eV higher than the bulk peak per oxidation state.

Much effort has been devoted to understanding the ALD of HfO₂ from TDMAHf and water^{27–29,123}. Recently, Timm *et al.* reported the first operando APXPS study of HfO₂ ALD on InAs²². In comparison to this study I have further improved the time resolution and, in addition, I have characterised not only the substrate, but also the precursor core levels.

Figure 3.9(a-e) illustrates the evolution of the O 1s, N 1s, and C 1s, Si 2p and Hf 4f core levels during the TDMAHf first half-cycle. For each core level 114 scans were collected, using a 700 eV photon energy. The combined beamline and analyser resolution was 200 meV. In order to avoid photon-induced changes of the surface species, the sample was moved continuously under the X-ray beam during the measurement. The energy scale of all core levels was calibrated with respect to the Si 2p_{3/2} bulk peak¹¹⁸ at 99.3 eV.

Figure 3.9(f-j) highlights selected scans from different regions of the surface plots in Figure 3.9(a-e), and each graph consists of scans from bottom to top (1-6): before the first TDMAHf dose, after the first dose, before the second dose, after the second dose, before evacuation and after evacuation. There are small initial components in C 1s and N 1s region at 283.3 and 397.7 eV, respectively, due to a small background pressure in the chamber from a previous TDMAHf experiment. The O 1s line contains two peaks that are related to O atoms in the “ins” (532.0 eV) and “tri” (352.8eV) configurations.

New components appear in the core levels after the first TDMAHf dose: the binding energies are 16.8 (Hf 4f), 398.6 (N 1s) and 286.1 eV (C 1s), respectively. These peaks are related to N and C in dimethylamido (-N(CH₃)₂, DMA⁻, and DNA⁻-bonded Hf. The Hf 4f doublet components have a separation of 1.7 eV and an intensity ratio of 1.33.

New components appear some minutes later, but before the second TMDAHf dose. They have binding energies of 16.2 (Hf 4f), 396.9 (N 1s) and 285.0 eV (C 1s), respectively, and are assigned to methyl methyleneimine (MMI)³⁴. It should be noted that MMI also contains a methyl group with a C 1s binding energy of 286.1 eV – the same as that of DMA⁻. In the O 1s spectra a component is found at 531.0 eV binding energy. This component is related to hafnium-bonded oxygen atoms.

To aid the understanding of the adsorption and decomposition pathways of TDMAHf, DFT calculations were carried out. In the modelling, the thermodynamically favourable (0001) and (10 $\bar{1}$ 0) surfaces were used (Figure 3.10).

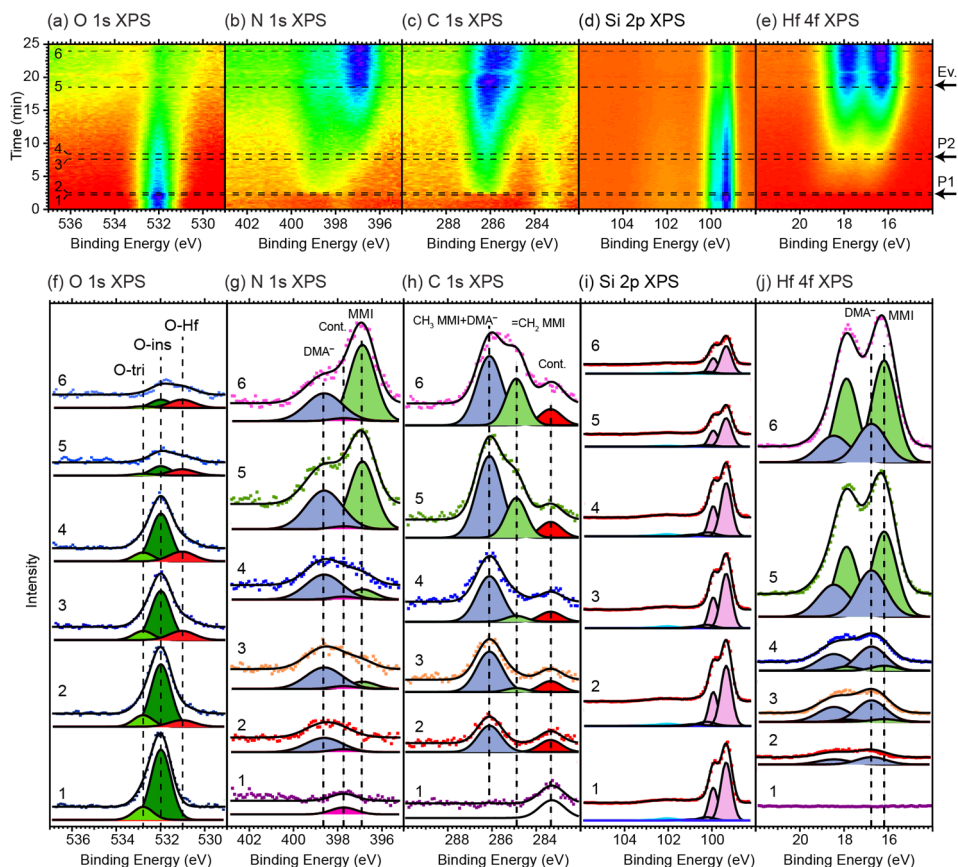


Figure 3.9.

XPS analysis of the first ALD half cycle of the HfO₂ growth on oxidised Si(111) from TDMAHf and H₂O. (a-e) XPS surface plots of O 1s, N 1s, Si 2p, C 1s and Hf 4f, respectively. (f-j) selected spectra from the surface plots from bottom to top: before the first dose, after the first dose, before the second dose, after the second dose, before evacuation and after evacuation. TMDAHf pulses and chamber evacuation are shown on the right hand side of the surface plots as P1 and P2 and Ev.

The (0001) surface was modelling using a supercell containing 480 atoms and lattice parameters of $a=19.71 \text{ \AA}$, $b=17.08 \text{ \AA}$, and $c=37.64 \text{ \AA}$. A vacuum layer of 20 \AA was placed on top of the SiO_2 (0001) surface to minimise the interactions between the supercells in the z -direction and to avoid any significant overlap between wave functions of periodically translated cells.

Figure 3.11 shows the homolytic cleavage of the Hf-N bond of TDMAHf in the gas phase, which requires $387.1 \text{ kJ mol}^{-1}$. It also shows the formation of DMA^- via a so called β -hydride elimination reaction. This process requires $\sim 160 \text{ kJ mol}^{-1}$. Thus, neither process is favourable in the gas phase, in good agreement with gas phase FTIR results and earlier DFT calculations.²³

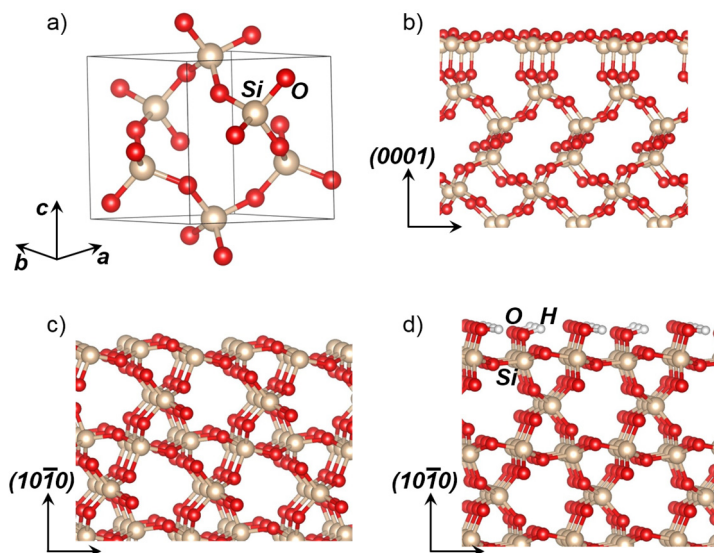


Figure 3.10. Structures of (a) unit cell of ideal SiO_2 crystal and (b) (0001) surface with the supercell containing 480 atoms. (c) and (d) $\text{Si}(10\bar{1}0)$ surface and hydroxylated $(10\bar{1}0)$ surface.

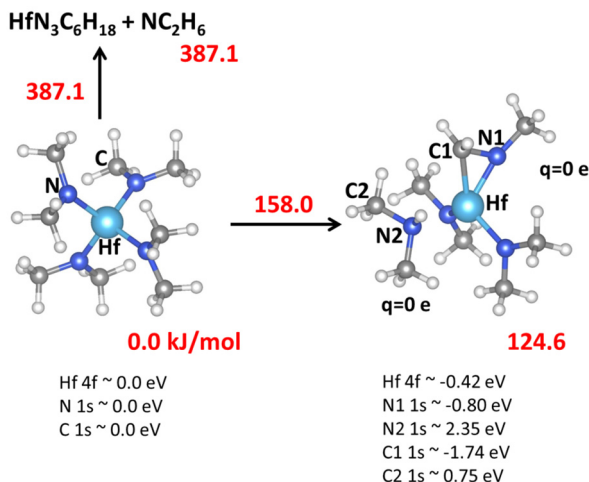


Figure 3.11.
DFT calculations of decomposition of isolated TDMAHf molecule. Core level shifts are indicated.

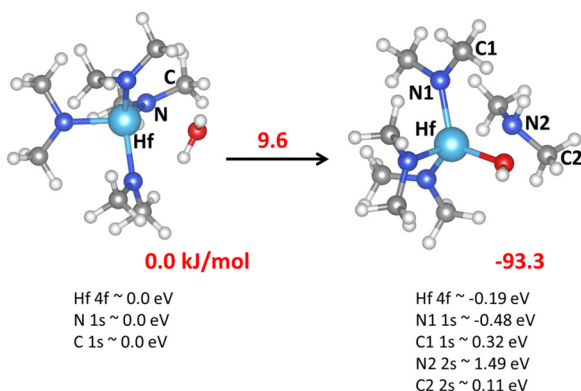


Figure 3.12.
DFT calculations of decomposition of TDMAHf molecule in presence of water molecule. Core level shifts are indicated.

Water renders the gas phase decomposition of TDMAHf favourable (Figure 3.12). The calculated activation barrier is only 9.6 kJ mol^{-1} . This indicates, that residual water in the chamber could lead to the present of both gas phase dimethylamine (DMA) and water-modified Hf complexes.

The surface-adsorption and -decomposition of TDMAHf was considered for a pristine SiO_2 surface (Figure 3.13), a SiO_2 (0001) surface with oxygen vacancy (Figure 3.14), a SiO_2 (0001) surface with oxygen vacancy in presence of water molecule (Figure 3.15), a SiO_2 (0001) surface with an oxygen vacancy and one hydroxyl group on the surface (Figure 3.16), a SiO_2 (10 $\bar{1}$ 0) surface with a monolayer

of hydroxyl (Figure 3.17) and a $\text{SiO}_2(10\bar{1}0)$ surface with a monolayer of hydroxyl and second TDMAHf molecule (Figure 3.18). From all these calculations it is obvious that few decomposition pathways are exothermic. However, even endothermic pathways could be followed if the chemical equilibrium is moved towards the product side by high temperature (280 °C in the experiments) and removal of products from the surface.

In more detail, the calculated adsorption energy of physisorbed TDMAHf on pristine SiO_2 is $-76.7 \text{ kJ mol}^{-1}$ (conf. I, Figure 3.13). A second adsorption configuration, conf. II, has an adsorption energy that is only 0.1 kJ mol^{-1} lower than that of conf. I. Thus, both configurations can co-exist. Further decomposition is unfavourable. Inspection of the core level energy shifts are presented in Table 3.4.

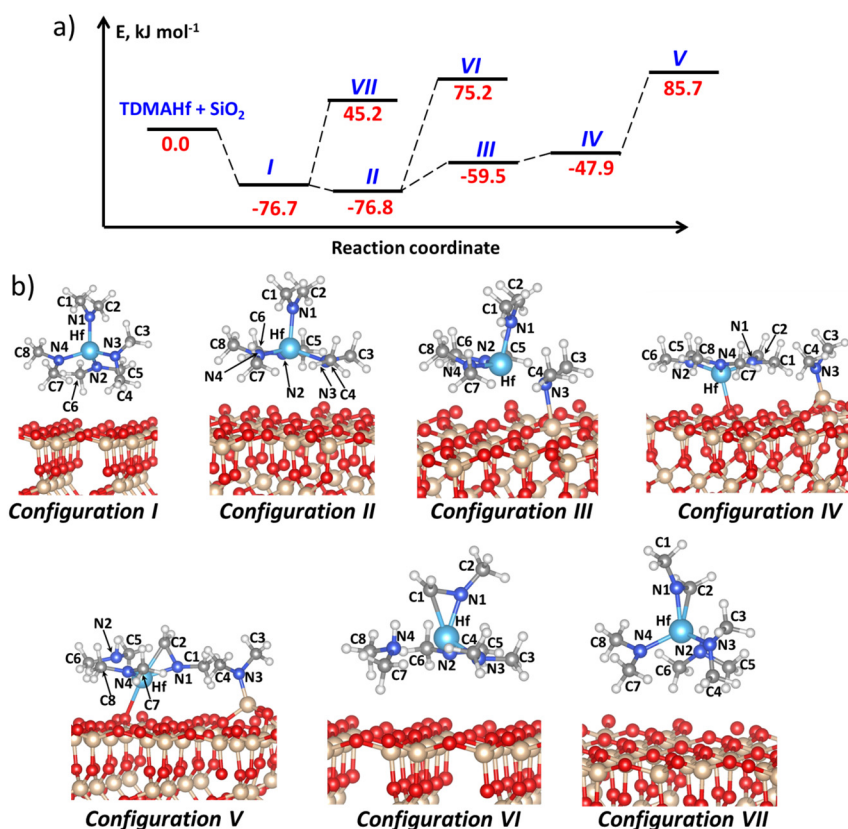


Figure 3.13.

(a) Calculated mechanisms of TDMAHf molecule decomposition on a pristine SiO_2 (0001) surface; (b) Structures involved in decomposition mechanism.

Table 3.4.

Calculated core level energy shifts for atoms of the different configurations in Figure 3.13b

Atom	Core level	Core level shifts						
		I	II	III	IV	V	VI	VII
Hf	4f	0.00	0.25	1.38	2.29	1.85	-0.07	-0.46
N1	1s	0.00	-0.12	0.76	1.83	1.14	-0.56	-0.76
N2	1s	0.00	0.23	0.88	1.72	3.69	-0.19	2.04
N3	1s	0.00	-0.02	1.71	1.59	1.39	-0.18	-0.19
N4	1s	0.00	0.26	0.87	1.84	1.50	2.04	-0.20
C1	1s	0.00	-0.15	0.48	1.09	0.57	-1.55	-0.74
C2	1s	0.00	-0.03	0.60	1.23	-0.04	-0.43	-1.69
C3	1s	0.00	0.07	0.76	1.18	0.99	-0.09	-0.29
C4	1s	0.00	-0.07	0.62	0.95	0.80	-0.10	-0.01
C5	1s	0.00	0.20	0.69	1.22	1.91	-0.018	0.75
C6	1s	0.00	0.18	0.63	1.23	2.01	-0.03	0.79
C7	1s	0.00	0.16	0.62	1.13	0.88	0.76	-0.13
C8	1s	0.00	0.16	0.66	1.15	1.20	0.78	-0.14

Removal of the native oxide layer from Si(111) surface and *in situ* oxidation of the surface was done in order to get a thin clean oxide layer with low thickness. This implies that surface might not be fully oxidised and that the presence of oxygen vacancies is probable¹¹⁸. DFT shows that the oxygen vacancy on SiO₂ surface has only a small effect on the adsorption of TDMAHf in comparison to the pristine surface and results in adsorption energy of -69.4 kJ mol⁻¹ for TDMAHf molecule (Figure 3.14, core level shifts in Table 3.5). Conf. V (Figure 3.14 b) is the final product of the β -hydride elimination reaction (Figure 3.14 a) from the initial Conf. I. Calculated Hf 4f, N1 1s and C2 1s core level energies in Conf. V are shifted relatively to Conf. I by -0.47, -0.76 and -1.71 eV, respectively. In spite of the fact that the calculated binding energy shifts are in agreements with experiment, presence of the DMA molecule and endothermic nature of the pathway indicates that current model falls short in interpretation of the experiment.

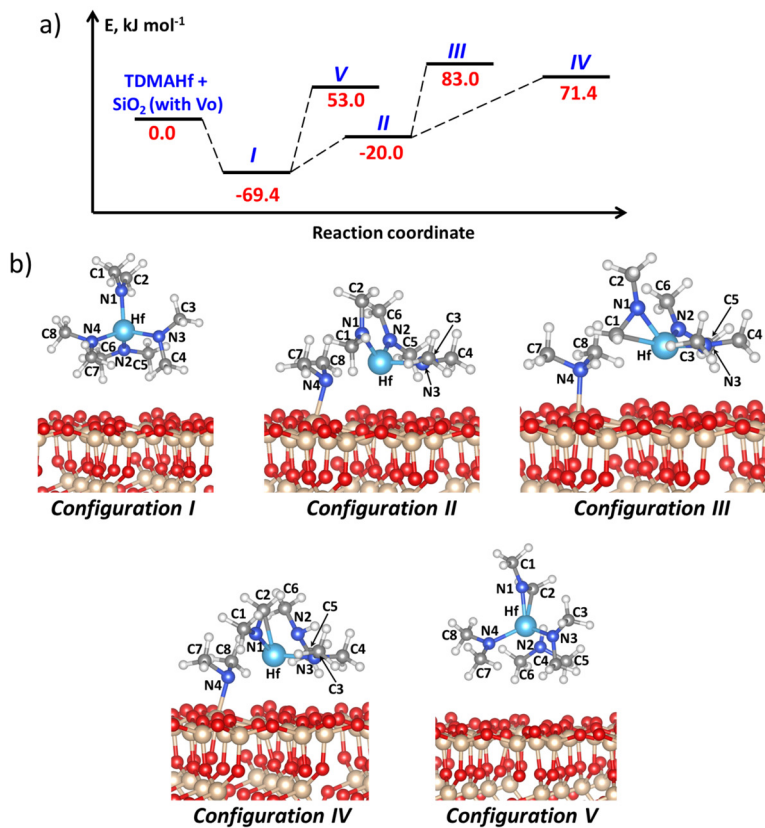


Figure 3.14.

(a) Energy path of TDMAHf molecule decomposition on a SiO₂ (0001) surface with oxygen vacancy; (b) Structures involved in decomposition mechanism.

Table 3.5.

Calculated core level energy shifts for atoms of the different configurations in Figure 3.14b

Atom	Core level	Core level shift				
		I	II	III	IV	V
Hf	4f	0.00	1.75	0.40	1.17	-0.47
N1	1s	0.00	0.87	0.01	0.46	-0.76
N2	1s	0.00	1.10	0.43	2.99	2.01
N3	1s	0.00	0.47	0.31	0.40	-0.20
N4	1s	0.00	1.35	2.55	1.52	-0.20
C1	1s	0.00	0.74	-0.82	0.29	-0.74
C2	1s	0.00	0.82	0.02	-0.58	-1.71
C3	1s	0.00	0.28	0.18	0.15	-0.30
C4	1s	0.00	0.08	-0.02	0.32	-0.04
C5	1s	0.00	0.82	0.42	1.38	0.75
C6	1s	0.00	0.91	0.24	1.37	0.80
C7	1s	0.00	0.32	0.89	0.43	-0.13
C8	1s	0.00	0.32	0.76	0.96	-0.14

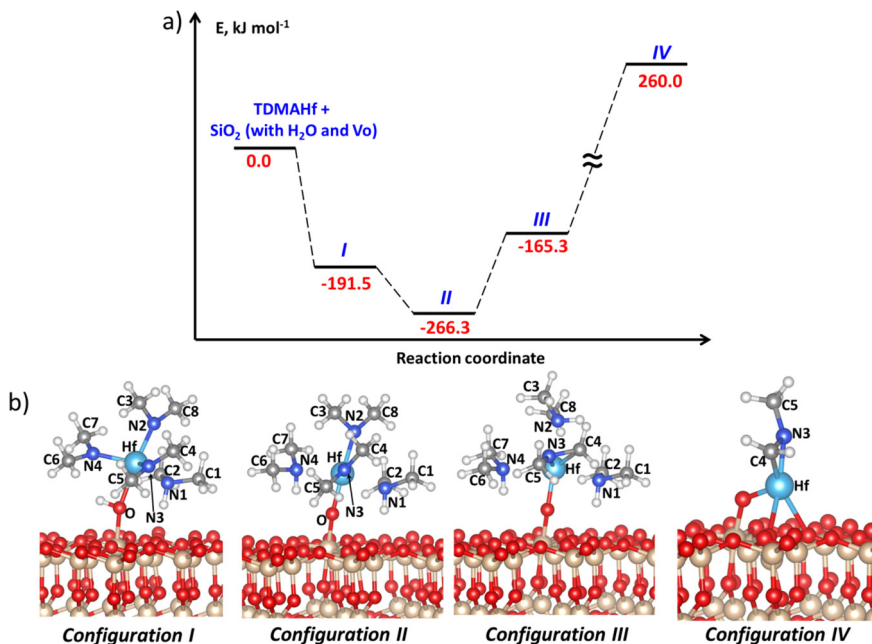


Figure 3.15.

(a) Energy path of TDMAHf molecule on a SiO₂ (0001) surface with oxygen vacancy and water molecule; (b) Structures involved in decomposition mechanism.

The presence of an oxygen vacancy and water molecule on SiO₂ surface has strong effect on the adsorption and decomposition of TDMAHf (Figure 3.15, core level shift in Table 3.6). Both the adsorption and initial decomposition are exothermic spontaneous and without activation barrier. In contrast, further decomposition to MMI is not favourable anymore, at odds with the experimental results.

Table 3.6.

Calculated core level energy shifts of the different configurations in Figure 3.15b

Atom	Core level	Core level shift			
		I	II	III	IV
Hf	4f	0.00	0.24	-0.35	0.50
N1	1s	0.00	0.08	-0.19	
N2	1s	0.00	0.17	2.66	
N3	1s	0.00	0.28	-0.29	0.34
N4	1s	0.00	2.46	2.11	
C1	1s	0.00	0.12	-0.21	
C2	1s	0.00	-0.05	0.08	
C3	1s	0.00	0.39	1.03	
C4	1s	0.00	0.23	-1.34	-0.43
C5	1s	0.00	0.13	-0.24	0.16
C6	1s	0.00	0.98	0.60	
C7	1s	0.00	1.01	1.01	
C8	1s	0.00	0.14	1.23	
O	1s	0.00	-1.31	-1.34	-0.38

In the experimental data there was no sign of any presence of OH groups on the surface. However, since it can be difficult to identify the hydroxyl peak in the O 1s line of SiO₂, also a hydroxylated surface was considered. Clearly, the decomposition of TDMAHf on this surface is exothermic, but also here there is a lack of MMI at odds with the experiment. One possibility that is considered in DFT calculations in my thesis is SiO₂ surface with oxygen vacancy in presence of OH group on the surface. DFT calculations in Figure 3.16.

A further considered possibility is that of TDMAHf decomposition on a SiO₂ surface with an oxygen vacancy and monolayer hydroxyl coverage (Figure 3.17). Here, exothermic decomposition pathways are available, both towards MMI via β -hydride elimination and employing a ligand exchange-type of reaction. It is, however, clear that the calculated binding energy shifts of the MMI configuration do not agree with experiment.

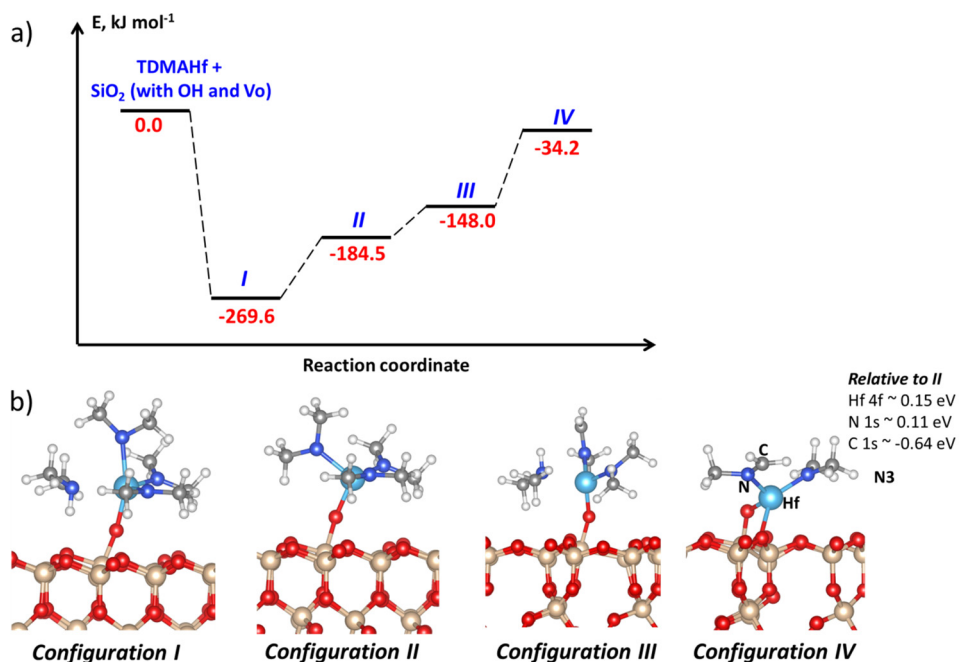


Figure 3.16. (a) Energy path of TDMAHf molecule on a SiO₂ surface with oxygen vacancy and one hydroxyl group; (b) Structures involved in decomposition mechanism. Core level shifts are indicated.

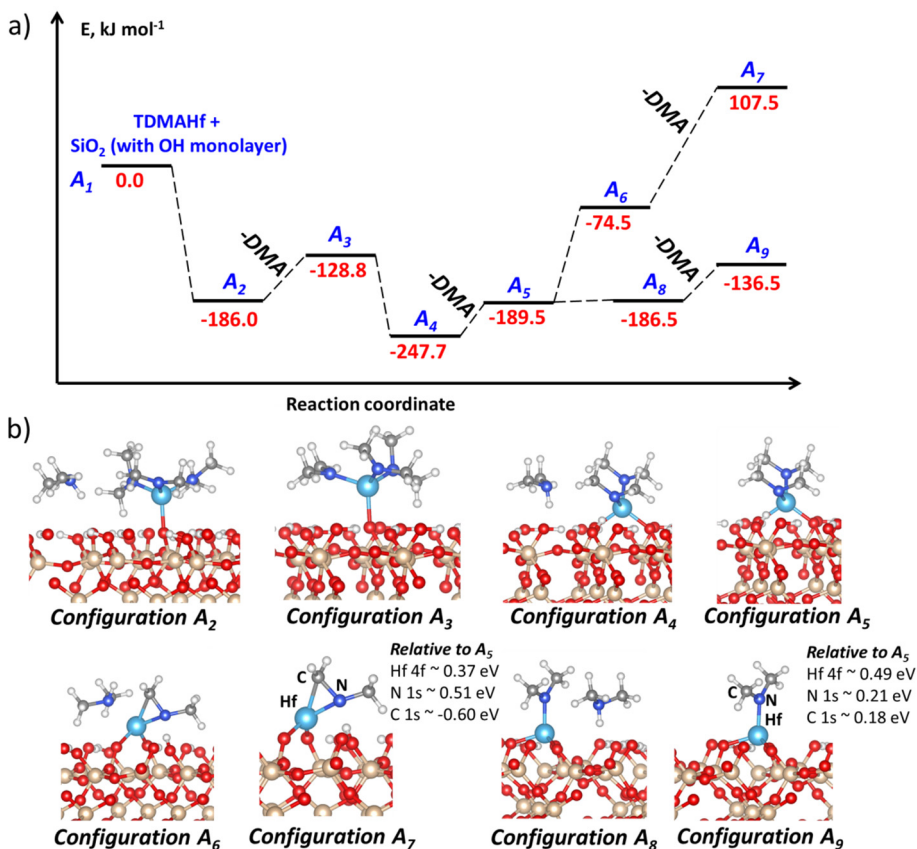


Figure 3.17. (a) Energy path of TDMAHf molecule on a SiO₂ (10 $\bar{1}$ 0) surface with one monolayer of hydroxyl groups; (b) Structures involved in decomposition mechanism. Core level shifts are indicated.

Finally, also a bimolecular reaction between two TDMAHf precursors was considered (Figure 3.18). Again, exothermic pathways are discernible, both along the β -hydride elimination route towards MMI and along a ligand exchange route. The calculated binding energy shifts of configuration B7 and B10, both of which are reached via overall exothermic pathways, are in qualitative agreement with the experimental results.

Although no final statement can yet be made as to which decomposition pathway is most likely, the DFT results give at least some preliminary indication of what is important: (a) bimolecular decomposition pathways seems to be a viable alternative, (b) any potential presence of water or surface hydroxyls would aid the decomposition and (c) kinetics will have to be considered to identify the most likely reaction scheme.

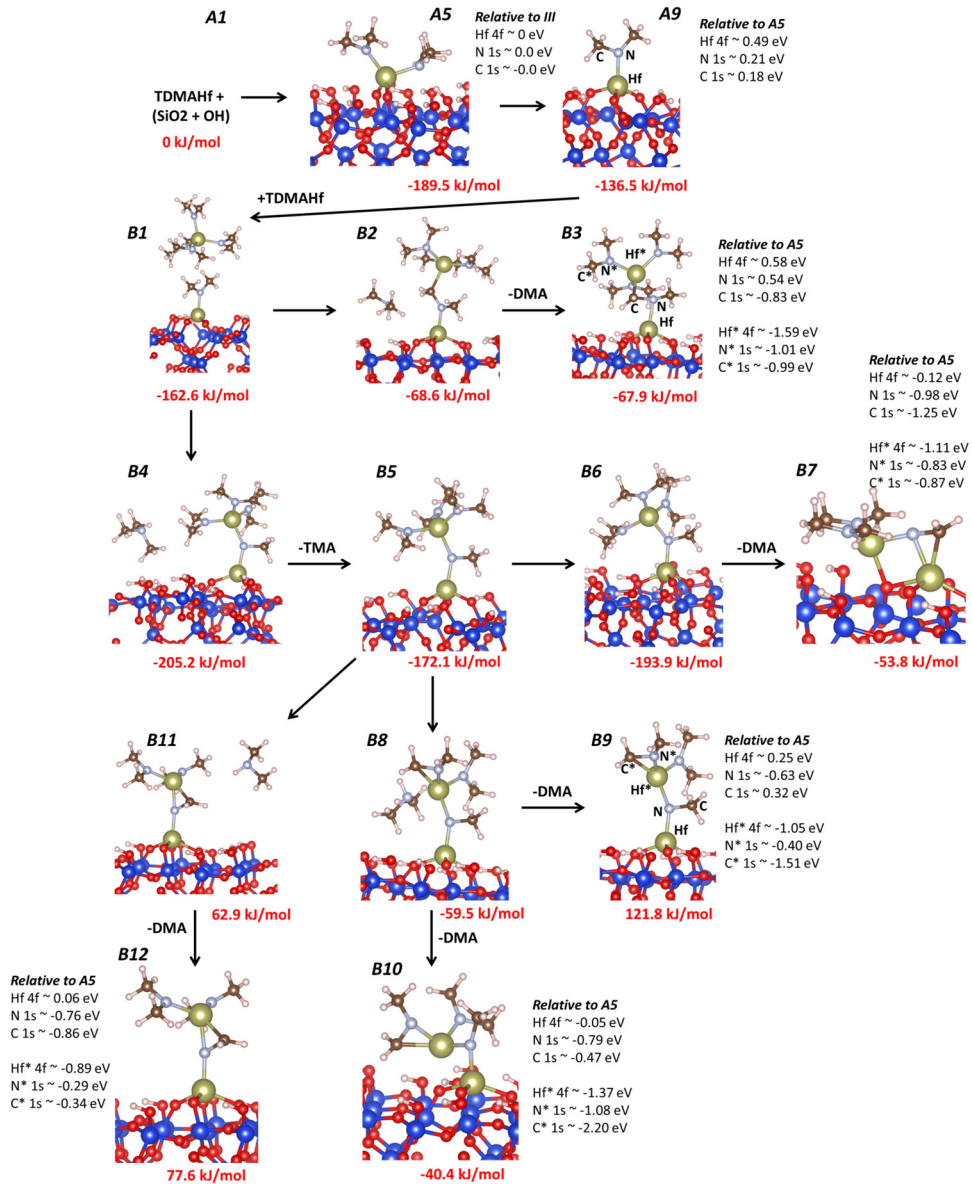


Figure 3.18. Decomposition of TDMAHf molecule on a SiO₂ (10 $\bar{1}$ 0) surface with one monolayer of hydroxyl groups and second TDMAHf molecule. Core level shifts are indicated.

4. Green Chemistry and Catalysis

Modern society relies heavily on a large variety of different chemicals, and, indeed, the production and consumption of chemicals continues to increase. Report published by United Nations environment programme (UNEP) show that global production and consumption of chemicals has increased. UNEP analysis shows that there has been a global increase in chemical industry output in all the regions in the world until 2010. Also estimations show that until 2020 the chemical industry output will increase around \$1200 billion¹²⁴. However, European chemicals production and consumption statistics show that after the lowest consumption in chemicals in 2008 due to the financial crisis there has been a sudden increase in consumption in 2010. However, in comparison with 2007 the consumption of chemicals has decreased approximately 53 million tonnes¹²⁵. Obviously, production at lower cost and in an environmental-friendly fashion in terms of energy consumption and waste production is highly desirable. The concept of *Green chemistry* addresses this goal by aiming at the design of chemical products and processes that have less impact on the environment. The principles of Green chemistry were formulated in *green chemistry: theory and practice* by Anastas and Warner¹²⁶:

- “It is better to prevent waste than to treat or clean up waste after it is formed.
- Synthetic methods should be designed to maximize the incorporation of all materials used in the process into the final product.
- Wherever practicable, synthetic methodologies should be designed to use and generate substances that possess little or no toxicity to human health and the environment.
- Chemical products should be designed to preserve efficacy of function while reducing toxicity.
- The use of auxiliary substances (e.g. solvents, separation agents, etc.) should be made unnecessary wherever possible and innocuous when used.
- Energy requirements should be recognized for their environmental and economic impacts and should be minimised. Synthetic methods should be conducted at ambient temperature and pressure.
- A raw material of feedstock should be renewable rather than depleting wherever technically and economically practicable

- Unnecessary derivatisation (blocking group, protection/deprotection, and temporary modification of physical/chemical processes) should be avoided whenever possible.
- Catalytic reagents (as selective as possible) are superior to stoichiometric reagents.
- Chemical products should be designed so that at the end of their function they do not persist in the environment and break down into innocuous degradation products.
- Analytical methodologies need to be further developed to allow for real-time, in process monitoring and control prior to the formation of hazardous substances.
- Substances and the form of a substance used in a chemical process should be chosen so as to minimise the potential for chemical accidents, including releases, explosions, and fires.”

Green chemistry can only be realised by using *catalysts*. The word catalyst was used for the first time by Jöns Jacob Berzelius in 1820 in his article that described the chemical conversion of starch to sugar, decomposition of hydrogen peroxide by metals and conversion of ethanol to acetic acid by Pt (for a sketch of the history of catalysis see e.g. Ref. 127). In 1904 Wilhelm Ostwald provided a modern definition of the term^{1,128}:

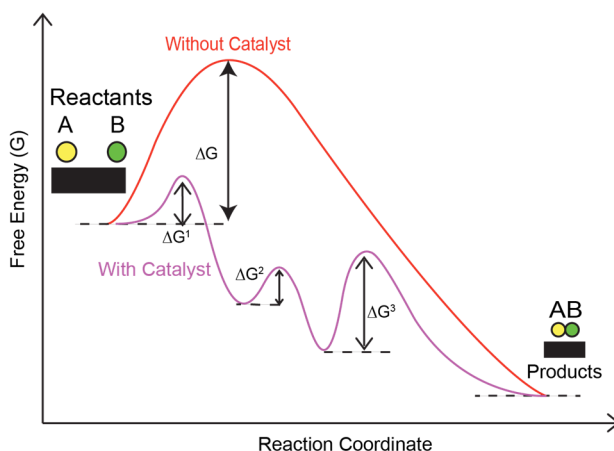


Figure 4.1.

Gibbs free energy diagram for an exothermic reaction with and without catalyst. The catalyst decreases the energy barrier for the reaction by changing the reaction path.

“A catalyst is a substance that affects the rate of a chemical reaction without being part of its end product”.

Hence, a catalyst is a substance that affects the kinetic of a reaction. This means that a catalyst will accelerate a reaction, preferably towards the desired end product of the reaction. Conversely, it does not and cannot affect the thermodynamics of the reaction. Figure 4.1 illustrates this concept: two different reaction paths are shown in a Gibbs free energy/reaction coordinate diagram for an exothermic reaction. The path without involvement of a catalyst has a high energy barrier which effectively prevents formation of the reaction product. The energy barriers on the path with involvement of a catalyst are much smaller and thus much easier to overcome: the reaction is accelerated. The catalyst makes the reactant more capable to react and form the final product.

Catalysts are used in all types of chemical industry, from the production of bulk petrochemicals (including e.g. fossil fuels) to fine chemicals (including e.g. many types of medicine). Naturally, catalysis plays a major role in the chemical and physical chemistry/chemical physics sciences, and the design and use of new catalysts, with potential great impact on economy and environment, is central to many pure and applied chemistry and physics research endeavours. Catalysis can roughly be divided into three different categories: homogeneous and heterogeneous catalysis.

4.1. Homogenous and Heterogeneous Catalysts

In homogenous catalysis the catalyst on the one hand and the reactants and products on the other are in the same phase, liquid or gas phase. An important example is the decomposition of atmospheric ozone in the presence of chlorine¹²⁶. The activity and selectivity of a homogeneous catalyst can often be tuned by relatively slight chemical modification of the catalyst, e.g. by exchanging a ligand with another. The main difficulties of homogeneous catalysis are that the product needs to be separated from the catalyst material and residual reactants, that the process cost typically is high, for transition metal catalysts metal leaching and contamination of the product, short catalyst lifetime and recovery of the catalyst. The advantages of homogeneous catalysis, accessible catalyst sites due to dissolved catalyst in solution, easily tenable selectivity by modifying catalyst complex and possibility to easily study the reaction mechanism, may outweigh the disadvantages, however, and many (fine chemical) industrial processes are done in the presence of homogenous catalysts¹²⁶.

In heterogeneous catalysis the catalyst is in a different phase than reactants and products. Schlögl has defined heterogeneous catalyst as¹²⁹:

“a functional material that continually creates active sites with its reactants under reaction conditions, these sites change the rates of chemical reactions of the reactants localized on them without changing the thermodynamic equilibrium between the materials”.

Heterogeneous catalysis benefits in particular from simple product separation and catalyst recovery processes and that a flow geometry can be applied, which is beneficial for industrial application. However, heterogeneous catalysts are typically less active and less selective than homogeneous ones¹³⁰. Approximately 90% of the industrial catalytic are heterogeneously catalysed, which shows the importance of the field^{6,126}.

An extremely important example of heterogeneous catalysis is the Haber-Bosch ammonia synthesis, one of the uniquely most important chemical processes^{5,126}. Heterogeneous catalysts has also had great impact on the fuel industry especially in so-called syngas i.e. synthesis gas, that is a mixture of carbon monoxide, carbon dioxide and hydrogen, conversion to ethanol and higher alcohols in order to substitute other fuels rooting from crude oil¹³¹. Today, petrochemical industry relies heavily on heterogeneous catalysis. Green chemistry also opened the doors for heterogeneous catalysts to enter the pharmaceutical and fine-chemicals industries, a rather complicated field since it requires the combination of physical chemistry, inorganic chemistry, organic and organometallic chemistry, surface science and material science⁵.

Many problems and issues in heterogeneous catalysis stay unresolved, such as the great difficulty in tuning the reaction, low selectivity and difficulties in defining the structure and reaction mechanism by means of advanced techniques such as X-ray analysis techniques. The lack of surface chemistry knowledge on heterogeneous catalytic reactions is not least due to the difficulty of measurements in *operando* conditions, but it is also a general difficulty of studying and understanding surfaces, which are inherently complex system. These issues make it more difficult to get insight about reaction mechanisms in heterogeneously catalysed reactions than in homogeneously catalysed ones¹³⁰.

A heterogenised catalyst can be seen as a homogenous catalyst, which is attached to an insoluble support covalently or non-covalently. Heterogenised catalysts are expected to be more stable in chemical reactions and make it easier to separate products in a chemical process. In principle, heterogenisation can modify and adjust a homogeneous catalyst's properties for higher efficiency, ease of recoverability and reusability and possibly using in a continuous flow reaction^{5,129}. Both covalently and non-covalently supported catalysts are studied in my thesis.

4.2. C-H Activation in Catalytic Oxygenation and Halogenation Chemistry

The inert nature of the C-H bond makes the activation of this bond a difficult process. At the same time, undirected C-H bond activation, i.e. a reaction in which no ligand or functional group is present to guide the catalytic reaction, is an important process in industrial chemical synthesis¹³². As an example conversion of methane that is found in natural gas to methanol in order to create an economically transportable liquid and makes the natural gas a more efficient energy source¹³³. One of the important class of reactions is the undirected selective oxidation of hydrocarbons, which is necessary in the synthesis of more complex molecules⁵. Figure 4.2 shows some simple examples of catalytic reactions that are discussed in this thesis, the acetoxylation of biphenyl and benzene and the halogenation of 2-phenylpyridine^{1,5}.

Earlier studies have shown that Pd complexes make efficient homogeneous catalysts for the replacement of the hydrogen atom in a C-H bond by functional groups containing N, O, C and halogen atoms. Moreover, when using Pd complexes mild conditions can be applied, i.e. conditions that are easily acquirable and manageable^{1,134,135}. In my thesis heterogenised homogeneous Pd catalysts complexes were considered: they were immobilised using three different approaches as discussed earlier, and they were used for C-H activation reactions.

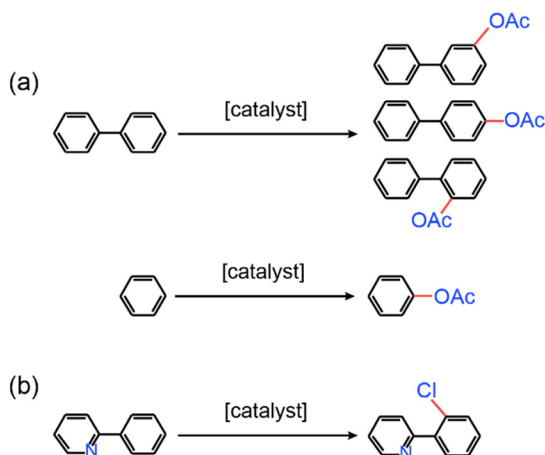


Figure 4.2.

Examples of catalytic reactions catalysts for which were analysed in this thesis. (a) Acetoxylation of biphenyl (the products can have one of the three structures depending on the aim of the reaction and type of the catalyst) and acetoxylation of benzene. Acetoxy group ($\text{CH}_3\text{-COO}^-$) is shown in the figure as OAc. (b) Chlorination of 2-phenylpyridine⁵.

4.3. XPS Studies of Catalyst Systems

In this section I describe how I have used electron spectroscopy to characterise the different heterogeneous catalyst samples prepared using the approaches discussed in Chapter 1.

Approach 1: Heterogenisation of the catalyst on a polymer support using covalent bonds – catalyst complex immobilised via two arms

Paper I reports a covalently bonded catalytic Pd complex in a polymer matrix for the acetoxylation reaction. I used XPS to characterise both the complex itself and the immobilised complex (cf. the chemical structures in Figure 2.8). More specifically, the studied samples were the catalytic complex (labelled **4b**), the polymer (**7b**) and the polymer after removing the pyridine ligand (**7bAN**). As will be reported below, also the catalyst after a catalytic reaction was studied.

The Pd 3d and Cl 2p XPS signals of three samples **4b**, **7b** and **7bAN** are shown in Figure 4.3. In Figure 4.3a the Pd 3d doublet is seen with binding energies of around 340 (Pd 3d_{5/2}) and 345.5 eV (Pd 3d_{3/2}) for all three samples. The values are in good agreement with a Pd^{II} oxidation state. A more precise look reveals that the binding energies are the same for the **4b** and **7b** samples, while a small shift is observed between the **4b/7b** samples on the one hand and the **7bAN** sample on the other. This is probably due to an exchange of the original pyridine ligand with acetonitrile. This ligand exchange causes a change in chemical environment of the Pd atoms, which then leads to the chemical shift.

An important result is that the highlighted region in the Pd 3d core level in Figure 4.3a at a binding energy of around 335 eV does not contain any peak. In this region one would find any signal related to the Pd⁰ oxidation state or Pd in the metallic state. That there is no peak for neither of the samples illustrates that no reduction of the Pd ions in the complex occurs during polymerisation and ligand exchange¹³⁶⁻¹³⁹.

The corresponding Cl 2p signals are shown in Figure 4.3b. For the **4b** sample one can see a single doublet with Cl 2p_{3/2} and Cl 2p_{1/2} binding energies of 199.8 and 201.4 eV, respectively. This is as expected from the structure of the palladium complex in Figure 2.8a: there is only one type of Cl in the structure and hence only a single doublet should be observed. After polymerisation (sample **7b**) the peak of a new species appears at lower binding energy. Thus, the polymerisation seems to introduce large differences in the chemical environment for the Cl atoms, depending on the exact configuration, and the signal suggests that there is more than one configuration. The polymerisation also goes along with a broadening of the signal, which is another sign of diversification of the chemical environments. For polymer **7bAN** a signal broadening towards higher binding energy is observed with a new doublet appearing at around 201.9 eV. This binding energy can be related to C-Cl

bonds^{53,140}. This signal is likely due to an addition of Cl to the vinyl groups during the washing step (with triflic acid). This washing step is carried out to remove the pyridine from the Pd centres of the bonded complex.

In order to study the recyclability of catalyst **7b** in the C-H acetoxylation of biphenyl (Figure 4.4a), the samples were used in four catalytic cycles and characterised after each step. Figure 4.4b shows corresponding Pd 3d spectra. Here, XPS was measured after washing and drying of the used catalyst. It is seen that a small shift towards lower binding energy occurs between the fresh polymer **7b** and that used in the catalytic reaction. The shift can be ascribed to ligand exchange between Cl bonded to Pd and acetate¹⁻⁵. After that the binding energy stays at around 339.3 (Pd 3d_{5/2}) and 344.6 eV (Pd 3d_{3/2}) in all catalytic cycles and, hence, the catalyst retains its state. Although no further investigation was carried out on additional, the results suggest that the catalyst remains active and effective.

Again, no Pd⁰ or Pd in metallic state can be observed. The absence of the zero oxidation state after synthesis and catalysis is important since it suggest that no Pd leaching occurs. This also implies that contamination of the final product with Pd is unlikely.

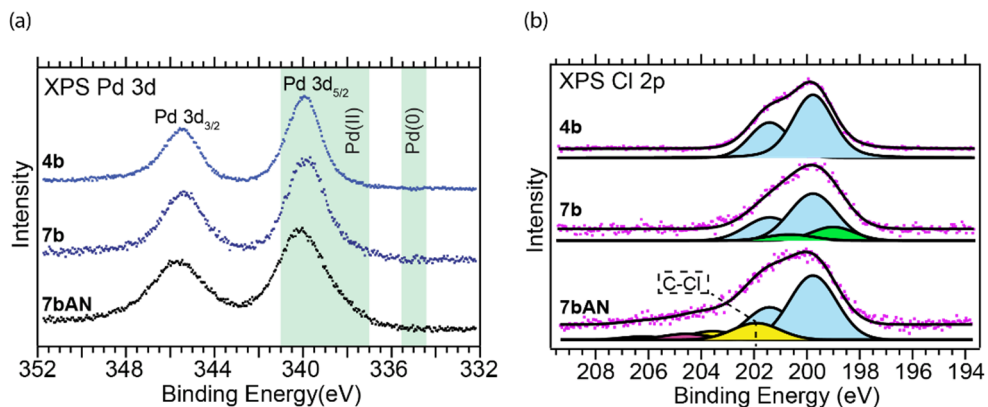


Figure 4.3.

(a) Pd 3d and (b) Cl 2p core levels of the **4b**, **7b** and **7bAN** samples. The graphs are modified from references 1,5.

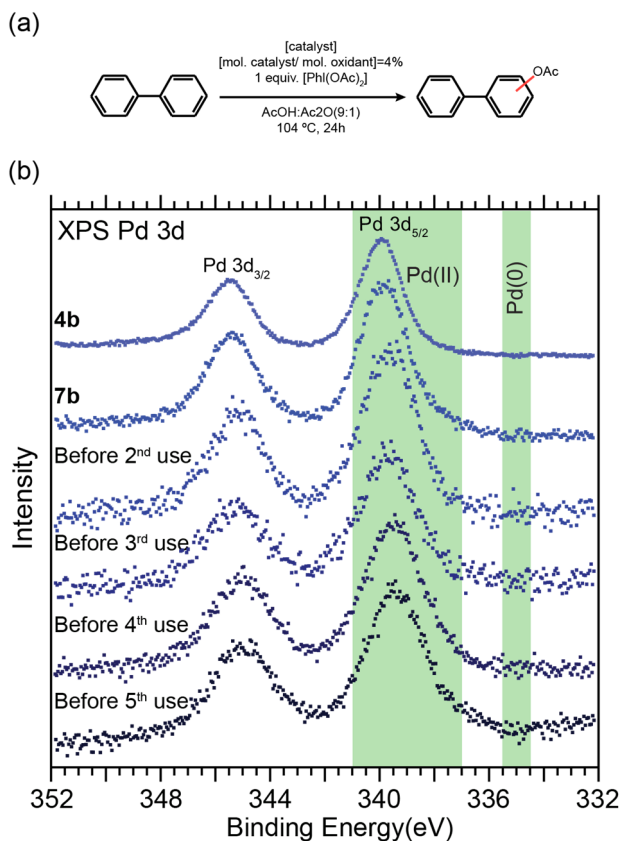


Figure 4.4.

Pd 3d core level of **4b**, **7b** and of **7b** after being used in the catalytic acetoxylation reaction of biphenyl. Graph is modified from reference 1 and 5.

Approach 1: Heterogenisation of the catalyst on a polymer support using covalent bonds – catalyst complex immobilised via one arm

In Paper II two new catalytic Pd complexes for C-H halogenation are reported. Their structures, together with their polymerised counterparts are shown in Figure 4.5. The main difference between Pd complex **4b** in paper I and complexes **1a** and **5b** in paper II is that the latter are immobilised via only one arm (Figure 4.5b and d). Samples with one arm have more freedom for mobility and hence can have different orientations during reaction. This can also help the reaction products to leave the catalytic active centre and go into solution faster. Further, in **5b** this arm is not even connected to any of the N atoms of the N-heterocyclic carbene (NHC) imidazole moiety, but instead through the backbone of the carbene ring. This configuration changes the electron density on the carbene ring which will in result in electron density change on Pd as the catalytic centre of the complex.

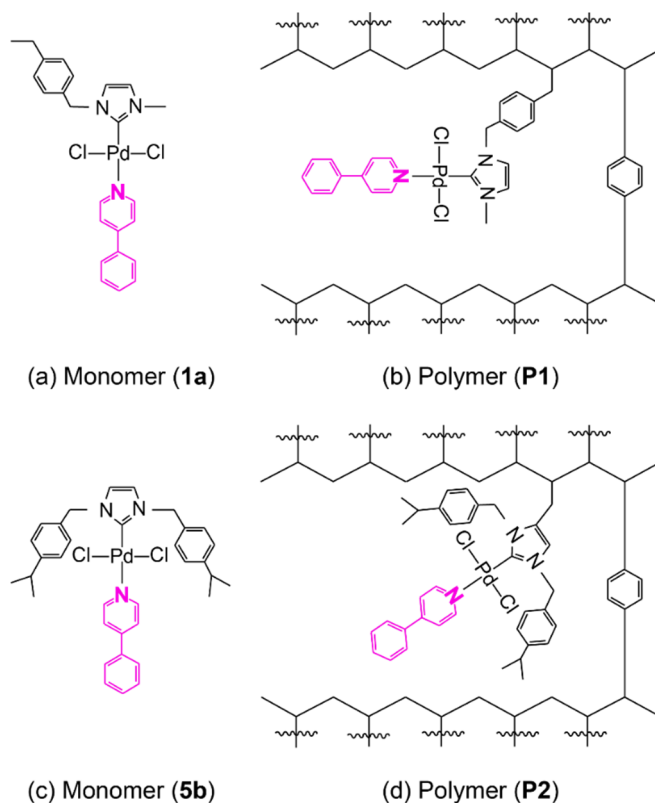


Figure 4.5.

Catalytic Pd complexes **1a** and **5b** for polymerisation via one arm together with their polymerised counterparts **P1** and **P2**. Figures are modified from reference 5.

The XP spectra of samples **1a**, **5b**, **P1** and **P2** are shown in Figure 4.6. In the Pd 3d spectra in Figure 4.6a, two regions are highlighted at around 335 and 338 eV. These are related to the Pd⁰ and Pd^{II} oxidation states, respectively¹⁴¹. Obviously, there is no sign for Pd⁰ or Pd in the metallic state for the Pd complexes and the polymer samples. Therefore, polymerisation does not cause any Pd complex reduction, but the original Pd^{II} oxidation state is retained.

In Figure 4.6b the corresponding Cl 2p core level spectra are presented. A slight broadening observed for the polymer samples suggests the presence of differences in chemical environment for the Cl atoms in these samples. The overall result is, however, quite much as expected from the similarities in the structures.

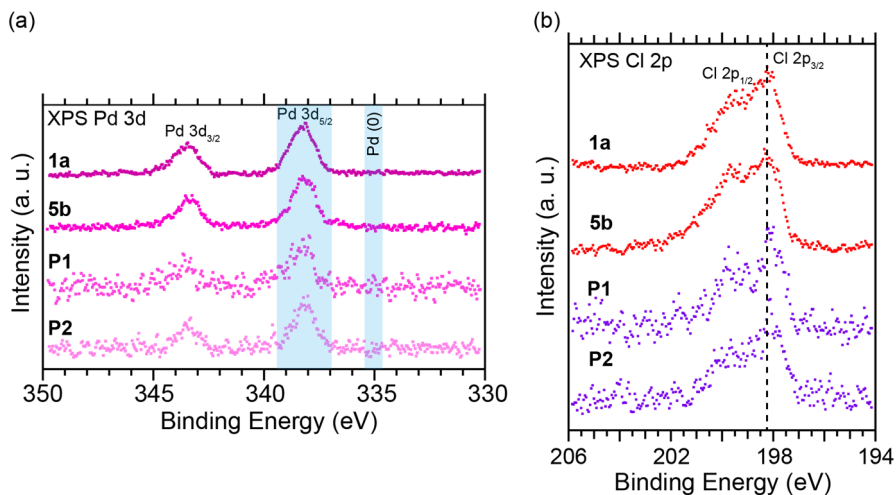


Figure 4.6. (a) Pd 3d and (b) Cl 2p core level spectra of the **1a**, **5b**, **P1** and **P2** samples. The graph is modified from reference 1 and 5.

Polymer-Supported Catalysts from heterogenisation approach 1 and XPS: Issues

Measuring XP spectra on organic or organometallic compounds can be difficult. The two main problems that occur – and that depend on the material, photon flux and photon energy – are sample charging and sample damage (also known as beam damage).

In conductive samples the electrons that leave the sample due to the photoexcitation are compensated by a current from the sample plate which is in contact with the sample holder and finally ground. Therefore, an infinite source of electrons is available to compensate the lack of electrons, and positive charge accumulation on the sample surface is avoided.

In the case of insulating and large-bandgap semiconductors, the situation is not the same. The lack of electrons causes a positive charge on the surface. This charge interacts with the outgoing photoelectrons and ultimately changes the peak positions. This change can amount from several eV to several tenths or even hundreds of eV. In order to solve this problem a good electrical contact with the sample holder, using a conductive mesh on the sample surface can sometimes overcome the problem. In other cases, charging is constant in time and homogeneous all over the sample, and then it is easy to calibrate all spectra with respect to a known peak's binding energy⁷¹. This solution is, however, not viable in the case of strong differential charging on an inhomogeneous sample.

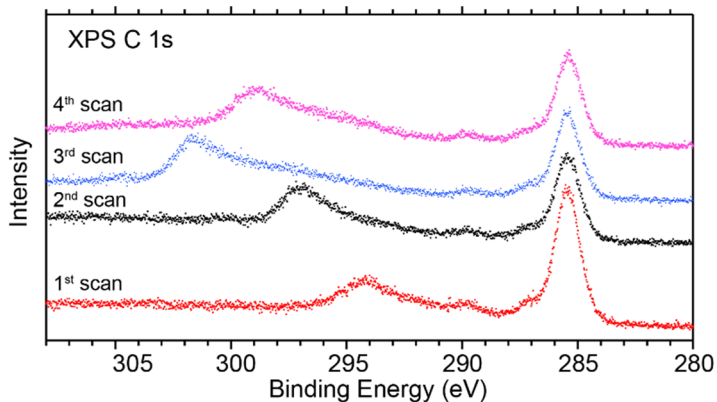


Figure 4.7.

XPS analysis of polymer **7b** samples at I311 beamline at MAX IV laboratory. The peaks position cannot be assigned correctly since the peak position is not reliable due to the charging on the sample surface.

One solution to avoid the effects of sample charging is to use an electron flood gun, which delivers low energy electrons to the sample surface. However, due to the interaction between the low-energy electrons and the sample, this can cause changes in the sample, which might be difficult to realise.

As described above, in my work I analysed polymerised catalyst complexes, i.e. transition metal complexes embedded in a block copolymer matrix. The samples are non-conductive enough and may experience sample charging. This is illustrated in Figure 4.7 for a measurement that I performed at beamline I311 at the old MAX-lab synchrotron radiation source. The figure shows four different, subsequent scans of a C 1s XPS measurement on polymer **7b** in paper I. During measurement the sample was moved in order to avoid beam damage. The differential charging effect is obvious: both different shifts, peak broadenings and extra peaks are seen, but also a non-perturbed C 1s peak.

In order to solve this issue samples were prepared with less amount of the material on the Si wafer substrate, and more importantly a lab source X-ray anode was used instead of synchrotron light. Using a lab source anode with lower flux and bigger beam spot reduced the intensity of light on the sample surface. This resulted in a lower signal and more scans had to be acquired and summed up later. While this is a disadvantage, it was outweighed by that charging was not observed anymore. It is important to note that there was no sign of change between separate scans.

Another issue that I had with the samples was strong beam damage due to the high photon flux. Beam damage using X-ray source can be due to direct interaction between incident beam and the sample causing photo degradation of the sample. It can also be due to the interaction of the secondary radiation produced by the incident beam. Auger and secondary electrons produced in the XPS process can also interact

with the sample and cause damage to the surface¹⁴². At the new SPECIES beamline, operated on the MAX II electron storage ring, the photon flux had increased so much that beam damage became forbidding: no result could be obtained in several attempts. Even though the sample was moved under the beam, beam damage was so fast that the catalyst samples were destroyed immediately and no meaningful data could be acquired. This means that a small beam spot and very high photon flux are not desirable for the polymer sample measurements. However, the use of a lower intensity X-ray light source was successful: the spectra that are shown above were measured using X-ray tubes at the SPECIES and HIPPIE beamlines. Of course, the lower photon flux and bigger beam spot resulted in intensity and less favourable statistics and thus slower data acquisition. Nevertheless, use of a lab source turned out to be more reliable for analysing the polymer samples.

Approach 2: Heterogenisation of the catalyst on a reduced graphene oxide support using non-covalent interactions

Papers III and IV deal with the immobilisation of catalytic Pd complexes (cf. Figure 4.8 for the structures of complexes **1@rGO** and **2@rGO**) on rGO using π - π stacking¹⁹, i.e. a non-covalent bond. The catalyst material is similar to that synthesised in conjunction with the work reported in papers I and II, but the Pd NHC complexes are now modified by the addition of either one (**1@rGO**) or two (**2@rGO**) anthracene groups to allow for π - π stacking. As with material **7a** the target catalytic reaction was the acetoxylation of benzene and biphenyl. The rGO support is catalytically inert and has a large surface area, which helps to disperse the immobilised catalyst and avoid catalyst agglomeration on the surface. It is also known that rGO can tune the activity and selectivity of some complex catalysts¹⁹.

The Cl 2p core level lines of **1**, fresh **1@rGO** and **1@rGO** after acetoxylation are shown in Figure 4.9. For comparison a Cl 2p reference XP spectrum of chloropyridine is also shown. The broadening of the peaks in the spectra of **1**, fresh **1@rGO** and **1@rGO** after acetoxylation suggests the presence of more than one species on the surface. The structure of Pd complex **1** suggests that the Cl 2p XP spectrum should contain two doublets. Indeed, two components are found at Cl 2p_{3/2} binding energies of 197.7 and 198.7 eV. The former is related to Cl binding to Pd and the latter to Cl in chloropyridine, bonded to Pd. These two components have the correct 2:1 intensity ratio.

The appearance of the Cl 2p spectra changes quite drastically after immobilisation of the complex **1** on rGO. For fresh **1@rGO** the Cl-Pd component is retained, but broadened, while the chloropyridine-Pd component has disappeared. A new component at higher binding energy has appeared instead. Only this latter component survives after use of the catalyst in the acetoxylation reaction (sample **1@rGO** after acetoxylation).

In order to identify the high-binding energy component, I made a reference measurement on rGO onto which chloropyridine was dropped. Chloropyridine has a high vapour pressure and thus the measurement had to be done quickly and on several identically prepared samples. Summing up all the Cl 2p spectra from these samples shows that the binding energy of Cl in rGO-bonded chloropyridine is at 200.3 eV. To my knowledge this result or any result for a similar graphite/graphene-like surface has not been reported before. The observation of a peak at the very same binding energy peak for the **1@rGO** samples is strong evidence for that that chloropyridine is separated from the complex after immobilisation on rGO. It sticks directly to the surface by π - π stacking.

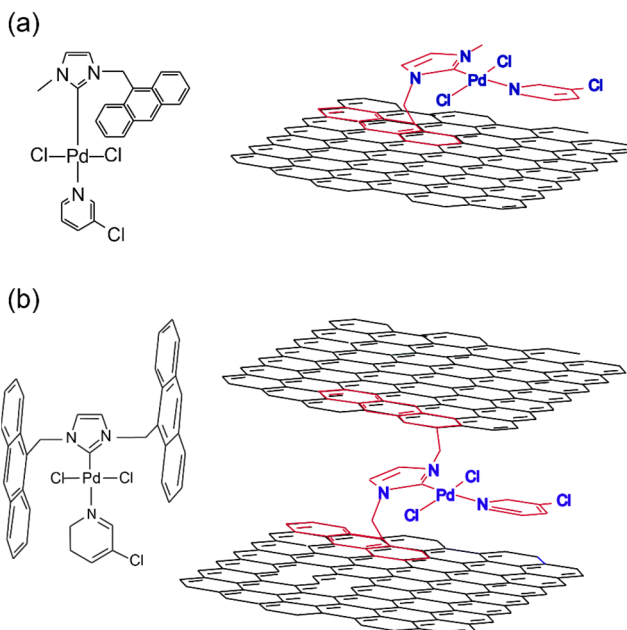


Figure 4.8.

Catalytic Pd complexes modified with (a) one or (b) two anthracene groups and sketch of the suggested immobilised structures on rGO using non-covalent . Figure modified from reference 1.

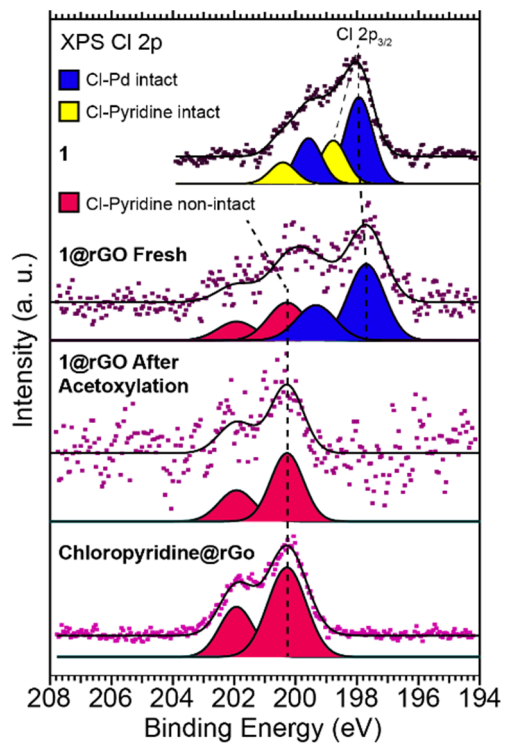


Figure 4.9.

Cl 2p XP spectra of **1c**, fresh **1@rGO**, **1@rGO** after acetoxylation and **chloropyridine@rGO**. Figure is modified from reference 5.

5. Conclusion and Remarks

The aim of my thesis was to synthesise a new heterogeneous transition metal catalyst for direct C-H activation by using concept similar to *molecular imprinting*, i.e. encapsulating the catalyst complex in a suitable cavity adapted to the desired reaction product. I studied catalytic transition metal complexes – NHC Pd complexes – that were heterogenised via three different approaches using covalent and non-covalent bonds: (1) heterogenisation of the catalyst on a polymer support using covalent bonds, (2) heterogenisation of the catalyst on a reduced graphene oxide support using non-covalent interactions and (3) immobilisation of the catalyst on an inorganic surface using covalent bonds and encapsulation in an inorganic matrix.

The first approach was used to synthesise new catalysts by anchoring the catalyst complex to the carbon chain using two linking groups attached to the nitrogen atoms in the carbene ring. In the second paper one arm was used for anchoring the catalyst complex to the polymer chain. Furthermore, in the second paper the anchoring arm was attached to the backbone of the imidazole moiety of the catalyst to provide more mobility and to avoid changes in the carbene ring properties, which potentially could lead to changes in the electron density of catalytically active Pd ions. These catalysts were also used in reactions, recycled and then analysed using UHV XPS. The XPS results show that the synthesis of the catalysts and their heterogenisation using a polymerisation approach were successful for both “one-arm” and “two-arm” catalysts. No change in the oxidation state of Pd was observed: the catalyst was stable during synthesis, polymerisation and catalytic reaction. TEM proved that there is no sign of Pd nanoparticles in the polymer matrix and, furthermore, the Pd atoms are distributed evenly in the matrix. It turned out that the approach did not allow proper encapsulation of the catalyst in a cavity due to the shape of the polymer: the catalysts are attached from one side to the carbon chain, and the polymer matrix cannot extend to cover the area around the catalyst. Nevertheless, the catalysts’ activity and selectivity was favourable.

In the second approach used in papers III and IV catalytic transition metal complexes were immobilised on an rGO surface using π -stacking between anthracene groups of catalyst complexes and the rGO surface. These catalysts were successfully used in halogenation reactions. The XPS analysis showed that there was no sign of Pd⁰, which proves that the Pd in the complex is stable throughout

synthesis, immobilisation on the rGO surface, catalysis and recovery. TEM also showed a homogenous distribution of the catalyst complexes on rGO and no sign of Pd nanoparticles. Again, encapsulation of the catalyst was not possible given the shape of the support.

In paper V I employed APXPS combined with DFT calculations to study the electronic structure of two widely used ALD precursors: TDMAHf and TDMAT. This study showed that π -donation from the amide ligands to the metal cause slight changes in the electronic structure, not only in the valence molecular orbitals, but also in the core levels. DFT contributed strongly to an increased understanding. This study is a good example of how DFT successfully can be combined with experiment.

Finally, in paper VI I report an *operando* study of ALD of HfO₂ on *in situ*-oxidised SiO₂/Si(111). In this study, surface chemical reactions were followed with 13 s temporal resolution. By using the snapshot mode of the analyser instead of the swept mode, the required measurement time for one core level could be decreased considerably. APXPS helped to bridge the pressure and time gaps between the ALD process and XPS measurements. *Operando* measurements helped to follow the surface species during each ALD half cycle and evacuation of the chamber. The results show that reactions start as soon as a TDMAHf precursor reaches the surface. Changes in Hf 4f, N 1s and C 1s clearly show that the precursor is adsorbed and reacts on the surface. MMI as a result of a β -hydride elimination reaction is observed at later stages of the reaction.

Also here, DFT helped to complete the understanding of the reaction mechanism and identify the spectral fingerprints of surface chemical species in APXPS. The calculations suggest that the reaction between the surface and precursor can be triggered by water or hydroxyls. Both ligand exchange and β -hydride elimination towards MMI seem feasible.

Also the ALD water half cycle was monitored. An abrupt shift in the binding energy of the Hf 4f core level occurs upon water dosing, which is due to the production of HfO₂ on the surface. A sudden decrease in the N 1s and C 1s intensities shows the removal of undesired precursor material from the surface, which, however, is far from complete.

6. Outlook

The fundamental studies reported in this thesis on the synthesis of a heterogeneous catalyst for direct C-H activation provides the possibility for further investigation on these systems. I would like to suggest the study of the heterogeneous catalysts designed within the context of this thesis in ambient pressure experiments. APXPS could give more insight about the reaction mechanisms and activity of the catalysts.

One could also pursue a DFT study of the one-arm and two-arm complexes studied in papers I-VI. This could expand the understanding of the difference between the electron density on the catalytically active centres of the immobilised one-arm and two-arm catalysts. An ambient pressure XPS investigation together with DFT calculation could help to understand reaction mechanisms and improve the design or synthesis process.

Another suggestion is to study the immobilisation of catalytic transition metal complexes on rGO using near-edge X-ray absorption fine structure (NEXAFS) spectroscopy. Such a study would help to find out about the orientation of the catalyst complexes on the rGO surface. Also here, APXPS and DFT could provide further insight into the nature of the catalysts and their reactivity behaviour.

The HfO₂ ALD investigation could be expanded to different surfaces. Experiments that I performed but where the results are not presented in this thesis include the ALD on a pristine Si(111) surface. In addition, the ALD of HfO₂ on a native oxide on Si(111) was also studied. As can be seen in Figure 6.1, the substrate structure can strongly affect the ALD growth of HfO₂: while the interaction of TDMAHf with clean Si(111) is slow, it is very rapid on the native oxide-covered surface. As soon as the TDMAHf dose is applied, the Si 2p line disappears in the measurement on the native oxide surface. However, in the case of the clean Si(111) surface very little change is observed. This shows a much less strong interaction between TDMAHf and the clean Si(111) surface in comparison to that between TDMAHf and the native oxide.

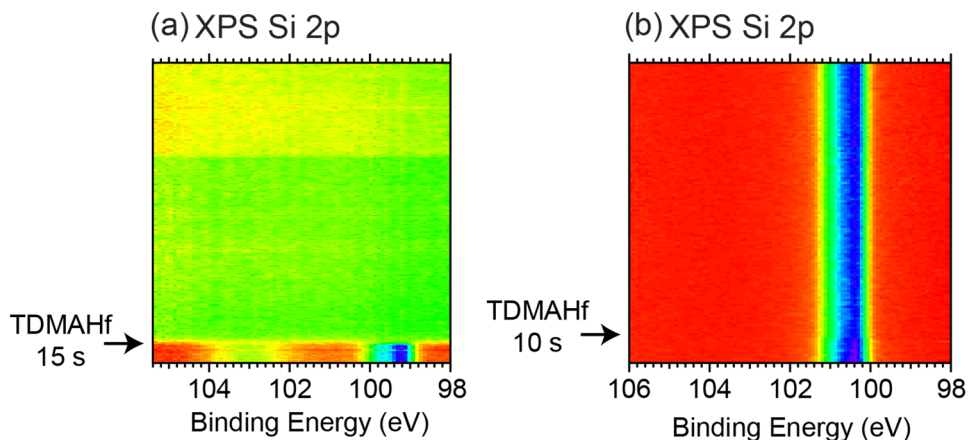


Figure 6.1.

Si 2p XPS surface spectra during dosing TDMAHf: (a) native oxide SiO₂/Si(111) and (b) clean Si(111). Surface XP spectra consists of 200 and 140 scans for native and clean surface, respectively.

Removing the native oxide layer from the SiO₂/Si(111) surface and hydrogen-terminating it, could also make for an interesting study. The surface is rather inert and can stay clean for longer time in air and even more so in a UHV chamber. This will limit the effect of any undesired contamination that can change the chemistry of TDMAHf on the surface. Hydrogen atoms on the surface can also trigger the interaction between TDMAHf and Si(111) surface in a different way in comparison to what has already been studied.

As mentioned in the introduction, the aim of my research was to apply the *molecular imprinting* concept by immobilising a catalytic transition metal complex on inorganic surface, encapsulating the catalyst inside an inorganic matrix and leaving a cavity close to the catalytically active centre of the catalyst by removing the template molecule attached to the catalyst complex. This design should in the end result in a good selectivity of the catalyst. In collaboration with the Chemistry Department a new catalyst for immobilisation has already been designed. Further studies can include the immobilisation of this new catalyst on an inorganic surface such as Si(111), employing NEXAFS to study the orientation of the catalyst, using APXPS to provide information about the interaction of the molecule with the surface and its surface chemistry of the surface during encapsulation. It is important to make sure that the catalyst is capable of orienting itself on the surface such that the catalytic active centre is not buried under the inorganic matrix. The catalyst should also be stable and not dissociate during immobilisation and ALD growth.

In order to be closer to real ALD conditions one could think of designing an APXPS reaction cell similar to industrial ALD cells. Potentially, this could very much improve the dosing and evacuating steps of the ALD half cycles. Gathering

information at high time resolution combined with faster process could help to answer important questions about the formation of the interfacial layer in ALD. By decreasing the amount of precursor dosed on to the surface and faster evacuation, changes in the chemistry of the surface could be observed better.

7. References

- (1) Majeed, M. H.; Shayesteh, P.; Wallenberg, L. R.; Persson, A. R.; Johansson, N.; Ye, L.; Schnadt, J.; Wendt, O. F. *Chemistry - A European Journal* **2017**, *23*, 8457–8465.
- (2) Ertl, G. *Angewandte Chemie International Edition* **2008**, *47*, 3524–3535.
- (3) Muratsugu, S.; Maity, N.; Baba, H.; Tasaki, M.; Tada, M. *Dalton Transactions* **2017**, *46*, 3125–3134.
- (4) Muratsugu, S.; Tada, M. *Accounts of Chemical Research* **2013**, *46*, 300–311.
- (5) Majeed, M. H. C-H Activation Reactions Mediated by Pd Based Heterogeneous Catalysts: Regioselective Formation of C-O and C-X Bonds, PhD thesis, Lund University: Lund, **2018**.
- (6) Barbaro, P., Liguori, F., Eds. *Heterogenized Homogeneous Catalysts for Fine Chemicals Production: Materials and Processes*, Springer: Dordrecht; New York, **2010**.
- (7) Hübner, S.; de Vries, J. G.; Farina, V. *Advanced Synthesis & Catalysis* **2016**, *358*, 3–25.
- (8) Copéret, C.; Basset, J.-M. *Advanced Synthesis & Catalysis* **2007**, *349*, 78–92.
- (9) Cole-Hamilton, D. J. *Science* **2003**, *299*, 1702–1706.
- (10) Blanksby, S. J.; Ellison, G. B. *Accounts of Chemical Research* **2003**, *36*, 255–263.
- (11) Adams, N. G.; Richardson, D. M. *Analytical Chemistry* **1953**, *25*, 1073–1074.
- (12) Verma, D. K.; Tombe, K. des. *AIHA Journal* **2002**, *63*, 225–230.
- (13) Alexander, C.; Andersson, H. S.; Andersson, L. I.; Ansell, R. J.; Kirsch, N.; Nicholls, I. A.; O'Mahony, J.; Whitcombe, M. J. *Journal of Molecular Recognition* **2006**, *19*, 106–180.
- (14) Tada, M.; Iwasawa, Y. *Journal of Molecular Catalysis A: Chemical* **2003**, *199*, 115–137.
- (15) Ye, L.; Mosbach, K. *Chemistry of Materials* **2008**, *20*, 859–868.
- (16) Wulff, Gü.; Liu, J. *Accounts of Chemical Research* **2012**, *45*, 239–247.
- (17) Haupt, K.; Mosbach, K. *Chemical Reviews* **2000**, *100*, 2495–2504.
- (18) Wolfgang A. Hermann, Schütz J., Frey G. D, Herdtweck Eb. *Organometallics* **2006**, *25*, 2437–2448.
- (19) Georgakilas, V.; Tiwari, J. N.; Kemp, K. C.; Perman, J. A.; Bourlinos, A. B.; Kim, K. S.; Zboril, R. *Chemical Reviews* **2016**, *116*, 5464–5519.
- (20) Triyoso, D.; Liu, R.; Roan, D.; Ramon, M.; Edwards, N. V.; Gregory, R.; Werho, D.; Kulik, J.; Tam, G.; Irwin, E.; Wang, X. -D, La, L. B.; Hobbs, C.; Garcia, R.; Baker,

- J.; White Jr., B. E.; Tobin, P. *Journal of The Electrochemical Society* **2004**, *151*, F220.
- (21) Lange, S.; Kiisk, V.; Reedo, V.; Kirm, M.; Aarik, J.; Sildos, I. *Optical Materials* **2006**, *28*, 1238–1242.
- (22) Timm, R.; Head, A. R.; Yngman, S.; Knutsson, J. V.; Hjort, M.; McKibbin, S. R.; Troian, A.; Persson, O.; Urpelainen, S.; Knudsen, J. *Nature Communications* **2018**, *9*.
- (23) Li, K.; Li, S.; Li, N.; Dixon, D. A.; Klein, T. M. *Journal of Physical Chemistry C* **2010**, *114*, 14061–14075.
- (24) Green, M. L.; Ho, M.-Y.; Busch, B.; Wilk, G. D.; Sorsch, T.; Conard, T.; Brijs, B.; Vandervorst, W.; Räisänen, P. I.; Muller, D.; Bude, M.; Grazul, J. *Journal of Applied Physics* **2002**, *92*, 7168–7174.
- (25) Li, K.; Li, S.; Li, N.; Klein, T. M.; Dixon, D. A. *The Journal of Physical Chemistry C* **2011**, *115*, 18560–18571.
- (26) Dkhissi, A.; Mazaleyrat, G.; Estève, A.; Rouhani, M. D. *Physical Chemistry Chemical Physics* **2009**, *11*, 3701.
- (27) Lee, J.-C.; Oh, S.-J.; Cho, M.; Hwang, C. S.; Jung, R. *Applied Physics Letters* **2004**, *84*, 1305–1307.
- (28) Wang, W.; Nabatame, T.; Shimogaki, Y. *Surface Science* **2005**, *588*, 108–116.
- (29) Deshpande, A.; Inman, R.; Jursich, G.; Takoudis, C. *Microelectronic Engineering* **2006**, *83*, 547–552.
- (30) Hackley, J. C.; Gougousi, T.; Demaree, J. D. *Journal of Applied Physics* **2007**, *102*, 034101.
- (31) Lee, B. H.; Kang, L.; Nieh, R.; Qi, W.-J.; Lee, J. C. T. *Applied Physics Letters* **2000**, *76*, 1926–1928.
- (32) Barrett, N.; Renault, O.; Damlencourt, J.-F.; Martin, F. *Journal of Applied Physics* **2004**, *96*, 6362–6369.
- (33) Cho, M.-H.; Roh, Y. S.; Whang, C. N.; Jeong, K.; Nahm, S. W.; Ko, D.-H.; Lee, J. H.; Lee, N. I.; Fujihara, K. *Applied Physics Letters* **2002**, *81*, 472–474.
- (34) Head, A. R.; Chaudhary, S.; Olivieri, G.; Bournel, F.; Andersen, J. N.; Rochet, F.; Gallet, J.-J.; Schnadt, J. *The Journal of Physical Chemistry C* **2016**, *120*, 243–251.
- (35) Cho, M.; Jeong, D. S.; Park, J.; Park, H. B.; Lee, S. W.; Park, T. J.; Hwang, C. S.; Jang, G. H.; Jeong, J. *Applied Physics Letters* **2004**, *85*, 5953–5955.
- (36) Miikkulainen, V.; Leskelä, M.; Ritala, M.; Puurunen, R. L. *Journal of Applied Physics* **2013**, *113*, 021301.
- (37) Harris, P. G.; Trigg, A. D. *Materials & Design* **1988**, *9*, 127–134.
- (38) Van Bui, H.; Grillo, F.; van Ommen, J. R. *Chemical Communications* **2017**, *53*, 45–71.
- (39) Turner, N. H. S. *Analytical Chemistry* **1988**, *60*, 377–387.
- (40) Siegbahn, K., *ESCA Applied to Free Molecules*; North-Holland Pub. Co: Amsterdam, **1969**.
- (41) Povstugar, V. I.; Tyurin, S. A.; Kodolov, V. I. *Polymer Science U.S.S.R.* **1985**, *27*, 1–18.

- (42) Hüfner, S. *Photoelectron Spectroscopy: Principles and Applications*; Springer Berlin Heidelberg: Berlin, Heidelberg, **2003**.
- (43) Powell, C. J. *Surface Science* **1974**, *44*, 29–46.
- (44) Jablonski, A.; Powell, C. *Journal of Electron Spectroscopy and Related Phenomena* **1999**, *100*, 137–160.
- (45) Berglund, C. N.; Spicer, W. E. *Physical Review* **1964**, *136*, A1030–A1044.
- (46) Werner, W. S. M.; Tratnik, H.; Brenner, J.; Störi, H. *Surface Science* **2001**, *495*, 107–119.
- (47) Damascelli, A.; Hussain, Z.; Shen, Z.-X. *Reviews of Modern Physics* **2003**, *75*, 473–541.
- (48) Seah, M. P.; Dench, W. A. *Surface and Interface Analysis* **1979**, *1*, 2–11.
- (49) Chaudhary, S.; *Modification of Oxide Surfaces with Functional Organic Molecules, Nanoparticles, and Hetero-Oxide Layers*; PhD thesis, Lund University, **2016**.
- (50) Manne, R.; Åberg, T. Koopmans' *Chemical Physics Letters* **1970**, *7*, 282–284.
- (51) Arman, M. A.; Klein, A.; Ferstl, P.; Valookaran, A.; Gustafson, J.; Schulte, K.; Lundgren, E.; Heinz, K.; Schneider, A.; Mittendorfer, F.; et al. *Surface Science* **2017**, *656*, 66–76.
- (52) Tissot, H.; Gallet, J.-J.; Bourmel, F.; Naitabdi, A.; Pierucci, D.; Bondino, F.; Magnano, E.; Rochet, F.; Finocchi, F. *The Journal of Physical Chemistry C* **2014**, *118*, 1887–1893..
- (53) Kang, E. T.; Ti, H. C.; Neoh, K. G.; Tan, T. C. *Polymer Journal* **1988**, *20*, 399–406.
- (54) Gao, J.; Teplyakov, A. V. *Catalysis Today* **2014**, *238*, 111–117.
- (55) Schnadt, J.; Knudsen, J.; Andersen, J. N.; Siegbahn, H.; Pietzsch, A.; Hennies, F.; Johansson, N.; Mårtensson, N.; Öhrwall, G.; Bahr, S.; et al. *Journal of Synchrotron Radiation* **2012**, *19*, 701–704.
- (56) Urpelainen, S.; Sâthe, C.; Grizolli, W.; Agâker, M.; Head, A. R.; Andersson, M.; Huang, S.-W.; Jensen, B. N.; Wallén, E.; Tarawneh, H.; *Journal of Synchrotron Radiation* **2017**, *24*, 344–353.
- (57) Baudalet, F.; Belkhou, R.; Briois, V.; Coati, A.; Dumas, P.; Et, A. *Oil & Gas Science and Technology* **2005**, *60*, 849–874.
- (58) Bartzsch, S.; Oelfke, U. *Physics in Medicine & Biology* **2017**, *62*, 8600–8615.
- (59) Salmeron, M.; Schlogl, R. *Surface Science Reports* **2008**, *63*, 169–199.
- (60) Starr, D. E.; Liu, Z.; Hävecker, M.; Knop-Gericke, A.; Bluhm, H. *Chemical Society Reviews* **2013**, *42*, 5833.
- (61) Knudsen, J.; Andersen, J. N.; Schnadt, J. *Surface Science* **2016**, *646*, 160–169.
- (62) Bluhm, H.; Hävecker, M.; Knop-Gericke, A.; Kiskinova, M.; Schlögl, R.; Salmeron, M. *MRS Bulletin* **2007**, *32*, 1022–1030.
- (63) Eriksson, S. K.; Hahlin, M.; Kahk, J. M.; Villar-Garcia, I. J.; Webb, M. J.; Grennberg, H.; Yakimova, R.; Rensmo, H.; Edström, K.; Hagfeldt, A.; *Review of Scientific Instruments* **2014**, *85*, 075119.
- (64) Ogletree, D. F.; Bluhm, H.; Lebedev, G.; Fadley, C. S.; Hussain, Z.; Salmeron, M. *Review of Scientific Instruments* **2002**, *73*, 3872–3877.

- (65) Axnanda, S.; Crumlin, E. J.; Mao, B.; Rani, S.; Chang, R.; Karlsson, P. G.; Edwards, M. O. M.; Lundqvist, M.; Moberg, R.; Ross, P.; *Scientific Reports* **2015**, *5*.
- (66) Kaya, S.; Ogasawara, H.; Näslund, L.-Å.; Forsell, J.-O.; Casalongue, H. S.; Miller, D. J.; Nilsson, A. *Catalysis Today* **2013**, *205*, 101–105.
- (67) Frank Ogletree, D.; Bluhm, H.; Hebenstreit, E. D.; Salmeron, M. *Nuclear Instruments and Methods in Physics Research Section A: Accelerators, Spectrometers, Detectors and Associated Equipment* **2009**, *601*, 151–160.
- (68) Shavorskiy, A.; Karslioglu, O.; Zegkinoglou, I.; Bluhm, H. *Synchrotron Radiation News* **2014**, *27*, 14–23.
- (69) Polack, F.; Silly, M.; Chauvet, C.; Lagarde, B.; Bergéard, N.; Izquierdo, M.; Chubar, O.; Krizmancic, D.; Ribbens, M.; Duval, J.-P.; Basset, C.; Kubsy, S.; Sirotti, F. *AIP Conference proceedings* **2010**, 185–188.
- (70) Roy, K.; Artiglia, L.; van Bokhoven, J. A. *ChemCatChem* **2018**, *10*, 666–682.
- (71) Niemantsverdriet, J. W. *Spectroscopy in Catalysis: An Introduction*, 3rd completely rev. and enl. ed.; Wiley-VCH, Chichester, **2007**.
- (72) Rullik, L. Industrial Alloys Studied by Surface Sensitive Techniques, PhD thesis, Lund University, **2018**.
- (73) Published Specifications for SU9000 HITACHI's New Premium SEM. <https://www.hitachi-hightech.com/html>. **2019**.
- (74) Liu, J. High-Resolution Scanning Electron Microscopy. In *Handbook of Microscopy for Nanotechnology*; Yao, N., Wang, Z. L., Eds.; Kluwer Academic Publishers: Boston, **2005**; pp 325–359.
- (75) Goldstein, J. *Scanning Electron Microscopy and X-Ray Microanalysis*, 3rd Ed.; Kluwer Academic/Plenum Publishers: New York, **2003**.
- (76) Anka, P. *International Journal of Current Microbiology and Applied Sciences* **2018**, *7*, 743–747.
- (77) Kaiser, U.; Muller, D. A.; Grazul, J. L.; Chuvilin, A.; Kawasaki, M. Direct Observation of Defect-Mediated Cluster Nucleation. *Nature Materials* **2002**, *1*, 102–105.
- (78) Liu, J. *Microscopy* **2005**, *54*, 251–278.
- (79) Kisielowski, C.; Freitag, B.; Bischoff, M.; van Lin, H.; Lazar, S.; Knippels, G.; Tiemeijer, P.; van der Stam, M.; von Harrach, S.; Stekelenburg, M.; et al. *Microscopy and Microanalysis* **2008**, *14*, 469–477.
- (80) Li, C.; Habler, G.; Baldwin, L. C.; Abart, R. *Ultramicroscopy* **2018**, *184*, 310–317.
- (81) Burke, K. *The Journal of Chemical Physics* **2012**, *136*, 150901.
- (82) Koch, W.; Holthausen, M. C. *A Chemist's Guide to Density Functional Theory*, 2nd ed.; Wiley-VCH: Weinheim ; New York, **2001**.
- (83) Sholl, D. S.; Steckel, J. A. *Density Functional Theory: A Practical Introduction*; Wiley: Hoboken, N.J, **2009**.
- (84) van Mourik, T.; Buhl, M.; Gageot, M.-P. *Philosophical Transactions of the Royal Society A: Mathematical, Physical and Engineering Sciences* **2014**, *372*, 20120488–20120488.

- (85) McDouall, J. J. W. *Computational Quantum Chemistry: Molecular Structure and Properties in Silicon; Theoretical and Computational Chemistry Series*; Royal Society of Chemistry: Cambridge, **2013**.
- (86) Zhan, C.-G.; Nichols, J. A.; Dixon, D. A. *The Journal of Physical Chemistry A* **2003**, *107*, 4184–4195.
- (87) Patrick, C. E.; Giustino, F. *Physical Review B* **2011**, *84*.
- (88) Zhao, Y.; Truhlar, D. G. *Theoretical Chemistry Accounts* **2008**, *120*, 215–241.
- (89) Head, A. R.; Tsyshevsky, R.; Trotochaud, L.; Yu, Y.; Karshoğlu, O.; Eichhorn, B.; Kuklja, M. M.; Bluhm, H. *Journal of Physics: Condensed Matter* **2018**, *30*, 134005.
- (90) Puurunen, R. L. *Chemical Vapor Deposition* **2014**, *20*, 332–344.
- (91) Kim, H. *Journal of Vacuum Science & Technology B: Microelectronics and Nanometer Structures* **2003**, *21*, 2231.
- (92) Sperling, B. A.; Hoang, J.; Kimes, W. A.; Maslar, J. E.; Steffens, K. L.; Nguyen, N. V. *Journal of Vacuum Science & Technology A: Vacuum, Surfaces, and Films* **2014**, *32*, 031513.
- (93) Johnson, R. W.; Hultqvist, A.; Bent, S. F. *Materials Today* **2014**, *17*, 236–246.
- (94) Miikkulainen, V.; Leskelä, M.; Ritala, M.; Puurunen, R. L. *Journal of Applied Physics* **2013**, *113*, 021301.
- (95) Puurunen, R. L. *Journal of Applied Physics* **2005**, *97*, 121301.
- (96) Ma, Q.; Guo, H.; Gordon, R. G.; Zaera, F. Uptake of Copper *Chemistry of Materials* **2010**, *22*, 352–359.
- (97) Elers, K.-E.; Blomberg, T.; Peussa, M.; Aitchison, B.; Haukka, S.; Marcus, S. *Chemical Vapor Deposition* **2006**, *12*, 13–24.
- (98) Kanomata, K.; Ohba, H.; Pungboon Pansila, P.; Ahmmad, B.; Kubota, S.; Hirahara, K.; Hirose, F. *Journal of Vacuum Science & Technology A: Vacuum, Surfaces, and Films* **2015**, *33*, 01A113.
- (99) Yao, Y.; Coyle, J. P.; Barry, S. T.; Zaera, F. *The Journal of Physical Chemistry C* **2016**, *120*, 14149–14156.
- (100) Li, K.; Li, S.; Li, N.; Klein, T. M.; Dixon, D. A. *The Journal of Physical Chemistry C* **2011**, *115*, 18560–18571.
- (101) Lin, J.-M.; Teplyakov, A. V.; Rodríguez-Reyes, J. C. F. *Journal of Vacuum Science & Technology A: Vacuum, Surfaces, and Films* **2013**, *31*, 021401.
- (102) Sperling, B. A.; Kimes, W. A.; Maslar, J. E. *Applied Surface Science* **2010**, *256*, 5035–5041.
- (103) Zhang, L.; Liu, M.; Ren, W.; Zhou, Z.; Dong, G.; Zhang, Y.; Peng, B.; Hao, X.; Wang, C.; Jiang, Z. -D, Jing W., Ye, Z. -G. *RSC Advances* **2017**, *7*, 8388–8393.
- (104) Shahin, D. I.; Tadjer, M. J.; Wheeler, V. D.; Koehler, A. D.; Anderson, T. J.; Eddy, C. R.; Christou, A. *Applied Physics Letters* **2018**, *112*, 042107.
- (105) Shi-Jin Ding; Hang Hu; Lim, H. F.; Kim, S. J.; Yu, X. F.; Chunxiang Zhu; Li, M. F.; Byung Jin Cho; Chan, D. S. H.; Rustagi, S. C.; et al. *IEEE Electron Device Letters* **2003**, *24*, 730–732.
- (106) Yu, H. Y.; Li, M. F.; Kwong, D. L. *Thin Solid Films* **2004**, *462–463*, 110–113.

- (107) Triyoso, D. H.; Hegde, R. I.; Grant, J.; Fejes, P.; Liu, R.; Roan, D.; Ramon, M.; Werho, D.; Rai, R.; La, L. B.; Baker, J.; Garza, T.; Guenther, T.; White Jr., B. E.; Tobin P. J. *Journal of Vacuum Science & Technology B: Microelectronics and Nanometer Structures* **2004**, *22*, 2121.
- (108) Ye, L.; Kropp, J. A.; Gougousi, T. *Applied Surface Science* **2017**, *422*, 666–674.
- (109) Tallarida, M.; Karavaev, K.; Schmeisser, D. *Journal of Applied Physics* **2008**, *104*, 064116.
- (110) Park, B.-E.; Oh, I.-K.; Lee, C. W.; Lee, G.; Shin, Y.-H.; Lansalot-Matras, C.; Noh, W.; Kim, H.; Lee, H.-B.-R. *The Journal of Physical Chemistry C* **2016**, *120*, 5958–5967.
- (111) Pinčík, E.; Kobayashi, H.; Matsumoto, T.; Takahashi, M.; Mikula, M.; Brunner, R. *Applied Surface Science* **2014**, *301*, 34–39.
- (112) Platt, C. L.; Li, N.; Li, K.; Klein, T. M. *Thin Solid Films* **2010**, *518*, 4081–4086.
- (113) Ruhl, G.; Rehmet, R.; Knižová, M.; Merica, R.; Vepřek, S. *Chemistry of Materials* **1996**, *8*, 2712–2720.
- (114) Musschoot, J.; Xie, Q.; Deduytsche, D.; Van den Berghe, S.; Van Meirhaeghe, R. L.; Detavernier, C. *Microelectronic Engineering* **2009**, *86*, 72–77.
- (115) Assaud, L.; Pitzschel, K.; Barr, M. K. S.; Petit, M.; Monier, G.; Hanbücken, M.; Santinacci, L. *Applied Physics A* **2017**, *123*.
- (116) Novak, I.; Kovač, B.; Jokić, M. *The Journal of Physical Chemistry A* **2014**, *118*, 5636–5641.
- (117) Mann, J. B. Atomic structure calculations II. Hartree-Fock wavefunctions and radial expectation values: hydrogen to lawrencium. Los Alamos Scientific Lab., N. Mex., **1968**.
- (118) Gallet, J.-J.; Silly, M. G.; Kazzi, M. E.; Bournel, F.; Sirotti, F.; Rochet, F. *Scientific Reports* **2017**, *7*.
- (119) Wang, Y.-L.; Guo, H.-M.; Qin, Z.-H.; Ma, H.-F.; Gao, H.-J. *Journal of Nanomaterials* **2008**, *2008*, 1–18.
- (120) Schubert, B.; Avouris, P.; Hoffmann, R. *The Journal of Chemical Physics* **1993**, *98*, 7593–7605.
- (121) Lee, S.-H.; Kang, M.-H. *Physical Review Letters* **2000**, *84*, 1724–1727.
- (122) Lee, S.-H.; Kang, M.-H. *Physical Review B* **2000**, *61*, 8250–8255.
- (123) Han, L.; Pan, J.; Zhang, Q.; Li, S.; Chen, Z. *ECS Journal of Solid State Science and Technology* **2014**, *3*, 155–160.
- (124) Kemf, E.; United Nations Environment Programme. *GCO-Global Chemicals Outlook: Towards Sound Management of Chemicals*; **2013**.
- (125) https://ec.europa.eu/eurostat/statistics-explained/index.php/Chemicals_production_and_consumption_statistics#Total_production_of_chemicals. **2019**.
- (126) Rothenberg, G. *Catalysis: Concepts and Green Applications*; WILEY-VCH: Weinheim, **2008**.
- (127) Roberts, M. Birth of the Catalytic Concept. *Catalysis Letters* **1800**, No. 67, 1–4.
- (128) Oswald, W. *Annalen Der Naturphilosophie*; **1904**.

- (129) Schlögl, R. Heterogeneous Catalysis. *Angewandte Chemie International Edition* **2015**, *54*, 3465–3520.
- (130) Fadhel, A. Z.; Pollet, P.; Liotta, C. L.; Eckert, C. A. *Molecules* **2010**, *15*, 8400–8424.
- (131) Subramani, V.; Gangwal, S. K. *Energy & Fuels* **2008**, *22*, 814–839.
- (132) Giri, R.; Liang, J.; Lei, J.-G.; Li, J.-J.; Wang, D.-H.; Chen, X.; Naggar, I. C.; Guo, C.; Foxman, B. M.; Yu, J.-Q. *Angewandte Chemie International Edition* **2005**, *44*, 7420–7424.
- (133) Crabtree, R. H. *Journal of the Chemical Society, Dalton Transactions* **2001**, No. 17, 2437–2450.
- (134) Chen, X.; Engle, K. M.; Wang, D.-H.; Yu, J.-Q. *Angewandte Chemie International Edition* **2009**, *48*, 5094–5115.
- (135) Seregin, I. V.; Gevorgyan, V. *Direct Transition Chemical Society Reviews* **2007**, *36*, 1173.
- (136) Arrigo, R.; Schuster, M. E.; Abate, S.; Wrabetz, S.; Amakawa, K.; Teschner, D.; Freni, M.; Centi, G.; Perathoner, S.; Hävecker, M.; Schlögl, R. *ChemSusChem* **2014**, *7*, 179–194.
- (137) Arrigo, R.; Schuster, M. E.; Xie, Z.; Yi, Y.; Wowsnick, G.; Sun, L. L.; Hermann, K. E.; Friedrich, M.; Kast, P.; Hävecker, M.; Knop-Gericke, A.; Schlögl, R. *ACS Catalysis* **2015**, *5*, 2740–2753.
- (138) Kumar, G.; Blackburn, J. R.; Albridge, R. G.; Moddeman, W. E.; Jones, M. M. *Inorganic Chemistry* **1972**, *11*, 296–300.
- (139) Militello, M. C.; Simko, S. J. *Surface Science Spectra* **1994**, *3*, 387–394.
- (140) Clark, D. T.; Kilcast, D.; Adams, D. B.; Musgrave, W. K. R. *Journal of Electron Spectroscopy and Related Phenomena* **1975**, *6*, 117–134.
- (141) Xu, S.; Song, K.; Li, T.; Tan, B. *Journal of Materials Chemistry A* **2015**, *3*, 1272–1278.
- (142) Baer, D. R.; Engelhard, M. H.; Lea, A. S. *Surface Science Spectra* **2003**, *10*, 47–56.



LUND
UNIVERSITY

Faculty of Science
Department of Physics
Division of Synchrotron Radiation Research

ISBN 978-91-7753-968-1 (print)
ISBN 978-91-7753-969-8 (pdf)

